Functional analysis of oncogenic lesions in multiple myeloma with potential significance for refractory disease

Funktionelle Analyse onkogener Läsionen beim Multiplen Myelom mit potenzieller Bedeutung für einen refraktären Krankheitsverlauf

Doctoral thesis for a doctoral degree

at the Graduate School of Life Sciences,

Julius-Maximilians-Universität Würzburg,

Section: Biomedicine

submitted by

Umair Munawar

from

Lahore, Pakistan

Würzburg, 2020

Submitted on: . . . .

Members of the *Promotionskomitee*:

Chairperson: Prof. Manfred Gessler

Primary Supervisor: Prof. Ralf C. Bargou

Supervisor (Second): Prof. Harald Wajant

Supervisor (Third): Prof. Svenja Meierjohann

Supervisor (Fourth): Dr. Thorsten Stühmer

Date of Public Defence: . . . .

Date of Receipt of Certificates: . . . .

Contents

List of Figures

List of Tables

Summary

Despite the advancement in the treatment from genotoxic drugs to more targeted therapies, multiple myeloma (MM) remains incurable. MM is known for its complex genetic heterogeneity as different genetic lesion accrue over the course of the disease. The current work focuses on the functional analysis of genetic lesions found at the time of diagnosis and relapse and their potential role regarding therapy response and refractory disease.

Genetic lesions involving tumor suppressor gene *TP53*, are found at diagnosis and tend to accrue during disease progression. Different types of mono- and biallelic *TP53* alterations were emulated in the AMO1 cell line model, were functionally characterized and tested for their potential role in therapy response. Both types of single hit *TP53* alteration (deletion 17p and *TP53* point mutations) were found to have similar adverse effects on the functionality of the p53 system and response to genotoxic drugs which were completely abolished in the case of double hit *TP53* alterations (no p53 expression, or mutant overexpression in wild type *TP53* deletion background). Whereas, sensitivity to proteasome inhibitors remained unaltered. Using the clonal competition assay (CCA), single *TP53* hit clones were found to have a fitness advantage over wildtype cells. Proliferative cell fitness was further enhanced in double hit *TP53* clones, as they dominated wildtype and single hit *TP53* clones in the CCA. Presence of external selection pressure in the form of low dose melphalan expedited the intrinsic fitness advantage.

Alterations found in CUL4B, a component of CRL4-CRBN protein complex, a target of immunomodulatory drugs (IMiDs), were also functionally analyzed in the current study. Hotspot mutations and mutations found in IMiDs refractory patients were modelized in L363 cells and their role in IMiDs sensitivity was studied. *CUL4B* mutations were found not to be involved in providing lenalidomide resistance to the cell, whereas knocking *CUL4B* out was observed to provide negative fitness to the cells in CCA. In the presence of external selection pressure, these clones showed fitness, which was lost in the case of lenalidomide withdrawal. This shows that some alterations may play a role in refractory patients only in the presence of therapy, and as soon as therapy is discontinued, these altered clones may disappear such as clones with alterations in *CUL4B*. On the other hand, some alterations provide drug-independent intrinsic positive fitness, however, be further enhanced by drug exposure, such as seen in case of *TP53* altered clones. Therefore, close monitoring and functional analysis of evolving clones is desired during disease progression, as it can be helpful in therapeutic guidance to achieve a better outcome for patients.

Zusammenfassung

Das Multiple Myelom (MM) ist im Normalfall eine unheilbare Erkrankung, trotz etlicher Fortschritte hinsichtlich der Behandlung, angefangen von genotoxischen Medikamenten bis hin zu zielgerichteten Therapien. Eine komplexe genetische Heterogenität, bei der sich Läsionen im Verlauf der Krankheit ansammeln, ist typisch für das MM. Diese Arbeit beschäftigt sich mit der funktionellen Analyse von genetischen Läsionen zum Erstdiagnose-Zeitpunkt bzw. Rezidiv und ihrer potenziellen Bedeutung bezüglich des Ansprechens auf die Therapie und einer refraktären Verlaufsform.

Genetische Veränderungen des Tumorsuppressorgens *TP53* sind mitunter schon bei der Erst-Diagnose nachweisbar und nehmen im Krankheitsverlauf weiter zu. Deshalb wurden verschiedene mono- und biallelische *TP53* Mutationen in AMO1 Zelllinien-Modellen nachgebildet, funktionell charakterisiert und auf ihre potenzielle Rolle im Therapie-Ansprechen getestet. Dabei wurden für beide Formen von *single hit TP53* Alterationen (17p Deletionen und *TP53* Punktmutationen) ähnlich nachteilige Effekte auf die Funktionalität des p53 Systems und das Ansprechen auf genotoxische Medikation gefunden. Im Falle von *double hit TP53* Alterationen (keinerlei p53 Expression oder aber hohe Spiegel von mutiertem p53 bei *TP53* wildtype deletierem Hintergrund) wurden diese Effekte noch weiter verstärkt. Die Sensitivität gegenüber Proteasom-Inhibitoren blieb indessen unbeeinträchtigt. Mithilfe des *Clonal Competition Assays* (CCA), wurde festgestellt, dass *single hit TP53* Klone gegenüber wildtypischen Zellen einen Fitnessvorteil haben. In *double hit TP53* Klonen war die proliferative Zell-Fitness zu dem gesteigert, sodass diese über wildtypische und *single hit TP53* Klone im CCA dominierten. Die Anwesenheit eines externen Selektionsdrucks in Form von Niedrigdosis-Melphalan verstärkte zusätzlich den intrinsischen Fitnessvorteil.

Aberrationen in CUL4B, einer Untereinheit des CRL4-CRBN Protein Komplexes, dem Angriffspunkt der Immunmodulatoren (IMiDs), wurden in dieser Studie ebenfalls funktionell analysiert. Hotspot Mutationen und solche Mutationen, die gehäuft in IMiD refraktären Patienten auftreten, wurden in L363 Zellen modelliert und hinsichtlich ihres Einflusses auf die IMiD Sensitivität untersucht. *CUL4B* Mutationen waren nicht in Lenalidomid-Resistenz involviert, ein Knockout von *CUL4B* äußerte sich aber in einer negativen Allgemeinzustand der Zellen im CCA. In Anwesenheit eines externen Selektionsdrucks, zeigten diese Klone einen Fitnessvorteil, der wieder verloren ging, wenn kein Lenalidomid mehr zugegeben wurde. Dies zeigt, dass manche Alterationen nur dann eine Rolle in refraktären Patienten zu spielen scheinen, wenn diese therapiert werden. Sobald die Therapie eingestellt oder unterbrochen wird, könnten solche Klone verschwinden wie z.B. *CUL4B*-Alterationen. Auf der anderen Seite bedingen manche Veränderungen wiederum einen Medikamenten-unabhängigen, intrinsisch Fitnessvorteil, der jedoch durch Medikamenten-Exposition noch zusätzlich verstärkt werden kann, wie beispielweise bei *TP53* mutierten Klonen. Daher ist eine engmaschige Überwachung während der Krankheits-Progression sowie eine funktionelle Analyse der sich entwickelnden Klone wünschenswert. Dies könnte für die therapeutische Beratung hilfreich sein um somit ein besseres Behandlungsergebnis für die Patienten zu erzielen.

Chapter 1

Introduction

1.1 Multiple myeloma

Multiple myeloma (MM) is a type of non-hodgkin lymphoma, characterized by clonal proliferation of malignant plasma cells in the form of localized tumors at single or multiple locations in the pelvis, ribs, skull and vertebral column. Further characteristics are high levels of M protein in blood or urine and associated organ dysfunction e.g. kidney failure. These tumors can be either medullary (confined within a bone) or extramedullary (developing in soft tissues outside the bones) [1]. It is the second most common hematological malignancy and accounts for approximately 13% of all hematological cancers. The incidence of multiple myeloma has increased uniformly since 1990. Cases of myeloma increased 126% and the death rate increased 94% from 1990 to 2016. The global increase in the incidence rate was contributed by population growth, aging population and rise in the age-specific incidence rate. The age-standardized incidence rate is 2.1 per 100,000 persons [2]. It is a disease of the old age as the median age at diagnosis is 70 years with 37% of patients being older than 75 years at the time of diagnosis [3].

1.2 Clinical symptoms

The clinical symptoms of MM include pathological fractures in the skeleton, anemia, impaired hematopoiesis and renal failure. The uncontrolled proliferation of MM cells disrupts the bone homeostasis by activating osteoclast and inhibiting osteoblast activity. This dysregulation of bone formation and resorptions results in pathological bone fracture, causing severe debilitating pains and sometimes even leads to spinal compressions because of collapsed vertebrae [4]. Although erythroid cells do not have direct lineage with the myeloma cells, anemia is a characteristic feature of MM. Myeloma cells uniformly infiltrate bones and disrupt erythropoiesis. Thus, the severity of anemia depends on the extent of infiltration into the bone, the number of the osteolytic lesions and the proliferation of MM cells. But this disruption of erythropoiesis is a reversible phenomenon [5, 6]. Abnormal monoclonal proliferation of the plasma cells results in increased levels of atypical immunoglobulin fragments, also called M protein. The elevated level of M protein is also one of the diagnostic features of MM [7]. Furthermore, the deposition of monoclonal immunoglobulin light chains into the tubular network of nephrons impairs normal kidney function. Hypercalcemia, a consequence of bone damage plays an important role in decreasing renal filtration and may result in kidney failure in extreme cases [8]. Due to the compromised immune system, MM patients are at higher risk of developing infections. Infections are shown to be a major cause of mortality and morbidity in MM patients as they are prone to developing viral and bacterial infections 7-folds higher than the normal population. This is due to the lack of a normal level of functional antibodies in the blood

and impaired lymphocytic function. Infections pose a major threat to MM patients causing on average 22% of deaths per year [9]. Rarely MM patients develop a hyperviscosity syndrome due to increased concentration of circulating antibodies in the blood. This may result in variable neurological symptoms, blurred vision due to retinal hemorrhage, bleeding and even cardiac complications [10]

1.3 Staging/biology

Activated B cells have a high proliferation rate and they differentiate into plasmablasts and memory B cells. During this phase they undergo a series of genetic modifications which include somatic hyper-mutations, isotype switching and affinity maturation. These multistep genetic and microenvironmental modifications can give rise to myeloma cells, in case they go wrong. Multiple myeloma is usually, but not always, preceded by a non-symptomatic monoclonal gammopathy of undetermined clinical significance (MGUS) followed by smoldering myeloma (SMM). Genetic abnormalities which drive this transformation from activated B cells to MGUS to SMM to MM include interchromosomal translocations, copy number aberrations, somatic mutations and epimutations [11].

1.3.1 Non-symptomatic monoclonal gammopathy of undetermined clinical significance (MGUS)

MGUS is characterized by <3g/dL of M protein, the absence of lytic bone lesions, no end-organ damage and <10% clonal bone marrow plasma cells. It is present in 1% of the adults over the age of 25 and 3-4% above the age of 50 years [12]. The initial concentration of M protein is a significant predictor of progression from MGUS to MM. The average risk of progression is one percent per year. A major difference between MGUS and MM is the absence of circulating plasma cells and of end organ damage [13]. There are two types of MGUS, non-IgM and IgM MGUS. IgM MGUS develops into Waldenström macroglobulinemia [14, 15]. Waldenström macroglobulinemia is characterized by lymphoplasmacytic lymphoma in bone marrow with IgM monoclonal gammopathy in the blood. Patients do show the symptoms of hyperviscosity, splenomegaly and infiltration of hematopoietic tissues [16], whereas non-IgM MGUS develops into SMM which later leads to MM.

1.3.2 Smoldering multiple myeloma (SMM)

Smoldering multiple myeloma is an intermediate stage between MGUS and MM, it is also called asymptomatic MM. Patients with SMM have higher clonal bone marrow plasma cell levels as compared to MGUS, <60%, >3g/dL of M protein but absence of any end-organ damage or lytic bone lesions. Patients with SMM tend to progress to MM within 2 years, but the median time for this progression is around 7 months [17].

There are complex genetic events involved in the conversion of MGUS into MM. Primary genetic events include translocations on the IgH locus which most commonly affect the genes *MMSET*, *FGFR3*, *MAF*, *CCND1*, *CCND3* [18, 19]. Secondary genetic events include further translocations and mutations

which mostly promote proliferation. These events may include activating mutations in *NRAS*, *KRAS*, *NFkB*, the inactivation of the cyclin dependent kinase inhibitors *CDKN2A* and *CDKN2C*, or inactivating mutations in tumor suppressor genes such as *TP53* and even some complex karyotypic aberrations. Some epigenetic modifications and microRNA dysregulations can also be involved [20, 21]. These alterations also include hyperploidy of some odd-numbered chromosomes such as chromosome number 3,5,9,11,15,19 and 21. Some of these hyperploidies are even found at the MGUS stage, thus they are rather considered pathogenic than progressive in nature [22, 23].
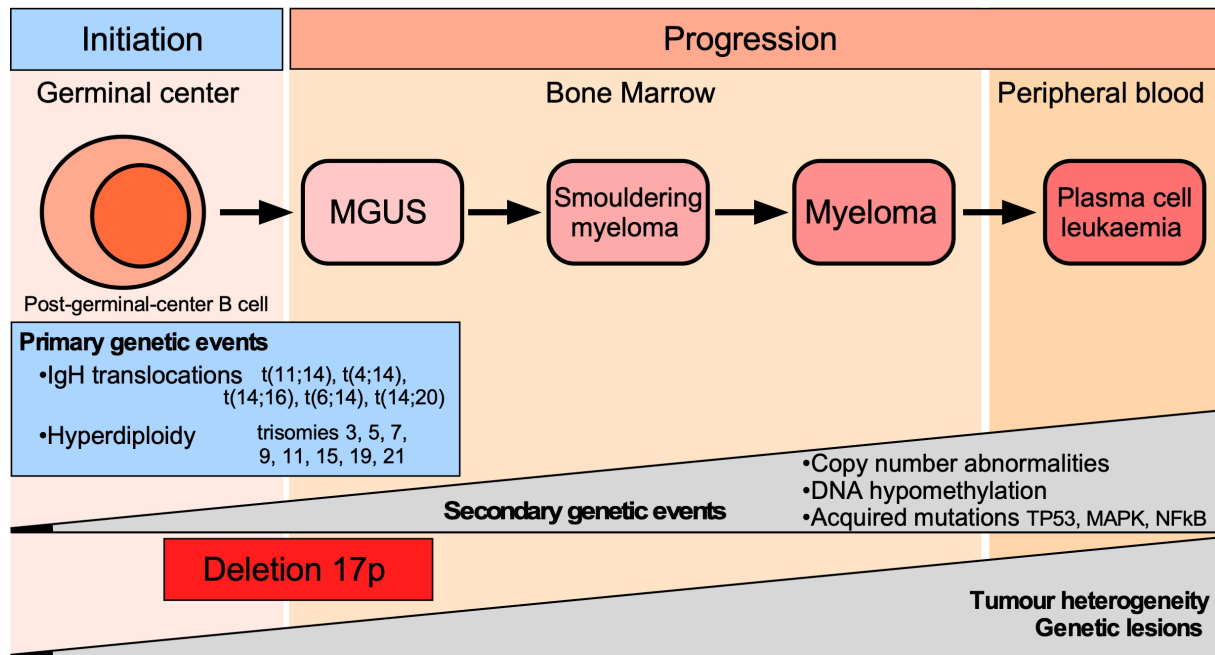
Figure 1.1: Staging of MM. Primary genetic alterations can happen in post germinal center B cells which initiate a series of changes leading towards MM. These primary alterations include IgH translocations involving chromosome 14, and/or hyperdiploidy of odd-numbered chromosomes. These events are considered pathogenic and not progressive and they can occur in bone marrow in addition to the germinal center. Secondary genetic events and extensive tumor heterogeneity tend to accumulate with the progression of the disease (adapted from [24]).

1.4 Treatment

Treatment of multiple myeloma has strongly improved over time. The very first reported case of myeloma was treated with rhubarb pills and orange peel infusion in the year 1844 [25]. The first drug reported to be useful in treating multiple myeloma was urethane. It remained the standard therapy from 1947 to 1966 when it was shown by a randomised clinical trial to be not better than a placebo [26]. The first try with an alkylans as a treatment was conducted by Blokhin in the year 1958, when he used sarcolysin (melphalan) to treat MM patients. In this initial study melphalan showed good response in patients which was later confirmed in bigger patient cohorts and also reported by many others [27, 28, 29].

The next class of treatment introduced was corticosteroids e.g prednisone. Used as a single drug, it did not have any impact on the overall survival of patients, but in combination with melphalan it showed an improvement in survival of 6 months as compared to melphalan alone [30]. The next substantial

improvement in treatment was the introduction of stem cell transplantations. The initial class of transplantations, called allogeneic stem cell transplantation, uses bone marrow from HLA-compatible sibling donors. One of the earliest studies on treating MM patients with allogeneic bone marrow transplants revealed a 12 month prolonged survival of patients post-transplantation [31]. As a next step, patients were tested with autologous stem cell transplants where they are initially given high dose melphalan along with the required support of antibiotics and platelets, followed by intravenous autograft, which was previously obtained from the same patient during remission. Initial studies showed that it did not significantly improve the survival and patients had a median survival duration of around 19 months [32]. Later, studies from intergroupe Francophone du Myeloma and UK medical research council showed the improved event free survival with autologous stem cell transplant (ASCT) [33, 34]. High dose chemotherapy with ASCT had been a standard treatment for MM until the development of novel therapies.

1.4.1 Novel therapies

Thalidomide was the first important advancement initiating an area of novel therapies for multiple myeloma. Thalidomide initially was developed in the 1950s and approved as a sedative but later was found to be causing teratogenic effects [35]. In 1994, it was reported to have antiangiogenic properties. Thanks to the increased awareness of importance of the angiogenesis in myeloma, it was tested in myeloma patients. The first clinical trial tested thalidomide as a single agent on 84 patients and with a response rate of 34% [36]. Thalidomide gave rise to the important class of antimyeloma drugs called immunomodulatory drugs (IMiDs). One of the most important derivatives of thalidomide, called lenalidomide (Len) showed promising results in randomized clinical trials [37]. Later, further studies were done to test it on newly diagnosed and relapsed refractory patients and it showed variable results as a single agent and in combination therapy and was approved in 2006 for MM patients which failed one prior therapy [38, 39]. Pomalidomide (Pom), sister compound of the same family had limited cross resistance with Len, showed good response in Relapsed Refractory Multiple Myeloma (RRMM) patients, thus was approved by The Food and Drug Administration (FDA) in 2013 [40].

When the mechanism of protein degradation by ubiquitination and subsequent degradation by the proteasome system was fully understood, several proteasome inhibitors (PIs) were developed. The first highly specific PI, Bortezomib (Bor) was developed in 1995 by Adams et al. and it demonstrated potent cytotoxic and growth inhibitory effects and antimyeloma activity in preclinical [41] and initial phase I studies [42]. In phase 2 trials, which tested it on 202 relapsed refractory MM patients, its response rate was around one third, which lead to its FDA approval as standard therapy in 2003 [43]. Currently Bortezomib (Bor), Carfilzomib (Car) and Ixazomib (Ixa) are used in PI therapy.

Venetoclax is a BCL-2 inhibitor, that was emerging as a new effective treatment option in relapsed and refractory MM. BCL-2 is overexpressed in patients with translocation (11;14) which has a prevalence rate of approximately 20% [44].

Moreover, monoclonal antibodies are one of the most recent treatment options in MM. Anti-CD38 antibodies, such as daratumumab, have shown impressive results as part of triple therapy and currently are being evaluated as a quadruple therapy approach [45]. Along with CD38 other targets expressed on

MM cells including CD138, CD74, CD48, SLAMF7 and BCMA are currently being studied as potential tumor-specific targets for monoclonal antibodies or bispecific T-cell engagers.

Most recently, BCMA directed CAR T-cells were developed and are being tested for their safety and efficacy in phase 2 clinical trials [46] in relapsed or refractory multiple myeloma patients. These recent studies offer the promise of adding new agents to the already existing pool of therapies against MM.

1.4.2 Current therapy regimen

In newly diagnosed multiple myeloma (NDMM) triplet therapy is recommended which should contain an IMiD (Len), a proteasome inhibitor (Bor) and a corticosteroid (Dex) [47]. The components of these triplets vary based on the patients' tolerance. For example, it can include cyclophosphamide instead of IMiDs. In some other patients doublet therapy containing Bor-Dex or Len-Dex is preferred. In transplant eligible patients post triple therapy ASCT is done followed by maintenance therapy with Len or Len-Bor in case of patients matching high-risk criteria. On the other hand in transplant-ineligible MM patients, based on the tolerance and health condition of the patient, therapy can be adapted from standard triple therapy. Especially in older patients the occurrence of treatment related side effects can be worse, hence, based on the patient's frailty, triple therapy can be attenuated or be replaced by double therapy which may include Bor-Dex or Len-Dex [48].
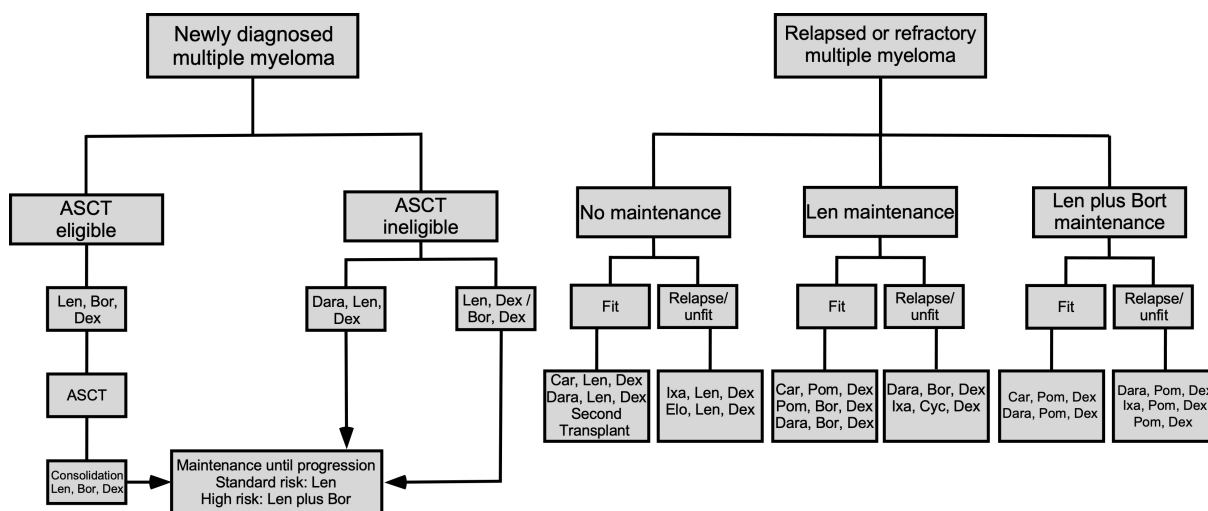
Figure 1.2: Current treatment regimen for multiple myeloma. NDMM patients are given triple therapy followed by ASCT. After ASCT patients are being given consolidation therapy. Maintenance therapy in the form of Len in case of standard risk or Len-Bor in high-risk patients. ASCT ineligible patients are given doublet or triplet therapy followed by maintenance therapy. In MM patients based on the previous therapy, they are given a new triplet therapy which includes at least one new class of drug.

In relapsed and refractory MM (RRMM) patients, a deep response is desirable as it is known to be associated with a longer survival. Treatment decisions for RRMM patients depend upon several factors including cytogenetic data at relapse, previous therapies and aggressiveness of the tumor growth. New therapies usually contain at least one novel class of drugs, not used in previous triplet or doublet therapies. Transplant deferred patients are recommended ASCT in case of relapse [49]. MM still remains incurable but with the development of several effective novel drugs, it has become quite a manageable disease.

1.5   Drug resistance

In the past decade many advancements in therapy development have improved patient overall survival drastically. Still, the acquisition of drug resistance and relapse is a major problem in MM. The underlying molecular mechanisms are being extensively studied by comparative genomic analysis of NDMM and RRMM patients.

A front line therapy with prolonged PI treatment usually results in PI resistance. In vitro studies with MM cell lines show that a continuous exposure to a certain PI induces resistance toward this particular PI as well as cross-resistance to some extent. The underlying molecular mechanisms are not fully understood yet and can vary. For example, point mutations in *PSMB5*, the responsible gene for PI binding, induced Bor resistance in cell culture [50]. Using a targeted sequencing approach this has also been confirmed to happen in vivo in a relapsed patient [51]. Mutations in other proteasome subunit genes after relapse have also been validated to induce resistance under laboratory settings, but in vivo occurrences are rather rare making it likely that other regulatory mechanisms, e.g. epigenetic gene silencing or RNA interference (RNAi), are also involved in the development of PI drug resistance [52].
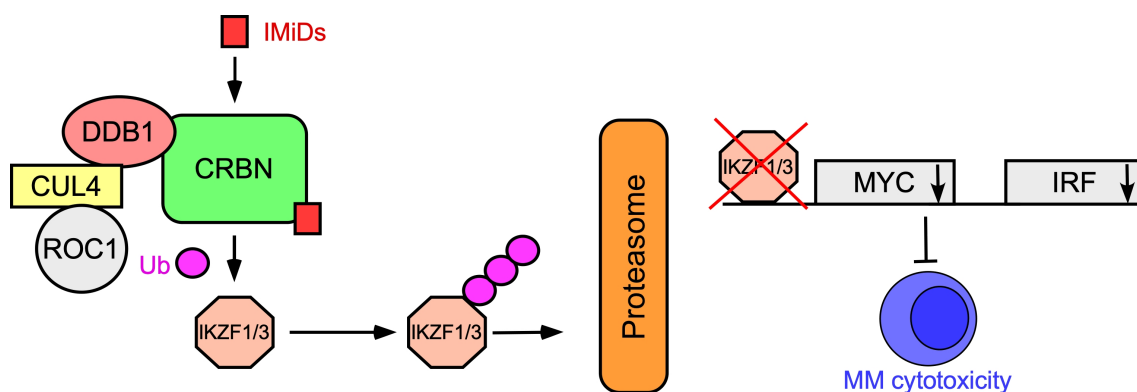
Figure 1.3: Mode of action of IMiDs. Immunomodulatory drugs act on the CRL4 protein complex. They bind to CRBN and enhance the CRL4-mediated transfer of ubiquitin to IKZF1/3. IKZF1/3 normally acts as a transcription factor and enhances the progression of MM cells, but when ubiquitinated, they get degraded by proteasomes, and are no longer functional. In this way IMiDs accomplish their anti-myeloma activity.

The phenomenon of drug resistance is similarly known for IMiDs, another frontline therapy. IMiDs target the CRL4 complex (CRBN-DDB1-CUL4B-ROC1) and enhance the depletion of the transcription factors IKZF1 and IKZF3 (also known as Ikaros and Aiolos) by ubiquitination, resulting in cytotoxicity of MM cells [53, 54]. As cereblon (CRBN) is the only known binding protein for all IMiDs, mutations in this gene can induce IMiD resistance [55]. Several analyses of different NDMM cohorts compared to IMiD treated RRMM indicate an increased mutation rate in *CRBN* and other subunits of the CRL4 complex in the latter [55, 56, 57, 58].

A statistical association of mutations in CRL4 complex subunits and IMiD resistance has been shown, but functional validation of in vivo found individual mutations is yet to be determined.

1.6 Clonal heterogeneity

Clonal heterogeneity is a well known feature of MM. It can be dynamically acquired with progressive disease. Such genomic alterations result in inter- and intra-patient heterogeneity, which translates into diverse clinical outcomes [59]. With the help of recent techniques like SNP arrays or Next Generation Sequencing (NGS) based whole genome or panel sequencing techniques, it has been shown that within the same patient there can be clonal and/or subclonal diverse tumor populations containing different genetic aberrations [60]. A recent study by Leo Rasche, et al. based on 51 MM patients has shown that more than 75% patients exhibited spatial clonal heterogeneity. These different clones contained mainly alterations in *TP53*, *CDKN2C* and other important genes [61]. Molecular data suggests that clonal heterogeneity is not linear but a result of the branching evolutionary pathways following Darwinian principles. According to this model, the acquisition of mutations help clonal cells to adapt to the microenvironment. Consequently new and fitter clones outcompete previously dominant clones by overgrowing [62, 63].

This clonal heterogeneity and evolution have direct implications on therapy. It has been shown in patients that a dominant clone at first relapse may have completely disappeared in the second relapse and can be replaced by an entirely different dominant clone with different genetic aberrations and sensitivity/resistance to previous therapy [64]. In this way, therapy acts as a selective pressure, in the favor of the resistant clones in context of the current therapy. This clone is likely to induce a new relapse. Therefore, understanding the implications of a patient's individual tumor composition under the current treatment phase is a key when it comes to in-time clinical decisions to best help the patients in an adaptive approach.

1.7 *TP53*

It took almost 10 years to finally establish the tumor suppressor role of p53 contrary to the popular belief of its function as an oncogene in 1989 [65]. Immediately after that inactivating *TP53* mutations began to be reported in different tumors and now these are reported to be found in almost 50% of all human cancers [66].

TP53 encodes for the 43.7 kDa protein p53 (apparent molecular weight 53kDa on Western blot) which acts as a transcription factor and binds to DNA in a sequence-specific manner [67]. Its active form exists as a homotetramer [68]. The p53 monomer consists of multiple domains, a transactivation domain (residues 1-73) and a proline-rich domain (residues 63-97) in the N terminal region. The C terminal region contains two domains, the transactivation domain (residues 324-355) required for the transcriptional activity and the nuclear localization signal (360-393). The central part of the protein is the highly conserved DNA binding domain (residues 94-312), where most of the commonly occurring mutations are found (Figure 1.7) [67].

In normal cells the level of p53 is very low, sometimes even undetectable. But under stress or DNA damage, the p53 level goes up and as a result causes cell cycle arrest or apoptosis. The p53 level is critical for the cell and it is therefore kept under tight control by MDM2. MDM2 is an E3 ubiquitin ligase that,

under normal conditions, ubiquitinates p53 resulting in proteasome-mediated degradation of p53. P53 acts as a transcription factor for MDM2, hence, controls its level in the cells. In this way a negative feedback loop between p53 and MDM2 is established in the cells [69] (Figure 1.4). To study the normal pathway of p53 in vitro, the cells can be treated with the MDM2 inhibitor called Nutlin 3a. It inhibits the binding of MDM2 to p53, by steric blockage of the binding groove of MDM2 for p53, hence, the p53 level increases. Transcription of genes responsive to p53 thus also increases, e.g. of *MDM2* and *CDKN2A* (coding for p21$^{\text{Cip1}}$), leading to a Nutlin 3a exposure mediated cell cycle arrest or apoptosis [70].
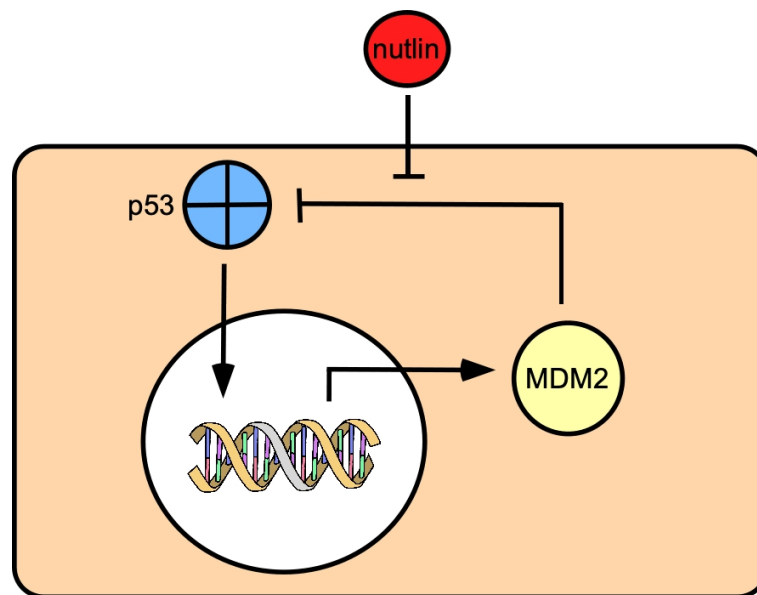
Figure 1.4: p53 MDM2 negative feedback loop. MDM2 inhibits/degrades p53 and p53 enhances the MDM2 level. To study the functionality of the p53 system in cells, the MDM2 inhibitor Nutlin 3a is being used. Nutlin 3a blocks the binding of MDM2 to p53, p53 does not get degraded and its level gets elevated. Due to an enhanced level of p53, its downstream targets are expressed at a higher level. One of these is MDM2.

The cancer genome atlas (TCGA) collected the genomic data from over 10,000 cancer cases and summarises the prevalence of *TP53* alterations. The data shows that 15.2% of all cases are mutation in *TP53*, 15.9% of cases are deletions and 22.02% of cases exhibit biallelic inactivations [71]. The prevalence of these abnormalities varies among different types of cancers such as paraganglioma with 0.5%, and lung, breast, ovarian and pancreatic cancers with 90% and does not always correlate with the prognosis. It has been reported to have prognostic relevance in few cancers which include some hematological malignancies such as multiple myeloma, acute myeloid leukemia, renal carcinomas and hepatocellular carcinomas [72]. In addition to the missense mutations, biallelic inactivation is also seen in multiple solid tumors with a prevalence of 91% as shown by TCGA. Even though many studies are showing high prevalence of *TP53* alterations in many cancer types, the functional effects of these alterations are still not well understood.

1.8 *TP53* alterations in multiple myeloma

Three types of p53 alterations are seen in MM patients: deletion of p arm of chromosome 17 (del 17p), monoallelic mutations and bi-allelic inactivation. They are not only found to be associated with the

pathogenesis of the disease but also with treatment resistance. These *TP53* aberrations can be present in NDMM or are being acquired during disease progression [73, 74]. Targeted sequencing of sequential paired samples and a cohort study on high-risk patients indicates that alterations of *TP53* tend to accrue over the course of disease and treatment [57, 58].
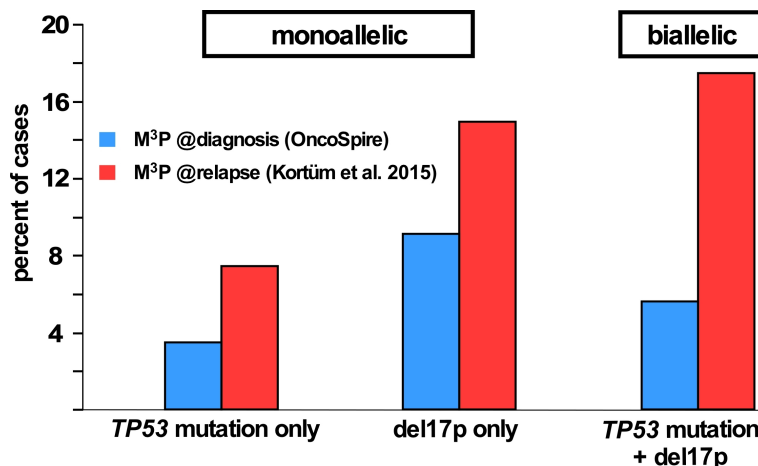
Figure 1.5: Acquisition of *TP53* alterations with time. All three types of *TP53* alterations accrue over the course of the disease. *TP53* point mutations increase from 4% at diagnosis to 8% at relapse. Del 17p cases increase from 9% to 16% from diagnosis to relapse. Biallelic alterations (mutation + del 17p) incidence rate increases from 5% to 19% over disease progression. (Image adapted from [57, 58])

1.8.1 Del 17p

Del 17p is one of the criteria of risk stratification of MM by the revised ISS and is considered one of the high-risk markers in MM. It has been shown by multiple studies that del 17p is present in approx. 11% of NDMM and these patients have a poor prognosis [75]. In most of the studies del 17p has retained the prognostic value for overall survival (OS) and progression free survival (PFS) and thus has become a staple of risk assessment of NDMM patients [76].

Criteria for considering a patient positive for del 17p are different among different studies conducted so far. Some studies consider a cut-off of >20% cells to be positive by fluorescent in situ hybridization (FISH), others consider 60% and some even consider the presence of 75% plasma cells with del 17p as high-risk determining feature [77]. In recent studies it has been shown that patients with more than 55% del 17p positive cells have median PFS and OS of 14 and 36 months respectively, whereas patients that had 55% or less del 17p positive cells showed median PFS and OS of 24 and 84 months. At the same time, patients with a high clonal cancer fraction (CCF) with del 17p are at higher risk of disease progression and early death as compared to patients with low CCF del 17p in both NDMM and RRMM settings [78, 79].
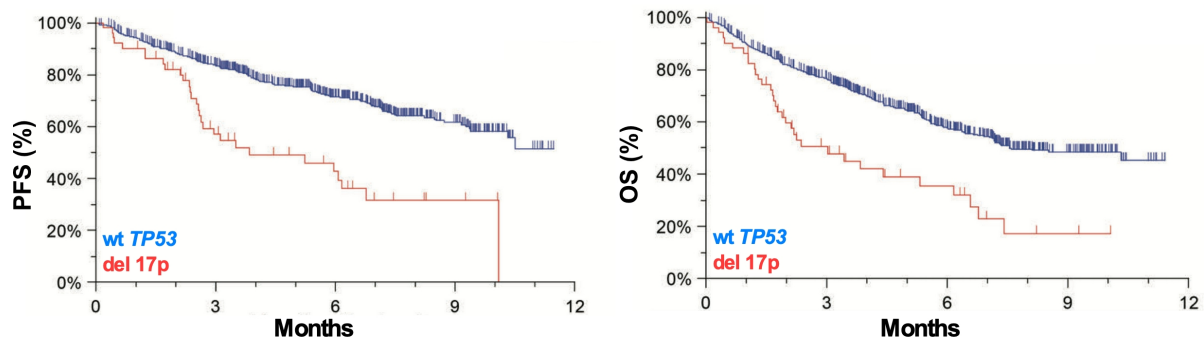
Figure 1.6: Kaplan-Meier plot showing PFS and OS of patients based on the 17p status. Patients with del 17p (determined by FISH) show worse progression free survival and overall survival as compared to patients with wild type *TP53*. (Adapted from [80])

Analysis of MM cohorts at diagnosis and relapse shows that the incidence of del 17p can increase during progression of the disease and translates into poor clinical outcomes (Figure 1.5) [56, 57]. The possible role of other genes present in the vicinity of *TP53* on chromosome 17 arm p is not fully ruled out. The potential involvement of co-deleted genes such as *Eif5a* and *Alox15b* in intensifying the impact of loss of the *Trp53* gene on the development of leukemia and lymphomas has been demonstrated in mouse models [81]. Conversely, studies have identified the presence of the *TP53* gene in a minimally deleted region on chromosome 17p [82] and revealed that hemizygosity caused the p53 haploinsufficiency and functional abnormalities in multiple myeloma [83]. The potential adverse role of *TP53* hemizygosity is strongly supported but remains inconclusive.

1.8.2 *TP53* point mutations

The incidence of *TP53* point mutations in NDMM is 3-8% [84, 57, 56]. These mutations, although present all across the *TP53* gene, concentrate mainly in the DNA binding domain (Figure 1.7). The exact prognostic role of *TP53* point mutations in MM is limited [85, 86]. A significant increase in the mutation frequency has been observed in late stage disease (25%) implying their possible role in disease progression and drug resistance [87].

    TP53 mutations are also reported to be a driver event in MM pathogenesis, helping in the propagation of disease in association with other driver gene mutations [88]. Normally *TP53* mutations are monoallelic and the cells completely inactivate the p53 system by loosing the second allele in the form of deletion 17p. This 'double hit' constellation is most commonly found in most MM cell lines. A higher prevalence of *TP53* point mutations at the sub-clonal level implies their acquisition during the clonal evolution of myeloma, which indicates that these mutations may have a progressive role as opposed to a founder event. Genomic analysis uncovers the association of co-occurrence of mutations and deletion of *TP53* [89]. Chng. *et al.* has shown that the incidence rate of *TP53* mutations is associated with a shorter OS compared to patients without mutations. In this study, as almost 50% of patients had del 17p, one can not differentiate if the observed effect was due to the monoallelic point mutations or biallelic alteration in *TP53* [90].
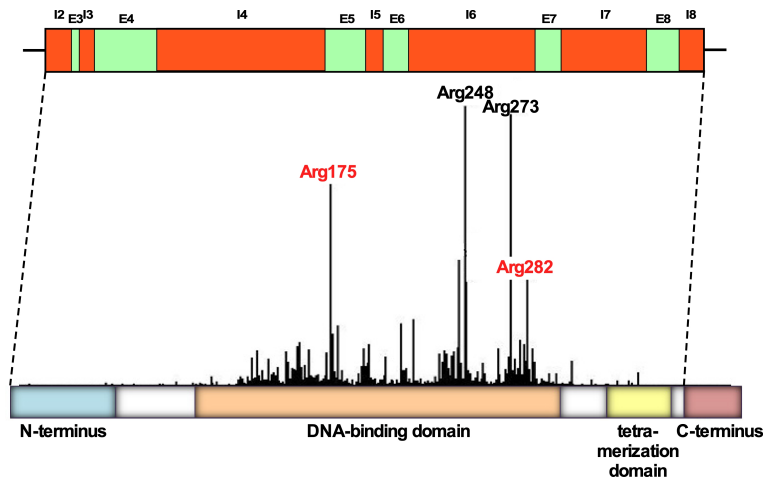
Figure 1.7: *TP53* point mutations. Almost 90% of the point mutations are found in the DNA binding domain of the p53 protein. Arg175 and Arg282 shown in red are two hotspot mutations whose functional implications in MM are analyzed in this thesis. (modified from www.proteopedia.org)

There are ways of appraising the functional impact of those mutations in silico via different algorithms such as used in programs like mutation assessor, sorting intolerant from tolerant (SIFT) or polymorphism phenotyping V2. These algorithms estimate the probability of phenotypic consequences of a mutation [91, 92, 93]. However, different algorithms may come to different predictive suggestions for the same mutation. To study the prognostic value of a *TP53* mutation, a long term follow-up of larger cohorts is needed together with a functional validation of these commonly occurring mutations in the wet lab.

1.8.3 Biallelic inactivation of *TP53*

A deletion of one allele in the form of del 17p and a mutation of the second allele putatively results in the complete inactivation of the p53 system. Early studies were showing a correlation between the incidences of mutations and del 17p, although the difference in OS or PFS between NDMM subgroups did not reach significance due to the small number of the patients included in the study [94, 90].
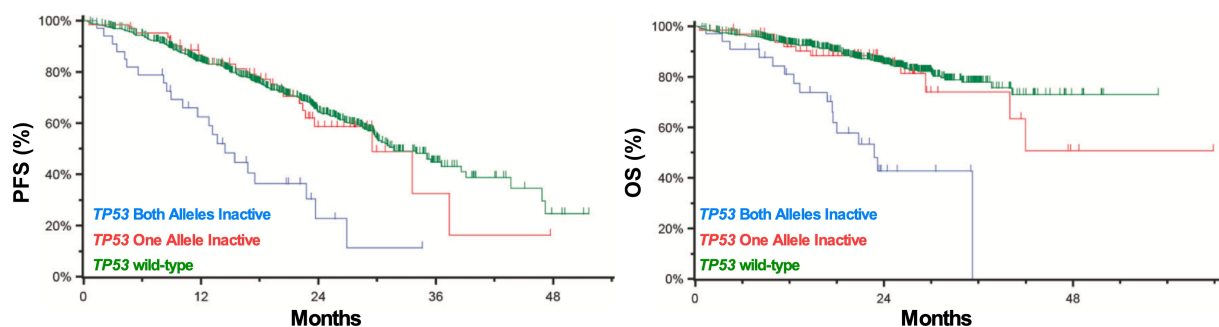
Figure 1.8: Kaplan-Meier plot showing PFS and OS of patients based on the *TP53* status. Patients with a monoallelic inactivation of *TP53* have worse progression free survival and overall survival as compared to patients having wild type *TP53*. If both alleles of *TP53* are inactivated, they have the worst PFS and OS as compared to the other two groups. (adapted from [84])

A recent study with bigger cohorts has not only shown a significant correlation between the incidence of mutation and deletion, but also showed that patients with biallelic inactivation had a worse PFS

and OS as compared to the patients with monoallelic inactivation. This study showed a 3 years OS of 84% of patients with a monoallelic hit as compared to 29% of patients with biallelic hits [80]. Different studies have shown that the incidence of biallelic *TP53* inactivation in NDMM patients is around 6-8% [84, 56, 57]. Walker et al. also showed that the incidence of mutation is associated with the incidence of a del 17p and patients with biallelic inactivation had the worst OS and PFS [84].

The order and timing of occurrence of these *TP53* lesions are not intensively studied yet but the occurrence of *TP53* mutations is somehow associated with del 17p. *TP53* mutations were found to occur simultaneously with del 17p or after occurrence of del 17p [89]. About one-third of del 17p carrying patients were found to have a *TP53* mutation and this concurrence increases upto 50% in case of refractory disease [94, 55]. Since these studies suggest that there is an association between the occurrence of del 17p and *TP53* point mutations and show that these alterations tend to accrue during the progression of the disease, the functional consequence of these intermediate states needs to be studied. As cells ultimately tend to attain biallelic hits and a drive is seen in patients from single hit situation to double hit situation, it makes perfect sense to analyze intermediate genomic alterations that lead to biallelic *TP53* inactivation.
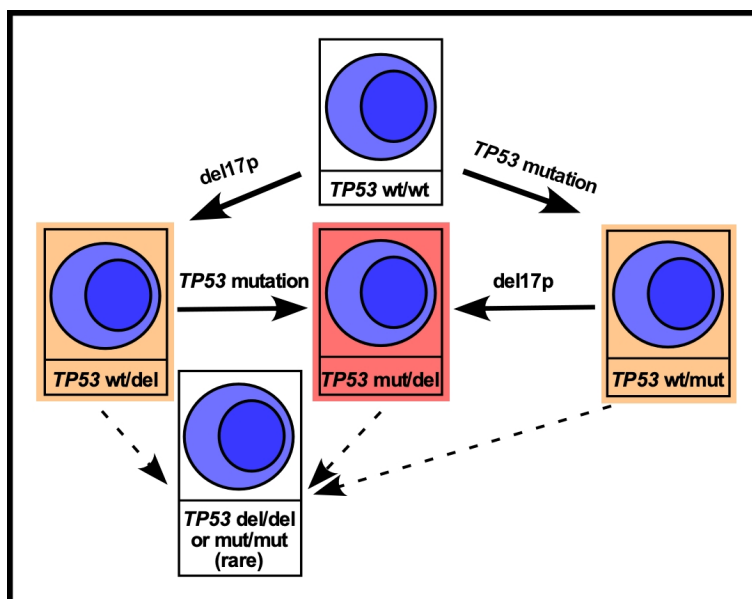
Figure 1.9: Pathway to *TP53* lesions. Primary MM cells having both wild type alleles of *TP53* acquire 'first hit' (highlighted in orange) as either an inactivating point mutation in one *TP53* allele or by losing one *TP53* allele as a consequence of del 17p. They attain 'second hit' in the form of point mutation (in case of already existing deletion) or deletion (in case of already existing point mutation) and give rise to 'double hit' status (highlighted in red), a condition most commonly found in most MM cell lines. Double deletion or double mutation constellation may also be possible but rarely found.

1.9   Targeting p53

With the advancement in the treatment of multiple myeloma from general genotoxic drugs to more targeted therapies such as IMiDs, PIs, monoclonal antibodies, or even CAR T-cells, the clinical outcome for MM patients has significantly improved, but still, patients tend to relapse, and MM remains incurable. Although the novel therapies are targeted towards specific proteins or pathways, studies still show

that high-risk group (*TP53* altered group) remains less responsive to certain therapies such as lenalidomide, and combination therapies of lenalidomide and dexamethasone in relapsed patients showing the underlying implications of *TP53* alterations against therapy response [95, 96].

The efforts to target p53 in MM mainly involved two approaches. First, inhibiting the interaction between p53 and its negative regulator MDM2, which results in a stabilization of p53 and consequently initiates downstream signaling to inhibit cell cycle and cause apoptosis [70], an approach potentially useful in wildtype (wt) MM cells, which are the majority of NDMM. Second, restoring the function of mutant p53 by using different agents, e.g. RITA (Reactivating p53 and Inducing Tumor Apoptosis) [97]. Other approaches included USP7 inhibitors [98] or PRIMA 1 [99] but none of the mentioned approaches has found its way to the clinic and *TP53*/p53 still remain untargetable in MM.

In order to improve the understanding of the implications of mono- and biallelic *TP53* lesions for MM pathobiology and treatment there is thus a necessity for deeper functional understanding of the different *TP53* alterations seen in patients.

1.10 Aims of the study

The first aim of this study was the functional characterization of clinically relevant *TP53* alterations in vitro as well as their impact on drug resistance. Several *TP53* alterations including monoallelic mutations, del 17p or biallelic inactivation are commonly detected in MM patients at NDMM and are known to accrue over disease progression in RRMM. The functional role of these different alterations is yet to be explored in detail. As these alterations have been shown to have a negative impact on disease outcome, deeper functional apprehension for these *TP53* alterations is essential. CRISPR-Cas9 generated AMO1 clones with single or double deleted *TP53* alleles (generated by Markus Roth) were used to establish different mono- and biallelic *TP53* alterations seen in patients using sleeping beauty transposon vector system. Two different monoallelic alterations were established: *TP53* hemizygosity (del 17p) or monoallelic *TP53* mutations (equal expression of mutant and wildtype cDNA genes in *TP53* deletion background) and two different biallelic *TP53* lesions were copied: biallelic *TP53* deletion or overexpression of mutant p53 in *TP53* deletion background. These cell line models were established to understand the predominant effects of different types of monoallelic lesions versus different biallelic alterations on the functionality of the p53 system and drug responsiveness in MM.
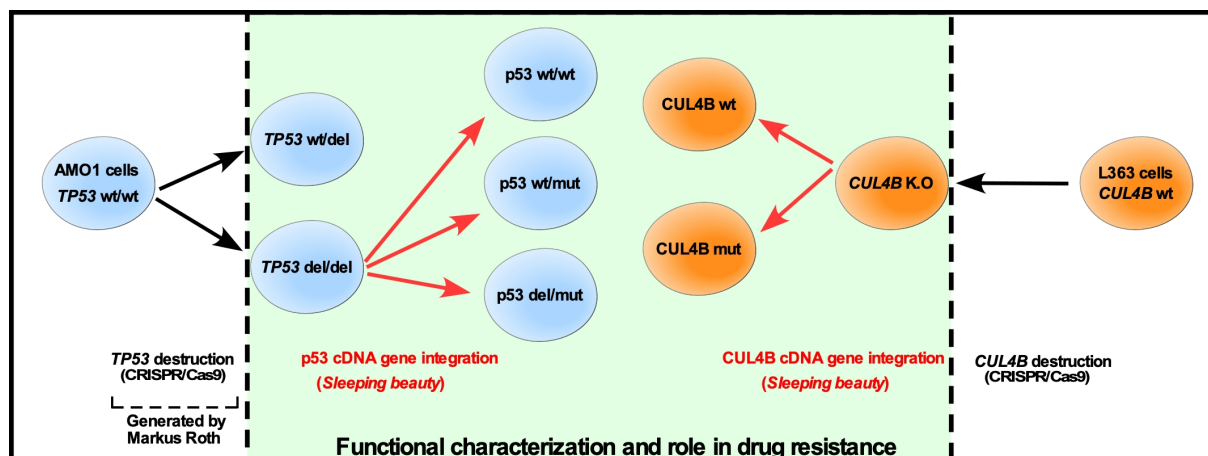
Figure 1.10: Aim of the study

The second aim of this study was to analyze the role of *CUL4B* and clinically relevant *CUL4B* mutations in IMiD sensitivity. CRL4/CRBN complex has been identified as a main target of immunomodulatory drugs. A statistical association of mutations in CRL4 complex subunits and IMiD resistance exists but functional validation of in vivo found individual mutations is yet to be determined. Present work focused on the role of CUL4B, one of the subunits of CRL4 complex, in IMiD sensitivity. CRISPR-Cas9 generated *CUL4B* knocked out cells were used for functional characterization of *CUL4B* hotspot mutations and to analyze their potential role in IMiD refractory patients. These cell line models were established to study the type of fitness provided by such alterations against wild type cells under lenalidomide exposure.

Chapter 2

Methods

2.1 Cell Culture

The cell lines AMO1 (DSMZ ACC 538) and L363 (DSMZ ACC 49) were bought from the German Collection of Microorganisms and Cell Cultures (DSMZ Braunschweig, Germany) and immediately expanded into stock and working banks. A new working bank aliquot was thawed for cell culture every 3-4 months. RPMI-1640 medium supplemented with 10% FBS, 1 mM sodium pyruvate, 2 mM glutamine, 100 U/ml penicillin, and 100 g/ml streptomycin (Table 3.1) was used for standard MM cell culture. Cells were kept at 37°C under 5% CO2. Cultures were split regularly every 3-4 days and routinely checked for mycoplasma negativity [100].

2.2 Electroporation

For electroporation the cells from the routine cultures were pelleted at 300 x g and resuspended in RPMI-1640 medium (without additives). The cell number was set around 10-40 million cells per ml. A total volume of 500 µl cell mixture containing the respective plasmids was transferred to the electroporation cuvettes (4mm), where a single exponential decay pulse of 280-300 Volts was applied using the Gene Pulser XCell (Bio-Rad Laboratories Munich, Germany). Cells were immediately transferred to 500 µl of plain RPMI-1640 medium already placed at 37°C for few minutes and later to complete RPMI-1640 medium and incubated at 37°C overnight [101].

2.2.1 Stable transfection

For sleeping beauty (SB) stable transfections, 20 µg/ml of the respective SB vector, 30 µg/ml pTX100 transposase expression plasmid were added in the cell mixture. Per electroporation 5 µg/ml EGPF expression plasmid was added to assess the transfection efficiency after 24 hours.

2.2.2 Transient transfection

For sleeping beauty transient transfections, 20 µg/ml of the respective SB vector and 5 µg/ml EGPF expression plasmid were used per electroporation reaction.

2.2.3 CRISPR

For CRISPR experiments, 5 µg/ml of the EGFP expression plasmid and 25 µg/ml of the respective GeneArt® CRISPR Nuclease vector were used in each electroporation.

2.3 OptiPrep

OptiPrep was performed to separate dead cells from alive cells 1-2 days after electroporation. The cell were pelleted at 300 x g for 5 minutes, resuspended in 1 ml of RPMI medium (without additives) and transferred to a 5 ml FACS tube where they were mixed with 300 µl of the OptiPrep medium (Axis-Shield, Dundee, UK) carefully to avoid bubble formation. This was followed by a careful overlying with 200 µl PBS, which forms a layer on the top of the cell suspension. The cells were centrifuged at 3500 x g for 7 minutes. The living cells form a ring on the boundary phase of PBS and the medium, were removed, washed with medium and transferred back to the culture.

2.4 Cytotoxicity assays

Two types of cytotoxicity assays were used to study the effects of drug treatment. Annexin V-PI measurement and the alamarBlue assay.

2.4.1 Annexin V-PI measurement

To measure apoptosis after drug treatment (cell death assay), the pelleted cells were washed with PBS and resuspended in 200 µl of cold annexin V-PI buffer (Table 3.5) containing 1 µl of annexin V-PromoFluor647 solution and 1 µg/ml Propidium iodide (PI). Flow cytometry was performed using FACS Calibur (BD Biosciences, Heidelberg, Germany). Data files were analyzed with Flowjo version 8.8.7. For determination of transfection efficiency, one day after electroporation, the cells were washed with PBS and resuspended in 200 µl of PBS containing 1 µg/ml propidium iodide and analyzed by flow cytometry.

2.4.2 AlamarBlue-Assay

AlamarBlue-Assay was performed to determine the metabolic activity of the cells, which is an indirect measurement of cell growth. After drug treatment in 96 well plates for a certain number of days (3-5 days, varying based on the drug used) 10% alamarBlue (440 µM solution of resazurin sodium salt) reagent was added. The plates were left in the cell culture incubator for 3-4 hours. The absorption of monochromatic color was measured at 570 nm and 600 nm with the microplate reader Model 680 (Bio-Rad). The relative percentage reduction of the alamarBlue reagent was calculated in comparison to the control cells. The reduction of the dye represents the metabolic activity of the cells, which indirectly represents the cell growth.

2.5 Selection of the transposed cells

After overnight recovery of the electroporated cells, the respective antibiotics were added to the culture to select for transposed cells and erase untransfected ones. AMO1 cells were selected with 1 µg/ml and L363 cells with 0.75 µg/ml of puromycin. For G418 selection 1 mg/ml of G418 was used for AMO1 and L363 cells. Culture was monitored regularly and the medium was replaced with the new medium

containing the respective antibiotic at day 7-10. It took 10-14 days to fully establish polyclonal cultures of the transposed cells.

2.6   CD4 purification

The cells co-transfected with CD4 expression vector or GeneArt® CRISPR vector (containing CD4 expression cassette) were subjected to CD4 purification using MACSelect 4 MicroBeads (Miltenyi Biotec, Gladbach, Germany) to separate positively transfected cells from untransfected cells. The cells were harvested 24-48 hours after electroporation at 300 x g for 3 minutes and the cell pellet was washed with PBS and MACS buffer respectively. The cell pellet was resuspended in 80 µl of MACSelect CD4 MiroBeads and incubated at 4°C for 10 minutes. Cell column was placed in the magnetic field of MACS separator, rinsed with 1-2 ml of MACS buffer and cell-beads suspension with an appropriate volume of MACS buffer was loaded on the column. Cell column was washed with 1-2 ml MACS buffer, removed from the magnetic field of MACS separator and cells were eluted with 2 ml RPMI medium.

2.7   Western blotting

2.7.1   Cell lysis and protein quantification

For Western analysis, fresh or frozen cell pellets (0.5-1 million cells) were resuspended in 50-100 µl cold lysis buffer (Table 3.8) and placed on ice for 20-25 minutes, followed by centrifugation at 16000 x g at 4°C for 10 minutes. After centrifugation supernatant was collected in a separate tube for protein quantification. Protein quantification was done using DC Protein Assay (Bio-Rad) following the manufacturer's instruction.

2.7.2   SDS-PAGE

The cell lysates were mixed with 2x Laemmli buffer (Table 3.7) and heated at 98°C for 5 minutes before loading on the gel. Initially the 10% polyacrylamide/SDS gel was run at 100 V for 5 minutes without samples before 15 µg protein per well was loaded. The gel was run at 120 V for 1-2 hours based on the size of protein to be detected by Western blotting.

2.7.3   Blotting and development

Separated proteins in the SDS gel were wet blotted on a nitrocellulose membrane using transfer buffer (Table 3.6) at 100 V for 50 minutes. To avoid overheating of the transfer buffer an ice block was placed in the blotting tank. After the transfer, the nitrocellulose membrane was stained with Ponceau-S Red (Table 3.10) to check the quality of the loading and blotting of the proteins. Protein marker bands were marked on the membrane and membrane was blocked with 5% non-fat dry milk in TBS-T (0.1% Tween in TBS, see (Table 3.13)) for 1 hour. Primary antibody dilutions were made in 5% non-fat dry milk in TBS-T and the cut membrane parts were incubated in respective primary antibody overnight at 4°C.

After washing the membrane 3 times, 5-10 minutes each with TBS-T, membranes were incubated with the respective secondary antibody dilution made in 5% non-fat dry milk in TBS-T for 1.5 hours at room temperature. The washing was repeated with TBS-T 3 times, 5-10 minutes each before developing the membrane with freshly prepared ECL solution (Table 3.15).

2.8 Drug treatment

2.8.1 Nutlin 3a

For the p53 induction experiment, the cells were seeded in a 12 well plate (100,000 cells per well) and treated with a final concentration of 10 µM Nutlin 3a overnight. Nutlin 3a was stored as a 10 mM stock solution in DMSO at -20°C. Solvent controls (DMSO for Nutlin 3a) were always set for each experiment. The next day, the cells were pelleted, washed with PBS and used for Western blot. For cytotoxicity experiments, 20000 cells per well were seeded in 96 well plates, treated with the respective concentration of Nutlin 3a. Annexin V-PI cell death measurement (See 2.4.1) was performed 72 hours after the Nutlin treatment.

2.8.2 Melphalan

Melphalan was dissolved in acidified ethanol and stored as a 20 mM stock solution at -20°C. To test melphalan sensitivity, cells were seeded in a 96 well plate (20,000 cells per well) in 100 µl RPMI medium. Another 100 µl of RMPI medium containing double the desired concentration of melphalan was added and the plates were incubated for 72 hours. Respective controls were set: solvent control (acidified ethanol) for the highest concentration of drug and no drug control. Based on the experiment, the cells were then subjected to the alamarBlue assay (See 2.4.2) or annexin V-PI assay (see 2.4.1).

2.8.3 Doxorubicin

Doxorubicin was stored as 10 mM stock solution in DMSO at -20°C. The cells were seeded in a 96 well plate (20,000 cells per well) in 100 µl RPMI medium and another 100 µl of RPMI medium containing double the desired concentration of the drug was added and the plates were incubated for 72 hours. Respective controls were set: solvent control (DMSO) for the highest concentration of doxorubicin and no drug control. Based on the experiment, the cells were then subjected to alamarBlue assay (See 2.4.2) or annexin V-PI assay (see 2.4.1).

2.8.4 Carfilzomib

Carfilzomib was dissolved in DMSO as a 20 mM stock solution. One time useable aliquots of 5 µl were stored at -20°C. For every use a fresh predilution of 10 µM was prepared. The cells were seeded (20,000 cells per well) as mentioned above in 100 µl RPMI medium and 100 µl of RPMI medium containing double the desired concentration of carfilzomib was added. The solvent control (DMSO) and no drug controls were set accordingly. The alamarBlue assay (see 2.4.2) was performed after 72 hours of incubation.

2.8.5 Bortezomib

Bortezomib was stored as a 10 mM stock solution in DMSO as one time useable aliquots of 5 µl at -20°C. For every use fresh predilution of concentration 10 µM was made. Cells were seeded as mentioned above in 100 µl of RPMI medium and 100 µl of RPMI medium containing double the desired concentration of bortezomib was added. Respective solvent control (DMSO) and no drug control were set. AlamarBlue assay (see 2.4.2) was performed after 72 hours of incubation.

2.9 Construction of the CRISPR plasmid

Commercially available CRISPR/Cas 9 plasmid (the GeneArt® CRISPR nuclease vector) was purchased from ThermoFisher Scientific (Walham, USA), (Table 3.18). It contained all the essential components of the CRISPR/Cas9 system and CD4 expression cassette which could be used for purification of positively transfected cells with CD4 beads after the transfection. Only the target-specific guide RNA sequence had to be cloned into the GeneArt® CRISPR vector.

2.9.1 Oligonucleotide design and annealing

Suitable PAM sequences (NGG) were identified in Exon 2 and Exon 3 of the Cul4B gene according to the manufacturer's instruction. Multiple target sequences of 19-20 bp length adjacent to PAM sequences were selected and their homology was checked with other genes to reduce the danger of off-target effects. Two target sequences with no significant homology with other genes were finally selected. A 3' overhang (GTTTT) on the top strand oligonucleotides and a 5' overhangs (CGGTG) on the bottom strand oligonucleotides were added as the GeneArt® CRISPR vector had complementary overhangs for cloning. Two pairs of oligonucleotides Cul4b-B-F/R and Cul4b-D-F/R (Table 3.19) with respective overhangs were ordered from Sigma-Aldrich (Steinheim, Germany). The oligonucleotides were dissolved in nuclease-free water to the final concentration of 200 µM. Next, they were mixed with the annealing buffer and heated at 98°C for 4 minutes and cooled down to room temperature for 10-15 minutes to make the stock solution of 50 µM annealed oligonucleotides.

Table 2.1: Components of oligonucleotide annealing reaction

Item	Volume (µl)
Forward Primer (200 µM)	2.5
Reverse Primer (200 µM)	2.5
10x oligonucleotide annealing buffer	1
Nuclease free water	4

Annealed double stranded (ds) oligonucleotides (50 µM) were diluted 1:100 as following to make the stock solution of 500 nM.

Table 2.2: Components for dilution to 500 nM oligonucleotide stock

Item	Volume (µl)
50 µM ds oligonucleotide stock	1
10x oligonucleotide annealing buffer	10
Nuclease free water	89

The ds oligonucleotide stock was further diluted 1:100 as following to make the working solution of 5 nM.

Table 2.3: Components for dilution to 5 nM oligonucleotide stock

Item	Volume (µl)
500 nM ds oligonucleotide stock	1
10x oligonucleotide annealing buffer	10
Nuclease free water	89
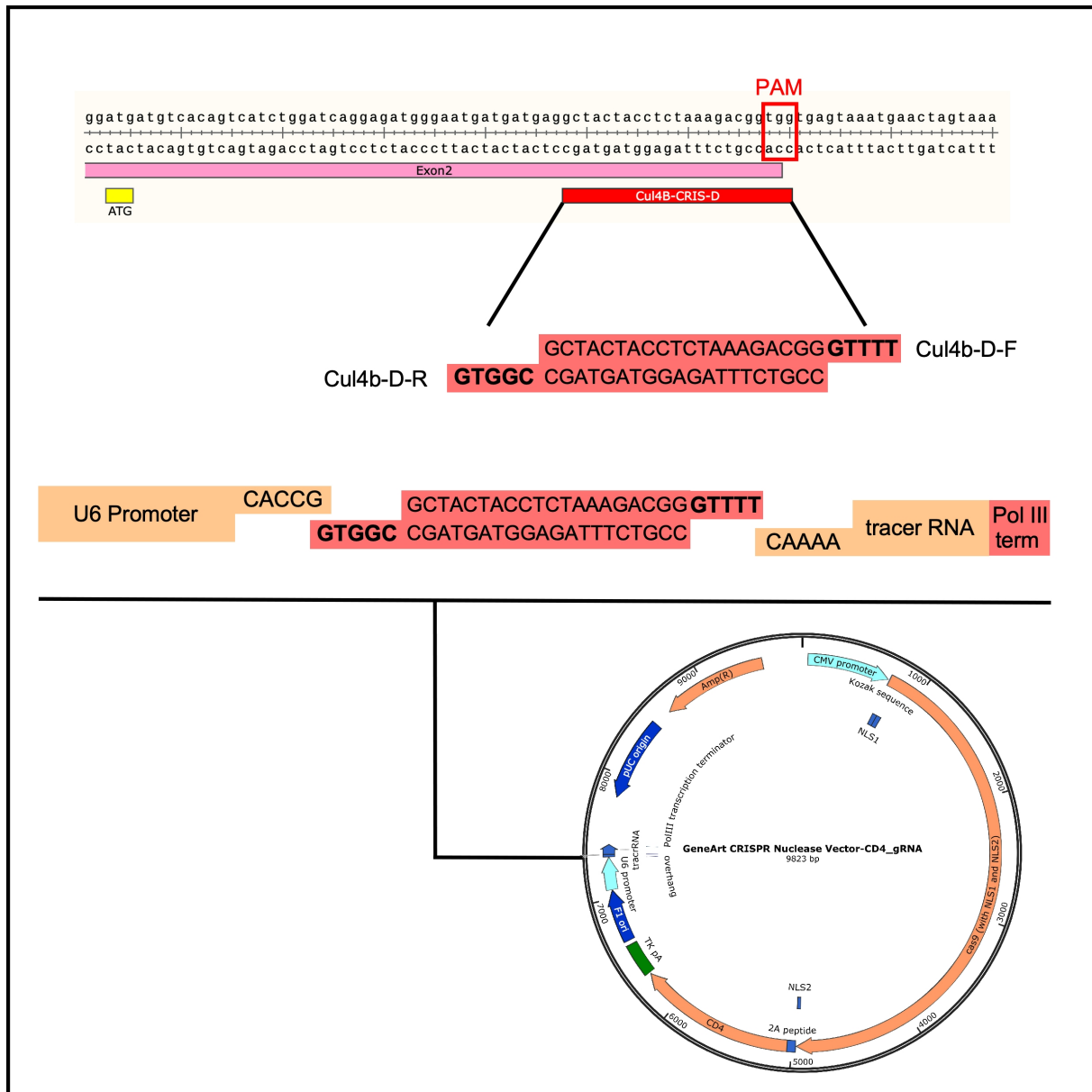
Figure 2.1: Assembly of Cul4B specific CRISPR vector. First the PAM sequence near the end of Exon 2 was identified and 20bp nucleotides adjacent to the PAM sequence were selected as target sequence and were ordered as oligonucleotides with required overhangs for subsequent cloning. Second, the annealed oligos were cloned into the GeneArt® CRISPR Nuclease Vector.

2.9.2   Cloning into the GeneArt® CRISPR vector

The annealed oligonucleotides (5 nM) were cloned into GeneArt® CRISPR vector as follows.

Table 2.4: Components of the ligation reaction with the GeneArt® CRISPR vector

Item	Volume (µl)
5x ligation buffer	4
ds oligonucleotides (5 nM)	2
GeneArt® CRISPR vector	2
T4 DNA ligase	1
Nuclease free water	11

Ligation reaction was mixed as mentioned above and incubated at room temperature for 15 minutes before 2 µl of the ligation mixture was transformed into chemically competent E.*coli* cells (Mix & go E.*coli* Zymo Research). The plates were incubated at 37°C overnight. The next day, plates were checked for colonies and in total 3-4 colonies were picked to set overnight cultures in 3 ml LB medium (containing 100 µg/ml Ampicillin) for DNA mini preparations. On the following day, plasmids were isolated and sent for Sanger sequencing with U6 primer (Table 3.19). The clones that contained the insert without any wrong bases (errors in nucleotides synthesis) as confirmed from sequencing were later grown from the original colony for midi preparations of plasmid DNA.

2.9.3   Generation of the single-cell clones

AMO1 and L363 cells were electroporated with the GeneArt® CRISPR vector containing the respective target sequence (Oligo B or Oligo D) (see 2.2). On the next day, the electroporation efficiency was measured by measuring the EGFP expression (plasmid was co-transfected) using FACS (see 2.4.1). Positively transfected cells were purified with CD4 microbeads (see 2.6) followed by a OptiPrep clean-up (see 2.3) to remove the dead cells. Single transfected healthy alive cells were picked with the help of an in-house tool, that consists of finely drawn out tips of the Pasteur pipette attached to some tubing and small filters (as shown in Figure 2.2). A 96 well plate with 100 µl RPMI medium in each well (except for the rim which was filled with PBS) and electroporated cells were equilibrated at room temperature for some time before starting the single-cell picking. As the EGFP plasmid was co-transfected with the GeneArt® CRISPR vector, it was possible to locate healthy-looking strongly transfected cells under the fluorescent microscope as these green cells would have probably also received a good amount of the GeneArt® CRISPR vector. Filling of the glass tip worked by capillary action and the single cells were released in each well very carefully by slow expulsion with mouth pressure. With some practice one could neatly position one cell in the bottom of the well and easily pick up surplus cells or debris out of the same well. All the wells were closely monitored in the next days to look for the clonal growth from a single location. In the case of multiple growth zones, extra cells were removed to ensure the expansion from one single cell. Cells were allowed to grow in the 96 well plate and subsequently were transferred to a bigger plate as soon as the cell number exceeded the capacity of the well.
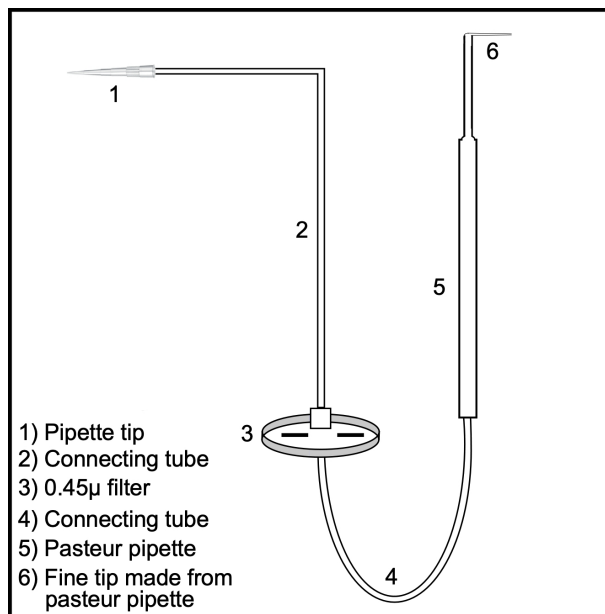
Figure 2.2: Self-made device for picking single cells.

2.9.4 Screening for knockout clones

During this expansion, when the cells had grown sufficient in number, their CUL4B protein level was analysed by Western blotting. Those clones that showed a protein knock out were selected for further expansion and stored as frozen cultures in liquid nitrogen.

Freezing cells

Cells were centrifuged, resuspended in the freezing medium (90% FBS and 10% DMSO), 5 million cells per ml were stored per cryotube. Cells were initially stored at -80°C in cryoboxes for 1-2 days and then were transferred into the vapor phase of liquid nitrogen tanks for long term storage.

Isolation of genomic DNA

For genomic DNA isolation 1-2 million cells were pelleted at 300 x g, washed with PBS, resuspended in 0.5 ml of cell lysis buffer (Table 3.9) and incubated at 60°C for 5 minutes. Proteinase K (2.5 µl) and RNase (2.5 µl) were added, mixed and incubated at 60°C for 45 more minutes. To precipitate the proteins 250 µl of 5 M NaCl was added and the tubes were placed on ice for 5 minutes before centrifugation at 9300 x g for 15 minutes. The supernatant was transferred to a fresh tube. An equal volume of isopropanol was added to precipitate the DNA. Tubes were centrifuged at 9300 x g for 10 minutes. The supernatant was discarded and the DNA pellet was washed with 1.2 ml of 70% cold ethanol. Pellet was air-dried and resuspended in a suitable volume of nuclease-free water. Last, the concentration of the isolated gDNA was determined with a NanoDrop spectrophotometer (ThermoFisher SCIENTIFIC).

TA cloning

Genomic DNA was used as a template for the polymerase chain reaction (PCR). Forward and reverse primers (CUL4b-int-F and CUL4b-int-R) were used to flank the respective target sequence in exons/introns of *Cul4b*. The PCR product was run on 1% agarose gel, cut and eluted with the PCR gel clean kit (MACHEREY-NAGEL) (Table 3.2). The elution was done with nuclease-free water. The DNA was quantified in eluted samples and was cloned into the pGEM®-T Easy vector (see Table 3.18).

Table 2.5: Components of the ligation reaction with the pGEM®-T Easy Vector

Item	Volume (µl)
10x ligation buffer	2
Eluted PCR product	1-4
pGEM®-T Easy Vector	1
T4 DNA ligase	1
Nuclease free water	upto 20

The ligation mixture was left at room temperature for 20 minutes followed by the transformation in competent E.*coli* cells.

Colony PCR

The colony PCR was performed to screen individual colonies seen on the plates next day, using T7-5' and SP6-3' primers (Table 3.19). The master mix for the colony PCR was prepared by mixing the following reagents and the colonies were picked from the plate with sterile toothpicks and transferred to the respective PCR tubes.

Table 2.6: Master mix for the colony PCR

Reagent	Volume (µl)
10x DreamTaq buffer	2.5
dNTP-Mix (2.5mM each dNTP)	0.5
T7-5' (10 µM)	1
SP6-3' (10 µM)	1
Dream Taq (5 u/µl)	0.1
Nuclease free water	20

The following program was run on the thermocycler for the colony PCR.

Table 2.7: Thermocycler conditions for the colony PCR

		Temperature°C	Time (min)
1X	Initial denaturation	94	4
	Denaturation	94	0.5
30X	Annealing	55	0.5
	Elongation	72	1

Positive colonies showing a band on the expected size in the agarose gel electrophoresis were picked again for DNA mini preparations and grown in 3 ml LB medium (containing 100 µg/ml ampicillin). Plasmids were isolated next day and samples were sent for Sanger sequencing with the T7-5' primer to LGC Genomics, Berlin according to the company requirements.

2.10   Construction of double cassette expression vector

To emulate the mutation first scenario in which one mutant and one wild type allele of *TP53* are expressed in the cell, a special vector to express two genes simultaneously on equal level was needed. To do so a pT2 sleeping beauty expression vector (pT2-SB) was modified in a way that it contains two independent but identical expression cassettes (with exception of a few nucleotides in the multiple cloning site (MCS)). A modified sleeping beauty vector (pT2-SB) that contained two pairs of the addressable restriction sites in the MCS; NheI / NotI and BsrGI / AgeI was used to construct double cassette expression vector as following.

2.10.1   Restriction reaction

In the first step, two derivatives of the pT2-SB were made, each one having only one pair of the restriction sites in the MCS. Sleeping beauty vector containing NheI / NotI as addressable cloning sites named pT2-N/N, and BsrGI / AgeI as addressable cloning sites named pT2-B/A. First of all pT2-SB vector was cut out with restriction enzyme NheI and NotI as mentioned below.

Table 2.8: Components of the restriction reaction

Reagent	Volume (µl)
10x Fast digest buffer	5
Vector (pT2-SB)	1µg
FD NheI	1
FD NotI	1
Nuclease free water	upto 50 µl

The restriction reaction mixture was incubated at 37°C for 30 minutes and 1 µl of Shrimp alkaline phosphatase (SAP) was added in the same tube and incubated for another 30 minutes. The reaction was heat inactivated at 80°C for 20 minutes and the DNA was precipitated by adding 2.5 vol of absolute EtOH

and 0.1 vol of 3 M sodium acetate, mixing and centrifuging at maximum speed. The DNA pellet was air dried after complete removal of ethanol and resuspended in nuclease free water. The concentration of the cut, dephosphorylated vector was determined by NanoDrop.

2.10.2 Oligonucleotide annealing and phosphorylation

Two sets of oligonucleotides were designed, set one called Pt2-NheNot-F/R and set two called Pt2-BsrAge-F/R (Table 3.19). Set one was designed to destroy the NheI and NotI sites in the MCS of the vector pT2-SB and set two of oligonucleotides was designed to remove the BsrGI and AgeI sites from the MCS of the same vector. All oligonucleotides were ordered from Sigma-Aldrich, dissolved in nuclease free water to have the final concentration 100 µM. Oligonucleotides annealing was performed in the following way.

Table 2.9: Components of the oligonucleotide annealing

Reagent	Volume (µl)
Forward oligonucleotide (100 µM)	1.5
Reverse oligonucleotide (100 µM)	1.5
1x oligo annealing buffer	47

The tubes were placed in the thermocycler and the following program was run.

Table 2.10: Thermocycler condition for the oligonucleotide annealing

Temperature°C	Time (min)
95	4
85	3
80	3
75	5
72	5
68	5

Double stranded oligonucleotides were kept at room temperature after annealing and then phosphorylated as following.

Table 2.11: Phosphorylation of the double stranded oligonucleotides

Reagent	Volume (µl)
ds Oligonucleotide	1
10x T4 PNK buffer	1
ATP (10 mM)	1
T4 PNK	0.5
Nuclease free water	upto 10 µl

The reaction was incubated at 37°C for 30 minutes followed by a heat inactivation at 70°C for 30 minutes. These phosphorylated ds oligonucleotides were used for ligation right away or stored at -20°C for later usage.

2.10.3 Ligation reaction

Ligation reactions were set in 1:3 molecular ratio of the vector and insert. Ligation reaction was set in the following way.

Table 2.12: Components of the ligation reaction

Reagent	Volume (µl)
ds phosporylated oligonucleotide	1
10x T4 DNA ligase buffer	1
Vector	50 ng
T4 DNA ligase	1
Nuclease free water	upto 10 µl

The ligation mixture was incubated at room temperature for 20 minutes. For transformation in competent E.*coli* cells, 1 µl of the ligation mixture was used and the plates were incubated overnight at 37°C.

2.10.4 Confirmation of positive clones

On the next day, the colonies seen on the plates were used to set up an overnight culture for DNA mini preparation. Plasmid DNA was isolated on the following day and was cut with the respective enzymes to confirm the positive cloning. Later, potential positive plasmids, indicated by the restriction reaction were sent for Sanger sequencing to confirm the correct cloning product.

2.10.5 PCR amplification of the expression cassette

Vector pT2-N/N was used as a template to amplify one expression cassette. Primers were designed to introduce a flanking BstX1 site on both sides of the expression cassette to be amplified (Figure 2.3). The PCR was set with the primers Pt2-BstX1-F/R (Table 3.19) using Q5 polymerase. A PCR product of 858 bp was seen, cut from agarose gel and was subjected to restriction reaction with BstX1 enzyme. Cut PCR product was cleaned with the PCR and gel clean kit and stored at -20°C for further cloning.

2.10.6 Subcloning into pSUSTER2

The amplified, cut expression cassette was initially subcloned in another smaller vector (pSUSTER2), which was cut with BstX1 following a regular restriction reaction and ligation protocol. Positive clones were confirmed via Sanger sequencing before further use.

2.10.7 Cloning into pT2-B/A

The pSUSTER2 vector containing the expression cassette was cut with BstX1, the released insert was cut from agarose gel and cleaned up with the PCR and gel clean kit. This single cassette insert was cloned into pT2-B/A vector which was already cut with BstX1 and dephosporylated. Since both of the expression cassettes were almost identical (except few bases in the MCS) it was complicated to screen for the clones containing both expression cassettes in the correct orientation by colony PCR. The CMV-5' primer which had binding site in both expression cassettes and PT2-3' primer which had one binding site down stream but outside the second expression cassette were used in the colony PCR (see Section 2.9.4). The clone with head to tail orientation of both cassettes was supposed to give two PCR products, one at 400bp and second at 1600bp in size. Negative clones or clones with tail to tail orientation were supposed to give only a 400bp band. The final expression vector with two expression cassettes was named pT2-DC (pT2-double cassette).
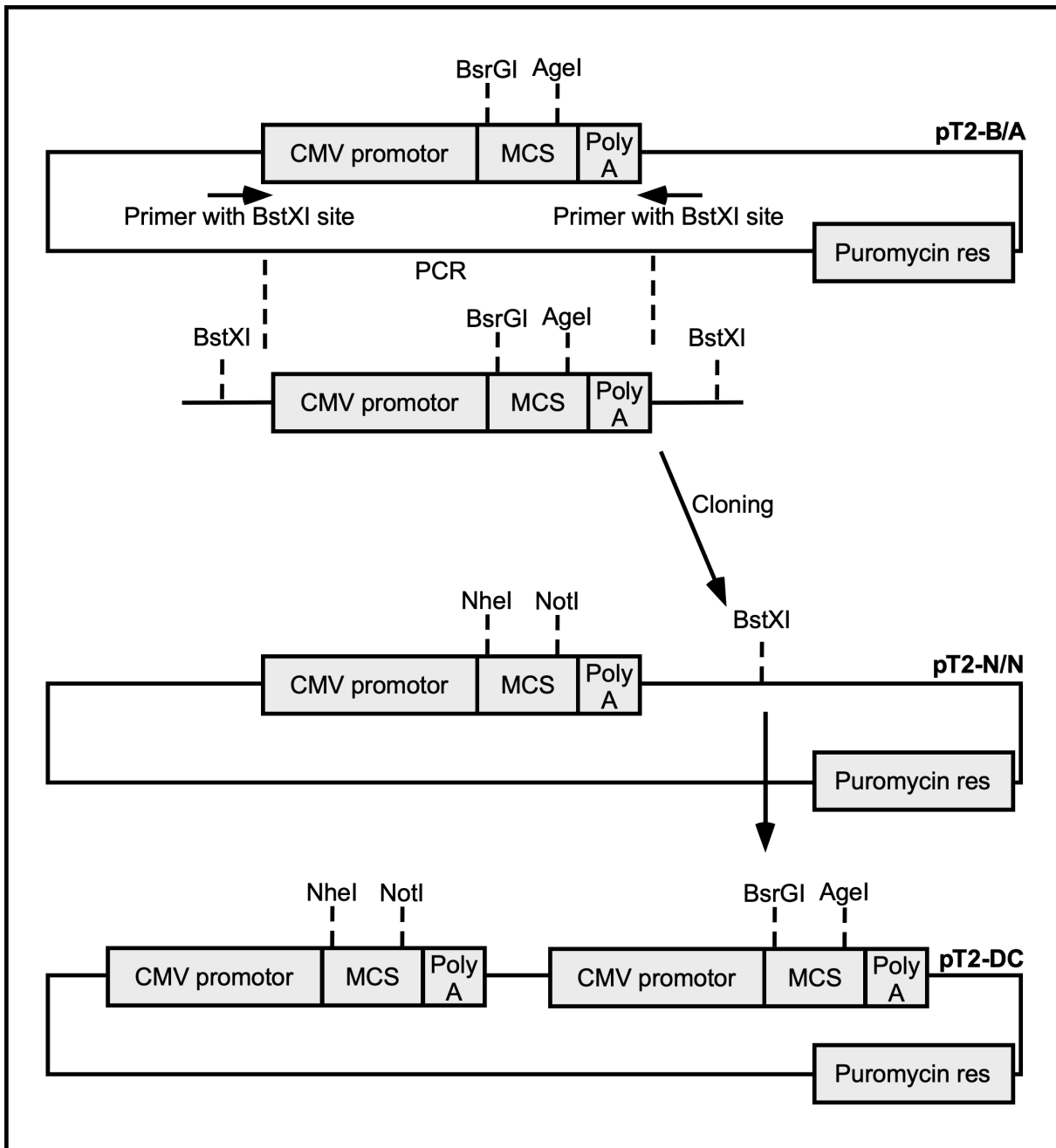
Figure 2.3: Cloning strategy for generation of two cassette mRNA/protein expression vector

2.11   Construction of p53 expression vectors

To construct a p53 expression vector, wt *TP53* was PCR amplified from cDNA of AMO1 cells, subcloned into the pBluescript vector and eventually cloned into the respective SB expression vector as described below.

2.11.1   wt *TP53* amplification

AMO1 cells were taken because they have wildtype *TP53* and a functional p53 system what is not the case for many other MM cell lines. For RNA isolation 0.5-1 million cells were pelleted and RNA was

isolated using the RNA isolation kit (Qiagen) (Table 3.2) according to the instructional manual.

cDNA preparation

Isolated RNA was used for the cDNA synthesis using the RevertAid Reverse transcriptase (Table 3.4) as following.

Reagent	Quantity
Template RNA	100 ng
Oligo(dT) (100 pM)	0.5 µg
Nuclease free water	upto 12.5 µl

The above mentioned reagents were mixed gently, incubated at 65°C for 5 minutes and then placed on ice. Following components were added in same tube in the indicated order.

Table 2.13: Components for the cDNA preparation

Reagent	Volume(µl)
5x Reaction buffer	4
RiboLock RNase Inhibitor	0.5
dNTP mix (10 mM)	2
RevertAid Reverse Transcriptase	1

The reaction mixture was incubated in the thermocycler at 42°C for 60 minutes. The reaction was terminated by heating at 70°C for 10 minutes and the cDNA was stored at -20°C for further usage.

PCR

This cDNA was used as a template for amplification of the wt *TP53* cDNA. Two primer sets were designed to amplify wt *TP53* cDNA, each primer set introducing a pair of restriction sites flanking the coding sequence of p53. Primer set 1 (p53-NheNot-F/R) was designed to introduce the NheI site on 5' of the coding sequence and NotI site on the 3' end, whereas primer set 2 (p53-BsrAge-F/R) to introduce BsrGI site on the 5' and AgeI site on the 3' end (Table 3.19). PCR was set up using the Q5 polymerase to avoid mistakes in the PCR amplification as Q5 polymerase has high fidelity. PCR was set up as following.

Table 2.14: Components of the PCR for amplification of *TP53* cDNA

Reagent	Volume (µl)
5x Q5 reaction buffer	10
dNTP-Mix (10 mM)	1
Forward Primer (10 µM)	2.5
Reverse Primer (10 µM)	2.5
Q5 DNA Polymerase (5 u/µl)	0.5
Template cDNA	1
5x Q5 GC Enhancer	10
Nuclease free water	upto 50

As these primers contain long overhangs to introduce new restriction sites on either side of the *TP53* cDNA, two step PCR was performed. In the first step, four cycles on the lower annealing temperature were set to promote the binding of the primers, and in second step, higher annealing temperature was used for the further amplification to reduce the unspecific amplification of the PCR product (Table 2.15)

Table 2.15: Thermocycler conditions for amplification of the *TP53* cDNA

		Temperature°C	Time (min)
1X	Initial denaturation	98	2
	Denaturation	98	0.5
4X	Annealing	52	0.5
	Extension	72	1.5
	Denaturation	98	0.5
30X	Annealing	65	0.5
	Extension	72	1.5
1X	Final extension	72	3

The PCR product was run on 1% agarose gel and PCR band of 1.5kb was cut from the gel and purified with the PCR and gel clean kit (Table 3.2).

Cloning into pBluscript vector

Cleaned-up PCR products were subjected to the restriction reaction with a pair of respective enzymes, NheI/NotI or BsrGI/AgeI and after restriction both variants of wt *TP53* cDNA were separately cloned in the modified pBluescript vector containing the respective pair of restriction enzymes (NheI/NotI or BsrGI/AgeI). In this way, two pBluescript vectors were prepared (pBS-p53^wt) containing wt *TP53* cDNA which could further be cloned in any other vector, using different sets of restriction enzymes.

2.11.2   Site-directed mutagenesis

The Agilent QuikChange Site-Directed Mutageneis Kit (Table 3.18) was used to introduce the point mutations in the wt *TP53* cDNA. Two primer sets were designed to introduce two different point mutations in the wt *TP53* cDNA. Set 1 (p53-R282W-F/R) for R282W and set 2 (p53-R175H-F/R) for R175H mutation (Table 3.19). Reagents for site-directed mutagenesis PCR were mixed and a proofreading *Pfu* DNA polymerase was used.

Table 2.16: Components of the site-directed mutagenesis PCR

Reagent	Volume (µl)
10x *Pfu* reaction buffer	3
dNTP-Mix (10 mM)	1
Forward Primer (10 µM)	2.5
Reverse Primer (10 µM)	2.5
Pfu DNA polymerase	1
Template Plasmid	10 ng
Nuclease free water	upto 30

The following PCR program was used on the thermocycler

Table 2.17: Thermocycler conditions for the site-directed mutagenesis PCR

		Temperature°C	Time (min)
1X	Initial denaturation	95	2
	Denaturation	95	0.5
16X	Annealing	55	1
	Extension	68	4.5

Right after the completion of the PCR, tubes were cooled down to the room temperature. The reaction mixture was incubated with 1 µl of DpnI at 37°C for 60 minutes and 2 µl was used for transformation in competent E.*coli* cells. Next day, the colonies were picked to set up miniprep cultures. On the following day the minipreps were sequenced to confirm the point mutations and final pBluescript vectors were named as pBS-p53^{282W} and pBS-p53^{175H}.

2.12   p53 expression vectors

In the first step wt *TP53* cDNA was subcloned into one cassette of pT2-DC using NheI/NotI restriction enzymes. The resulting vector was used for the subsequent cloning of another wt *TP53* cDNA or either of the mutant *TP53* cDNA into the second expression cassette with BsrGI/AgeI restriction enzymes. The resulting vectors express p53$^{wt/wt}$, p53$^{wt/R282W}$ or p53$^{wt/R175H}$. Single cassette expression vectors expressing only one copy of p53^{wt}, p53^{R282W} and p53^{R175H} were also prepared.

2.13   Clonal Competition Assay (CCA)

To study the long-term impact of mutations or genomic alterations on overall fitness of the cell, the CCA was designed.

2.13.1   Color coding of cell lines

SB vectors for the stable expression of EGFP or mKate/RFP were designed and prepared by MD student Nicole Müller. AMO1 cells, L363 cells and further clones to be analysed for their fitness advantage were stably transfected with either colour expressing plasmids under G418(neomycin) selection. These colour coded cells were expanded like a normal cell line and stored in liquid nitrogen as stock bank. These cells were grown under normal cell culture conditions (Section 2.1) and were subjected to the second transfection with the sleeping beauty vectors expressing variants of the *TP53* cDNA or *CUL4B* cDNA and were selected with puromycin. These double selected cells were used for setting up co-culture experiments.

2.13.2   Setting up co-cultures

Based on the experiment, cells were counted and mixed in a specific ratio, 1:10 or 1:3. In total two million cells were seeded in a T75 culture flask and were kept in the presence or absence of external drug exposure. Each approach was set up in triplicate. The cell culture was regularly split under normal culture condition and final concentrations of the drugs were kept on same concentration throughout the whole duration of the experiment. Every 4-5 days, a sample of the culture was taken out, washed and resuspended in 1x PBS for FACS analysis. The relative ratio of culture under study were measured with FlowJo.

Chapter 3

Materials

Table 3.1: Ingredients of the cell culture medium

Name	Manufacturer	Art. No
RPMI-1640	Sigma-Aldrich	R0883
FBS	Sigma-Aldrich	F7524
Pencillin/Streptomycin (1000 units Pen/ 10mg/ml Strep)	Sigma-Aldrich	P4333
L-Glutamine (200 mM)	Sigma-Aldrich	G7513
Sodium Pyruvate	Sigma-Aldrich	S8636

Table 3.2: Kits

Name	Manufacturer	Art. No
PCR and gel clean kit	MACHEREY-NAGEL	740609
Plasmid Midi Prep Kit	MACHEREY-NAGEL	740410
RNeasy Mini Kit	Qiagen	74104
Plasmid miniprep	Analytikjena	845-KS-5040500
MACSelect 4 MicroBeads	Miltenyi Biotec	130-070-101

Table 3.3: Machines

Name	Manufacturer
FACS Calibur	BD Biosciences, Heidelberg
Gene Pulser XCell	Bio-Rad Laboratories, Munich
Model 680 Microplate Reader	Bio-Rad Laboratories, Munich
NanoDrop 2000, spectrophotometer	ThermoFisher SCIENTIFIC, Dreieich
PowerPac Basic™ Power Supply	Bio-Rad Laboratories, Munich
Primus 25 advanced® Thermocycler	PEQLAB Biotechnologie, Erlangen
UP50H-Homogenisator	Hielscher Ultrasonics, Teltow
Western Blot Apparatur Mini-PROTEAN® 3-Cell	Bio-Rad Laboratories, Munich

Table 3.4: Enzymes

Name	Manufacturer	Art. No
Dream Taq Polymerase	ThermoFisher SCIENTIFIC	EP0703
Q5 DNA Polymerase	New England Biolabs	M0491
Pfu DNA Polymerase	ThermoFisher SCIENTIFIC	EP0572
T4 DNA Ligase	Fermentas	EL0011
Proteinase K	Fermentas	EO0491
RNase A	Fermentas	EN0531
Fast Digest NheI	ThermoFisher SCIENTIFIC	FD0974
Fast Digest NotI	ThermoFisher SCIENTIFIC	FD0594
Fast Digest BsrGI	ThermoFisher SCIENTIFIC	FD0933
Fast Digest AgeI	ThermoFisher SCIENTIFIC	ER1461
Fast Digest BstXI	ThermoFisher SCIENTIFIC	FD1024
Fast AP	ThermoFisher SCIENTIFIC	EF0651

Table 3.5: Annexin V-PI buffer

	Components	Quantity
	HEPES	10 mM
	NaCl	140 mM
Annexin-V/FITC binding buffer (pH 7.4)	CaCl$_2$	2.5 mM
	VE-Water	upto 100 ml

Table 3.6: Transfer buffer

	Components	Quantity
	Methanol	400 ml
	Glycin	28.8 ml
Transfer buffer	Tris-Base	6 g
	VE-Water	2 L

Table 3.7: Laemmli buffer

	Components	Quantity
	20% SDS	5 ml
	Glycerin	5 ml
	Tris-Base	3 ml
Laemmli buffer	β-Mercaptoethanol	5 ml
	Bromophenol blue	Small pinch
	VE-Water	upto 50 ml

Table 3.8: Lysis buffer

	Components	Quantity
	EDTA	5 mM
	NaCl	200 mM
Lysis buffer (pH 8.5)	Tris-Base	10 mM
	SDS	0.2%
	VE-Water	upto 50 ml

Table 3.9: Lysis buffer for gDNA isolation

	Components	Quantity
	Tris-Base	10 mM
	EDTA	5 mM
Lysis buffer for gDNA isolation (pH 8.5)	NaCl	200 mM
	SDS	0.2%

Table 3.10: Ponceau S Red

	Components	Quantity
	Ponceau S	0.1%
Ponceau-S red	Acetic Acid	5%
	VE-Water	Upto 100 ml

Table 3.11: PBS

	Components	Quantity
	KCl	0.2 g
	NaCl	8 g
PBS (pH 7.4)	$Na_2HPO_4.2H_2O$	1.75g
	KH_2PO_4	0.27 g
	VE-Water	upto 1 L

Table 3.12: TAE buffer

	Components	Quantity
	Tris-Base	2 M
	EDTA	10 mM
50X TAE buffer (pH 8.5)	Acetic acid	57.1 ml
	VE-Water	upto 1 L

Table 3.13: TBS

	Components	Quantity
	Tris-Base	20 mM
10X TBS Washing buffer (pH 7.6)	NaCl	136 mM
	VE-Water	upto 1 L

Table 3.14: TGS buffer

	Components	Quantity
	Tris-Base	60 g
	Glycin	284 g
10X TGS Running buffer	SDS	20 g
	VE-Water	upto 2 L

Table 3.15: ECL

	Components	Quantity
	Tris-Base	100 mM
	Luminol	2.5 mM
ECL (pH 8.8)	p-Coumaric acid	0.2 mM
	H_2O_2	3 mM

Table 3.16: Drugs

Drugs	Manufacturer	Art. No	Solvent	Stock Conc
Nutlin 3a	Selleckchem	S8059	DMSO	10 mM
Melphalan	Sigma-Aldrich	M2001	Acd. Ethanol	20 mM
Doxorubicin HCl	Calbiochem	324380	DMSO	10 mM
Carflizomib	Selleckchem	S2853	DMSO	10 mM
Bortezomib	Selleckchem	S1013	DMSO	5 mM

Table 3.17: Antibodies

Antibodies	Manufacturer	Art. No	Dilution
p53	Santa Cruz	sc-126	1:15000
MDM2	Santa Cruz	sc-965	1:1000
p21	Santa Cruz	sc-6246	1:10000
b-Actin	Sigma-Aldrich	A5316	1:10000
GAPDH	Sigma-Aldrich	G9545	1:10000
Cul4b	Cell Signalling	2699T	1:10000

Table 3.18: Commercial plasmids

Name	Manufacturer	Art. No
GeneArt® CRISPR Nuclease Vector	ThermoFisher SCIENTIFIC	A21175
pGEM®-T Easy Vector	Promega	A1360

Table 3.19: Primers

Primers	Sequence (5' > 3')
p53-NheNot-F	GGTC**GCTAGC**ATGGAGGAGCCGCAGTCAGA
p53-NheNot-R	AAGT**GCGGCCGC**TCAGTCTGAGTCAGGCCCTT
p53-BsrAge-F	GGTC**TGTACA**ATGGAGGAGCCGCAGTCAGA
p53-BsrAge-R	CACC**ACCGGT**TCAGTCTGAGTCAGGCCCTTC
Pt2-NheNot-F	CTAGCAGTTACAGACACGTGGAACGGTGAGTATACGTGC
Pt2-NheNot-R	GGCCGCACGTATACTCACCGTTCCACGTGTCTGTAACTG
Pt2-BsrAge-F	CTAGGAGTGTACAGACACGTGGAACCGGTGAGTATACGTCC
Pt2-BsrAge-R	GGCCGGACGTATACTCACCGGTTCCACGTGTCTGTACACTC
Pt2-BstX1-F	TCATA**CCACAGCTCTGG**AGTTCCGCGTTACATAACTT
Pt2-BstX1-R	TAGAAC**CCAGAGCTCTGG**CAATTCAGATACATTGAT
p53-R282W-F	CTGTCCTGGGAGAGAC**T**GGCGCACAGAGGAAGA
p53-R282W-R	TCTTCCTCTGTGCGCC**A**GTCTCTCCCAGGACAG
p53-R175H-F	GGAGGTTGTGAGGC**A**CTGCCCCCACCATG
p53-R175H-R	CATGGTGGGGGCAG**T**GCCTCACAACCTCC
p53-int-F	CCTGCCCTCAACAAGATGTTTTGCC
p53-int-R	TGGGGAGAGGAGCTGGTGTTGTTGG
U6	GGACTATCATATGCTTACCG
SP6	ATTTAGGTGACACTATAG
Pt2-MCS-R	CAACAACAATTGCATTCA
Cul4b-B-F	GCTTCTTCTGTATCGGTACGGTTTT
Cul4b-B-R	CGTACCGATACAGAAGAAGCCGGTG
Cul4b-D-F	GCTACTACCTCTAAAGACGGGTTTT
Cul4b-D-R	CCGTCTTTAGAGGTAGTAGCCGGTG
Cul4b-int-F	TGCTCCTCTGCCTGTTGACC
Cul4b-int-R	GATCACTAACTTCTTAGCAG

Table 3.20: Chemicals

Chemical	Company	Art Number
Ampicillin	Sigma-Aldrich	A9518
Agarose	Sigma-Aldrich	5210.3
APS	Roth	9592
Acrylamide/Bis-Acrylamide	Roth	3029.1
Bromophenolblue	Sigma-Aldrich	B5525
Calcium Chloride	Merck	2382
DMSO	Roth	A994
Disodiumhydrogenphosphate	Roth	T877.1
EDTA	Roth	ED255
Acetic Acid	Baker	6052
Ethanol 96%	Roth	T171.4
G418(Neomycin)	PAA	P25-011
D-Glucose	Roth	X997.1
Glycerin	Merck	104092
Glycin	Roth	3908.3
HD-Green	Intas	ISII-HDGreen Plus
HCl	Merck	100317
Hydrogenperoxide	Roth	9683
Isopropanol	Merck	100979
Luminol	Sigma-Aldrich	A8511
LB-Medium	Roth	X968002
β-Merceptoethanol	Roth	4227.1
Methanol	Sigma-Aldrich	32212
Nitrocellulose membrane	GR Healthcare	10600002
OptiPrep	Axis-Shield	LYS3782
P-Coumaric acid	Sigma-Aldrich	C9008
Ponceau-S	Applichem	A1405
Propidium Iodide	Sigma-Aldrich	P4170
Puromycin	Calbiochem	540222
di-Potassiumhydrogen phosphate	Merck	11.204
Potassium Chloride	Roth	6781.3
Resazurin Sodium (alamarBlue)	Sigma-Aldrich	R7017
SDS	Roth	2326.2

Chemical	Company	Art Number
Sodium Chloride	Sigma-Aldrich	30970
Di-Sodiumhydrogenphosphate	Sigma-Aldrich	S7907
TEMED	Roth	2367.3
Tris-Base	Roth	5229.2
TrypanBlue	Sigma-Aldrich	T6146
Tween 20	Roth	9127.1

Chapter 4

Results

4.1 Generation of mono- and biallelic deleted *TP53* clones in MM

A former MD student in our research group, Markus Roth designed 2 different guide RNA vectors to target two different exons of the human *TP53* gene. After electroporation with the CRISPR/Cas9 vector, single-cells were sorted manually and allowed to grow. The cultures grown from single-cell clones were tested for the functionality of the p53 system with the overnight treatment of Nutlin 3a followed by the genomic analysis of exact alterations produced by CRISPR/Cas9.

In current work, clones generated by Markus Roth were re-evaluated at molecular and functional level. In the first step, cultures grown from single-cells were treated overnight with MDM2 inhibitor, Nutlin 3a to evaluate the p53 system functionality via Western blot (WB), by analyzing the levels of p53, MDM2 and p21. Clones showing defective p53 function (based on WB analysis) were further analyzed to find the precise defects at the genomic level. PCR was performed with Taq DNA Polymerase using primers flanking the target sequence of the guide RNA (used in CRISPR/Cas9 vector) and PCR product was cloned into the pGEM®-T Easy vector via TA cloning. The cloned PCR products were Sanger sequenced to analyze the mono- and biallelic defects in *TP53* alleles. Four clones each with *TP53* +/- (single defected allele) and *TP53*-/- (both defected alleles) status were selected for further experiments.

In Figure 4.1 (A), lanes 1 and 2 represent the normal wt AMO1 culture, and lane 3 and 4 represent a wildtype culture grown from a single-cell (clone # 1). AMO1 and clone # 1 show a very low p53 level when treated with DMSO (solvent control for Nutlin 3a) as see in lanes 1 and 3, MDM2 and p21 are also low in protein level. Lane 2 and 4 show that overnight Nutlin 3a treatment increases p53 level in the AMO1 and clone # 1. This increase in p53 level is translated into the induction of the downstream targets of p53, MDM2 and p21. Similarly induced levels of proteins in AMO1 and clone # 1 show that the procedure of single-cell picking, and growth of cell culture from single-cell clone, did not alter the normal function of the p53 system.

Clone # 2 increased p53 level after Nutlin 3a treatment, but the increase was not as high as seen in the wildtype cultures, neither was that translated into equally high levels of MDM2 and p21 as shown in the lanes 5 and 6. Low level of p21, and MDM2 compared to AMO1 cells (lane 2) indicated a defected p53 system. Furthermore, a smaller sized p53 protein band was also seen in clone # 2. Sanger sequencing depicted that clone # 2 had one wt *TP53* allele (which gave correct band size in WB) and one defective allele of *TP53*. The defective allele had a deletion of 16bp, ensued a frameshift and generation of a smaller protein (estimated length 338 amino acids) (Figure 4.1 (B)). The smaller protein made from defective

allele was visible as a smaller band on WB.

Figure 4.1: Analysis of AMO1 clones with one allele of *TP53* deleted. (A) Characterization of p53 system functionality in p53 wt cells (AMO1 and clone # 1) and single-cell clones with one defective allele of *TP53*. Cells were treated overnight with MDM2 inhibitor Nutlin 3A (N) or applicable amount of solvent, DMSO (D) and analyzed for p53 system components by Western blotting. Staining with GAPDH served as a loading control. (B) Analysis of CRISPR/Cas9-generated *TP53* alterations in AMO1 clones. Genomic DNA was used to amplify PCR products covering the CRISPR target region. PCR products were cloned in the pGEM®-T Easy vector. Several plasmid minipreparations were made and sequenced. Representative parts of each type of read are shown to indicate the CRISPR-induced defects in respective AMO1 clones. The predicted protein changes are indicated on the right side.

Similar observations were made for clone # 3, there was not much induction of p53 or its downstream target (lane 7 and 8). Genomic sequencing (Figure 4.1 (B)) showed the presence of one wt *TP53* allele and one defective. The defective allele had a long deletion, which resulted in a relatively smaller size protein which was not clearly visible in WB.

Clone # 4 showed a higher steady state level of p53 in DMSO control (lane 9) and not proportionately

high induction of p53 after Nutlin 3a treatment (lane 10). A higher background level of p53 could be due to the inability of MDM2 to target mutant p53 for degradation. Sanger sequencing showed the insertion of 2 bp in one allele of *TP53*, whereas the frameshift resulted in the translation of slightly smaller size protein, which almost overlaps with the wt p53 band on WB. Almost near to zero induction was seen for downstream targets, i.e. MDM2 and p21.
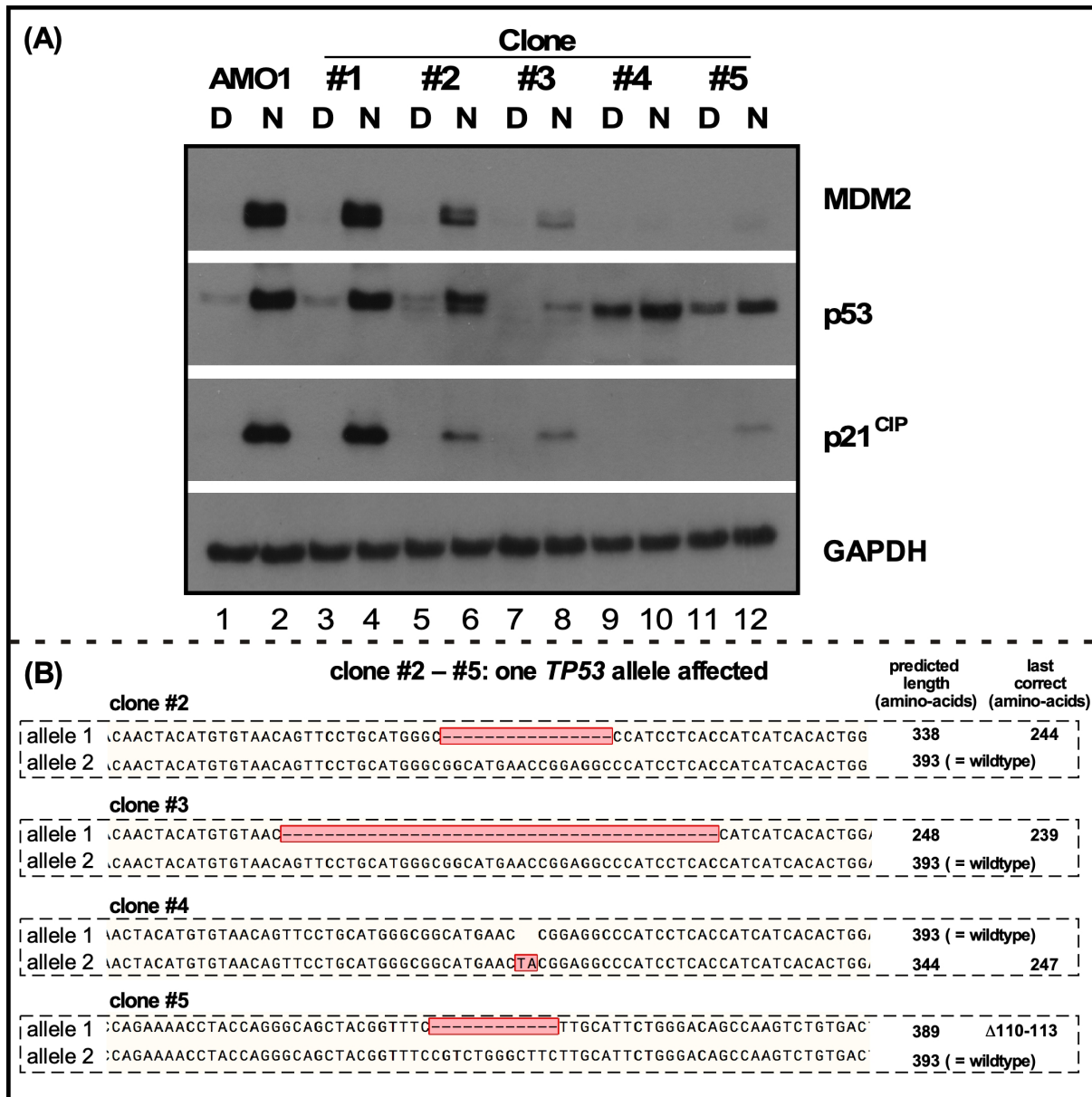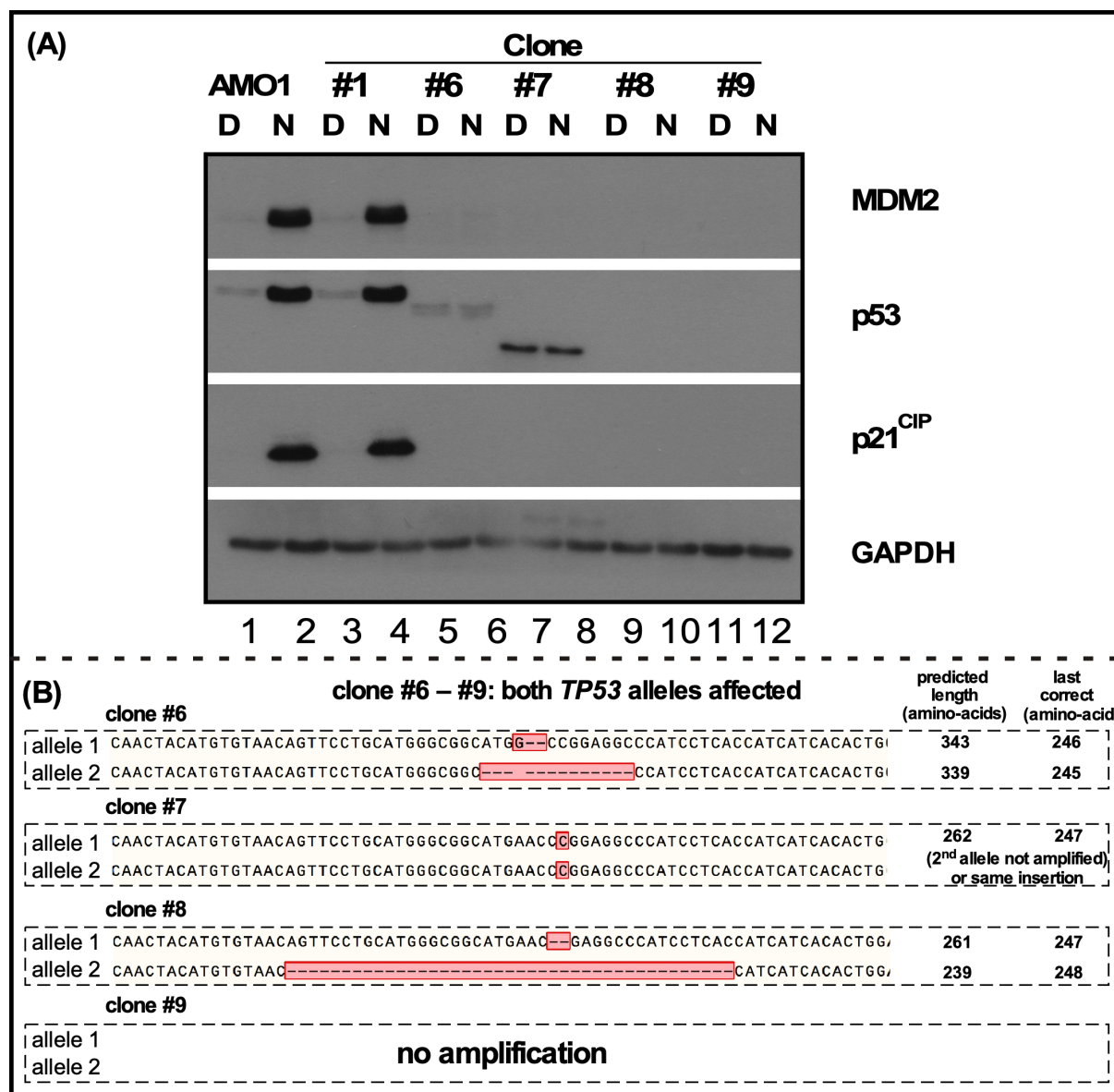

Figure 4.2: Analysis of AMO1 clones with both alleles of *TP53* deleted. (A) Characterisation of p53 system functionality in p53 wt cells (AMO1 and clone # 1) and single-cell clones with both defective allele of *TP53*. Cells were treated overnight with MDM2 inhibitor Nutlin 3A (N) or applicable amount of Solvent, DMSO (D) and analyzed for p53 system components by Western blotting. Staining with GAPDH served as loading control. (B) Analysis of CRISPR/Cas9-generated *TP53* alterations in AMO1 clones. Genomic DNA was used to amplify PCR products covering the CRISPR target region. PCR products were cloned in the pGEM®-T Easy vector. Several plasmid minipreparations were made and sequenced. Representative parts of each type of read are shown to indicate the CRISPR-induced defects in respective AMO1 clones. The predicted protein changes are indicated on the right side.

Similar results were seen in the case of clone # 5, where high background level and not enough

induction of p53 was seen. MDM2 and p21 were not induced either (lane 11 and 12 in Figure 4.1 (A)) and genomic analysis showed that it had an in-frame deletion of 12 bp in one *TP53* allele and other allele was wildtype (Figure 4.1 (B)).

Another set of 4 clones with biallelic disruption of *TP53* was analyzed. In Figure 4.2 (A) lane 1-4 represent wt AMO1 culture and wt culture grown from single-cell. Although a dim band of p53 (but lower than the original size) is seen in clone # 6, p53 level was not increased after overnight Nutlin treatment and MDM2 and p21 remained unchanged (lane 5 and 6). Sanger sequencing indicated the defects in both alleles of *TP53* (Figure 4.2 (B)).

For clone # 7, a smaller protein size predicted from the genomic analysis was seen as a smaller p53 band in lane 7 and 8 of Figure 4.2 (A). The insertion of a single nucleotide was seen in all reads (Figure 4.2 (B)). Either both the alleles had a similar insertion or the second allele was not amplified in the PCR, indicating that, defect/deletion produced by CRISPR/Cas9 was long enough that the primers used for PCR did not flank the whole region. In either case, this clone did not show a functional p53 system on WB.

In the case of clone # 8 and # 9, no expression of p53 was seen and signals from downstream targets MDM2 and p21 were not observed at all (Figure 4.2 (A)). As seen in Figure 4.2 (B), both alleles of *TP53* were affected in clone # 8. For clone # 9, there was no PCR amplification from genomic DNA, possibly due to the big deletions in both alleles. Therefore, based on the MDM2 and p21 signals, the p53 system was completely defected in clones # 6-9. Furthermore, genomic analysis confirmed the CRISPR/Cas9-mediated disruption of both alleles of *TP53* in these clones.

4.2 Analysis of p53 system functionality of AMO1 clones with mono- and biallelic *TP53* lesions

As Nutlin 3a treatment increases the p53 levels in the cells by blocking the binding of MDM2 to p53 and its subsequent degradation, accumulating higher levels of p53 results in apoptosis of *TP53* wt cells. AMO1 cells and clone #1 (*TP53+/+*) both showed sensitivity to the increasing concentration of Nutlin 3a. Both cultures showed almost no survival at a concentration of 7.5 µM and higher. In contrast, clones # 2-5, which harbor one wt copy of *TP53* and one CRISPR/Cas9 generated disrupted copy, showed variability in the response towards Nutlin 3a treatment. But in these clones, survival response was barely affected after treatment with MDM2 inhibitor Nutlin 3a when compared to the parental AMO1 cells (Figure 4.3 (A)). Although tested *TP53* hemizygous clones do have a wt *TP53* allele, but they possibly do not get enough contribution in the wt p53 level, to be translated into sensitivity towards Nutlin treatment.

TP53-/- clones were treated with three high concentrations of Nutlin 3a: 10, 15 and 20 µM and they showed no decline in cell survival. Clones # 6-9 showed complete resistance to the highest concentration of Nutlin 3a used in the experiment (Figure 4.3 (B)). As both alleles of *TP53* were defective in these clones, they did not produce any functional p53 in cells which could induce apoptosis after Nutlin 3a treatment. The absence of p53 in Western blot, and no increase of p53 seen after Nutlin treatment

overnight (Figure 4.2 (A) resulted into complete resistance against Nutlin 3a over a longer period of time (72 hours).
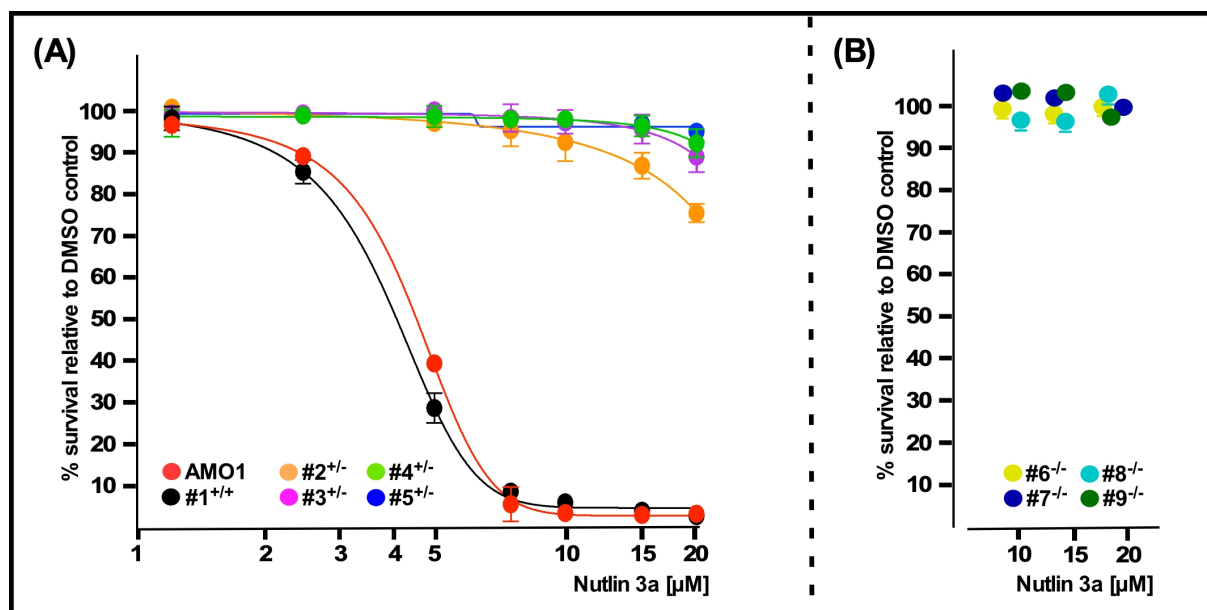
Figure 4.3: Dose response curves of AMO1 clones (*TP53+/+*, *TP53+/−* and *TP53−/−*) after 3 days treatment with Nutlin 3a. (A) *TP53+/+*, *TP53+/−* clones were treated with increasing concentration of Nutlin 3a for 72 hours followed by staining with Annexin V and propidium iodide. (B) *TP53−/−* clones treated with 3 high concentrations of Nutlin 3a (10, 15 and 20 µM) for 72 hours followed by Annexin V-PI staining. Survival curves represent two independent experiment and Error bars depict s.e.m.

In this way, two sets of clones were tested for the p53 system functionality. *TP53+/-* clones represented deletion first scenario (hemizygosity) and *TP53-/-* clones (both *TP53* alleles deleted) represented one of the double hit scenarios. Both of these sets of clones showed an impaired p53 system.

4.3 Equal expression of two p53 cDNA-gene copies is possible from a double cassette expression vector

In mutation-first scenario, cells should have equal expression from the mutant and wildtype alleles as promotors in both alleles are the same. Therefore, an expression system was needed which could express wildtype and mutant p53 simultaneously at the same level to emulate the mutation-first scenario when stably expressed in cells devoid of endogenous p53.

A double cassette SB expression vector with two individually addressable CMV promoter driven expression cassettes was developed (pT2-DC). To confirm the equal expression from both expression cassettes, a copy of the wt and mutant (R175H) *TP53* cDNA gene were cloned into the separate cassettes of the double cassette expression vector (pT2-p53$^{wt/R175H}$) (Figure 4.4 top). JJN3 cells were transiently transfected with the vector pT2-p53$^{wt/R175H}$ and with a CD4-Delta expression vector. Strongly transfected cells were purified with MACSelect CD4 microbeads and cDNA was prepared using a specific primer (PT2-MCS-3') that only recognizes mRNA made from both CMV promotor driven expression cassettes. PCR employing a different set of primers, (both 5' of the primer used for cDNA synthesis) was

performed to amplify *TP53* mRNA/cDNA expressed from the vector and the complete PCR products were Sanger sequenced. In Figure 4.4 bottom, peaks of equal height can be seen for the mutant and wildtype nucleotide base indicating that both variants of *TP53* were indeed expressed at a similar level. It confirmed that equal expression of two *TP53* cDNA-gene copies was possible from a double cassette expression vector and this vector could be used to express wildtype and mutant p53 simultaneously at the same level to emulate the mutation-first scenario when stably transposed in cells devoid of endogenous p53.
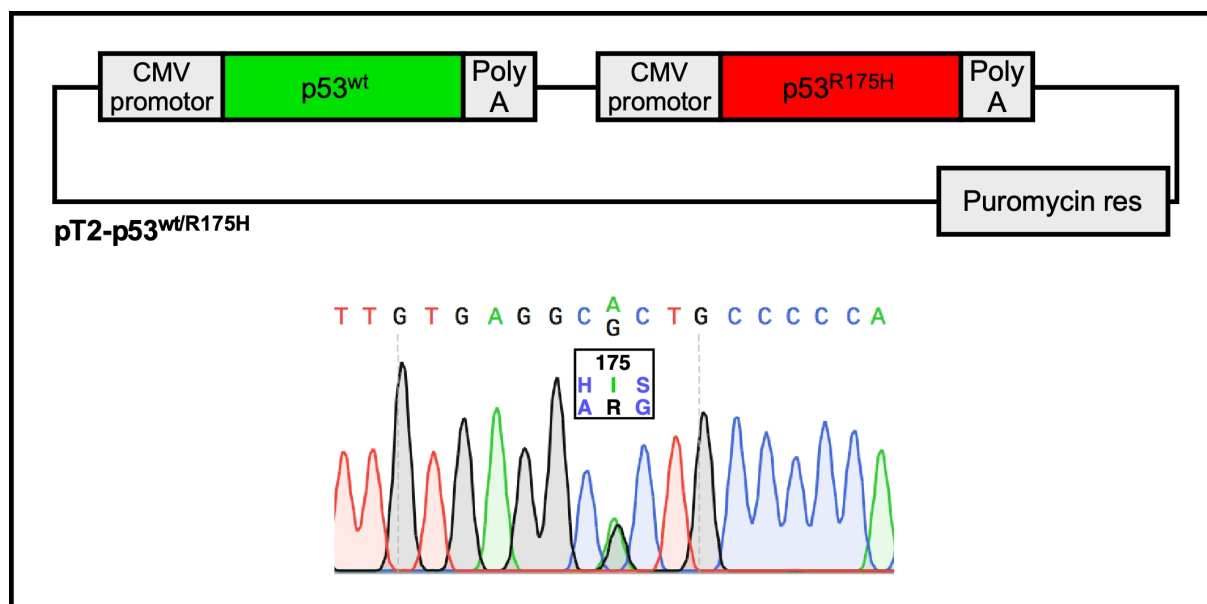
Figure 4.4: Equal expression system for p53 cDNA genes. Top: Schematic representation of double cassette SB vector (pT2-p53^{wt/R175H}) having a copy of the wt and mutant (R175H) p53 cDNA genes cloned into two individually addressable CMV-driven expression cassettes. Bottom: cDNA-analysis showing equal expression of wt and mutant (R175H) *TP53* cDNA genes from JJN3 cells transiently transfected with pT2-p53^{wt/R175H}.

4.4   Reinstatement of p53 system with double cassette expression vector

Next step was to test if stable integration of vector for constitutive re-expression of wt p53 into AMO1 *TP53*-/- clones was feasible and if cells were able to cope with the constitutive expression of p53 from a strong promoter (CMV) to restore the defective p53 signaling.

4.4.1   Expression of wt *TP53* cDNA reinstate the functionality of p53 system in a subset of *TP53* -/- clones

To test the reinstated of p53 system function in *TP53* -/- clones by exogenous expression of wildtype p53, a double cassette sleeping beauty expression vector was constructed with two wt *TP53* cDNA gene copies cloned into it (pT2-p53^{wt/wt}). Stable transfection of several *TP53*-/- clones was performed and polyclonal cultures were ready for further experiments within 10-14 days after selection with puromycin.

This was well within the normal time-frame established for sleeping beauty-mediated stable transfections with innocuous cargoes, indicating that no excessive death of stably transfected p53 expressing subclones had occurred.

First of all clone # 9 was transposed with vector pT2-p53$^{wt/wt}$ and after selection with puromycin, the polyclonal culture was treated with Nutlin 3a to test the p53 system. Western analysis showed a high steady-state expression of p53 (lane 5) as compared to AMO1 culture (lane 1), which was further enhanced when cells were treated overnight with Nutlin 3a (lane 4) (Figure 4.5 (A)). High steady-state and induced levels of p53 did not impact the expression of downstream targets of p53: MDM2 and p21, indicating that exogenous expression of p53 did not reinstate the broken MDM2/p53 loop. Furthermore, 3 days treatment with Nutlin 3a showed that SB-mediated expression of p53 in clone # 9 did not significantly impact the level of Nutlin sensitivity and cells remain fairly resistant to long-term Nutlin treatment (Figure 4.5 (B)). This indicated that in clone # 9 functionality of the p53 system could not be reestablished by exogenous wt p53 expression and it was not suitable for emulating other *TP53*/p53 constellations.

Figure 4.5: Failed reestablishment of the p53 system in clone # 9 via stable transfection with pT2 expression vector. (A) Sleeping Beauty-mediated introduction of two CMV promotor driven cDNA genes for wildtype p53 into the *TP53*-/- clone (clone # 9). Western analysis of p53 system components; p53, MDM2 and p21 after overnight treatment with 10 µM Nutlin 3a. Both parts of the blot were exposed as a unit and belong to the same strip of nitrocellulose membrane. (B) Cell survival analysis of AMO1 and clone # 9 with and without reintroduced p53 after 3 days incubation with 10 µM Nutlin 3a or an equivalent of DMSO as solvent control. Data represents 2 independent experiments and s.e.m is depicted by error bars.

A different *TP53* -/- clone (clone # 8) was transfected with the 2 x wt *TP53* cDNA expressing vector and the selected polyclonal culture was again treated with Nutlin 3a. Western analysis of p53 system components in Figure 4.6 (A) depicted that steady-state p53 level in transposed cells was comparable to the parental AMO1 cells (lanes 1 and 5). Overnight Nutlin treatment caused a significant increase in p53 level which was on a par to the level seen in wt cells, but again without significant changes in expression levels of the downstream p53 transcriptional targets MDM2 and p21. It indicated that exogenously expressed wt p53 was again either not suitable to act like endogenous p53, or that this particular clone harboured additional defects of the p53 system that set it apart from parental AMO 1 cells. Figure 4.6 (B) showed that clone # 8, even after expression of two wt *TP53* cDNA copies, remains fairly resistant

to 3 days treatment of Nutlin 3a, confirming that a functional p53 system could not be reinstated with exogenous expression of wt p53 in clone # 8 and this clone was not suitable to simulate other *TP53*/p53 arrangements.
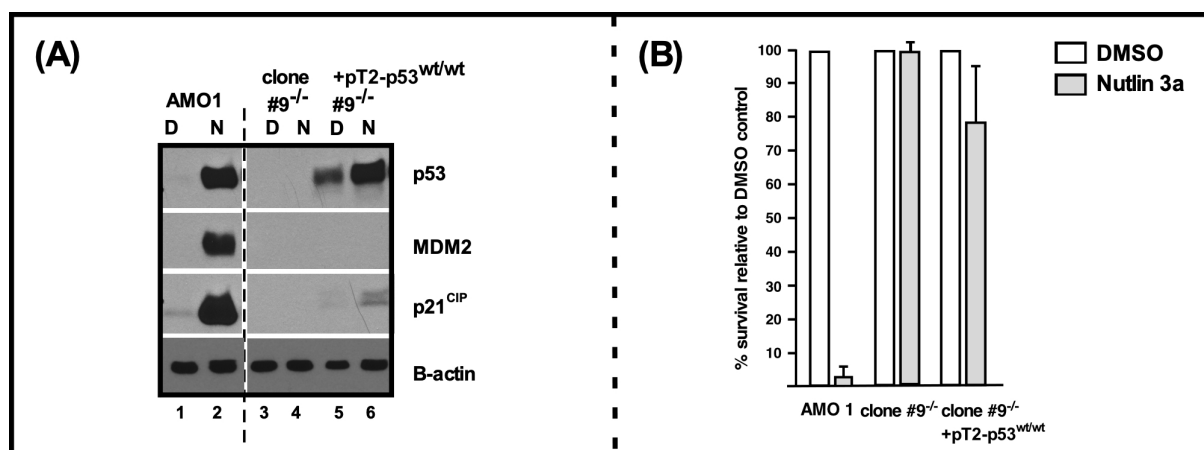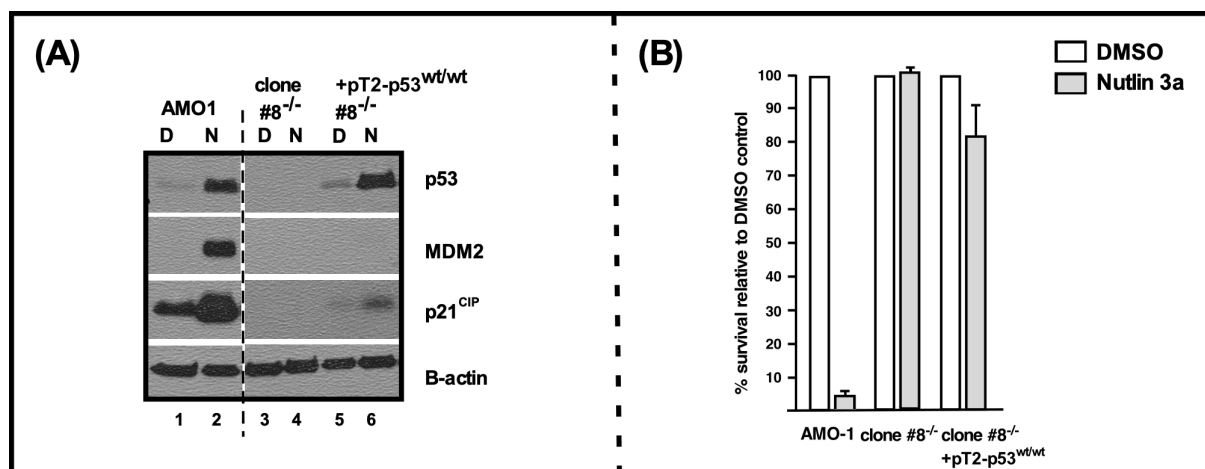

Figure 4.6: Failed reestablishment of the p53 system in clone # 8 via stable transfection with pT2 expression vector. (A) Sleeping Beauty-mediated introduction of two CMV promotor driven cDNA genes for wildtype p53 in the *TP53-/-* clone (clone # 8). Western analysis of p53 system components; p53, MDM2 and p21 after overnight treatment with 10 µM Nutlin 3a. Both parts of the blot were exposed as a unit and belong to the same strip of nitrocellulose membrane. (B) Cell survival analysis of AMO1 and clone # 8 with and without reintroduced p53 after 3 days incubation with 10 µM Nutlin 3a or an equivalent amount of DMSO as solvent control. Data represents 2 independent experiments and s.e.m is depicted by error bars.

To find a suitable clone in which the p53 system could be reestablished by exogenous p53 expression, another *TP53* -/- clone (clone # 7) was tested. The stably transfected polyclonal culture showed only slightly elevated steady-state level of p53 protein when compared to *TP53* wt AMO1 cells by Western blot (Figure 4.7 (A) lane 1 and 5). MDM2 and p21 levels were also identical between AMO1 and transposed cells. Overnight Nutlin 3a treatment enhanced the p53 level, which was roughly on a par with the increase seen in AMO1 cells (lane 2 and 6) Figure 4.7 (A). Western analysis showed pronounced increase in the levels of p53 downstream targets MDM2 (although to levels not quite as high as seen in parental AMO1) and p21 (comparable) after treatment with Nutlin 3a. It showed that this clone was thus indeed able to molecularly integrate exogenously introduced 2 copies of *TP53* wildtype cDNA into the MDM2/p53 degradation/transcription cycle that governs the level of p53 in AMO1 cells, even though their expression was driven by a strong and constitutively active promotor; CMV.

This molecular integration was also observed in another functional assay. *TP53-/-* clone (clone # 7) which had become resistant to the high concentration of Nutlin 3a, largely restored the p53-mediated death response after stable transfection with wt p53 expression vector (pT2-p53$^{wt/wt}$) (Figure 4.7 (B)). These cells showed apoptosis (similar to AMO1 cells) in Annexin V-PI staining 72 hours after the treatment with MDM2 inhibitor, indicating that this cellular model system indeed displayed the basic features to analyze p53 functions. These observations made clone # 7 a suitable clone to simulate other *TP53*/p53 constellations.
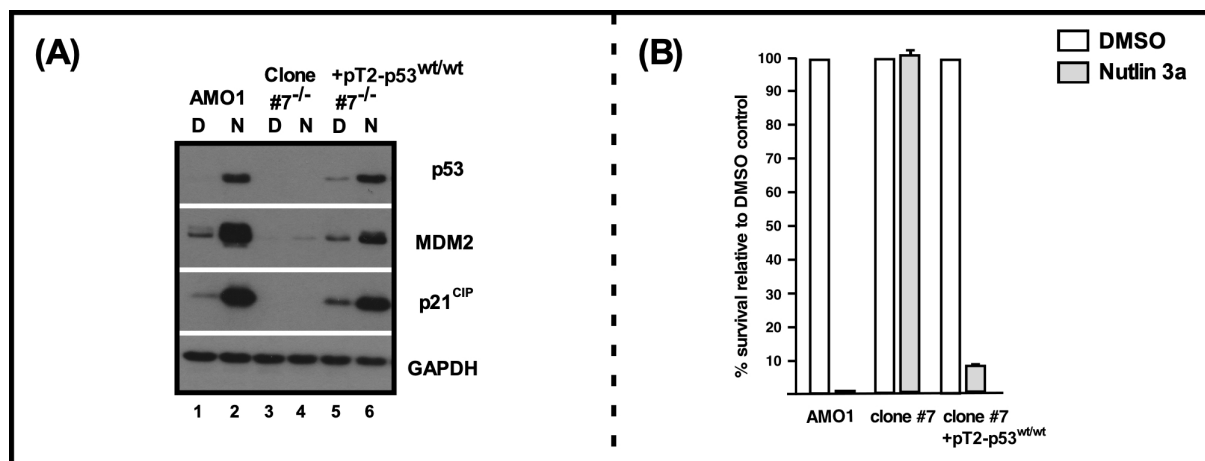
Figure 4.7: Functional analysis of the p53 system after stable transfection with pT2 expression vector. (A) Sleeping Beauty-mediated introduction of two CMV promotor driven cDNA genes for wildtype p53 into the *TP53-/-* clone (clone # 7). Western blot analysis of p53 system components; p53, MDM2 and p21 after overnight treatment with 10 µM Nutlin 3a. (B) Cell survival analysis of AMO1, clone # 7 with and without reintroduced p53 after 3 days incubation with 10µM Nutlin 3a or a suitable measure of DMSO as solvent control. Data represents 2 independent experiments and s.e.m is depicted by error bars.

Lastly, a similar stable transposition in another *TP53-/-* clone (clone # 6) was performed to confirm the results. Clone # 6 when transposed with wt *TP53* cDNA, showed a slight increase in steady levels of p53 which increased just like the wildtype culture upon Nutlin treatment. Increase in p53 levels also enhanced MDM2 and p21 levels ((lanes 7 and 8) Figure 4.10 (A)). Reintroduction of wildtype p53 made this clone sensitive to prolonged Nutlin treatment as seen in Figure 4.10 (B), implying that clone # 6 was again a good candidate clone to study the p53 system. In later experiments, both clones (# 6 and # 7) were thus used to functionally analyze other *TP53*/p53 constellations.

To better understand the stability of these reestablished wt p53 systems, *TP53-/-* clones stably transposed with wt p53 expressing vector were monitored for p53 system function for up to 30 days. It was found that these selected polyclonal cultures lost their efficacy of the p53 system over time. The overall response of the culture to the Nutlin treatment decreased with time and by day 30 (post-selection) almost 50 % of the response was lost in the same culture, which right after the antibiotic selection, was almost completely sensitive to 3 days Nutlin treatment (Figure 4.8). This indicated that the reestablishment of the 'wildtype' p53 system was a transient feature, most probably because over time those subclones with the least wildtype p53 activity still have an advantage in survival and become the dominant subclones in the culture. However, with a number of similar experiments performed it was also obvious that for clones # 6 and # 7 the initial sensitivity could faithfully be reproduced between independent experiments (Figure 4.9 and Figure 4.10). These tests indicated a time window within which experiments that involved clones with the SB-mediated reinstated p53 systems must be performed i.e. the first 1-2 weeks right after the selection of polyclonal cultures.
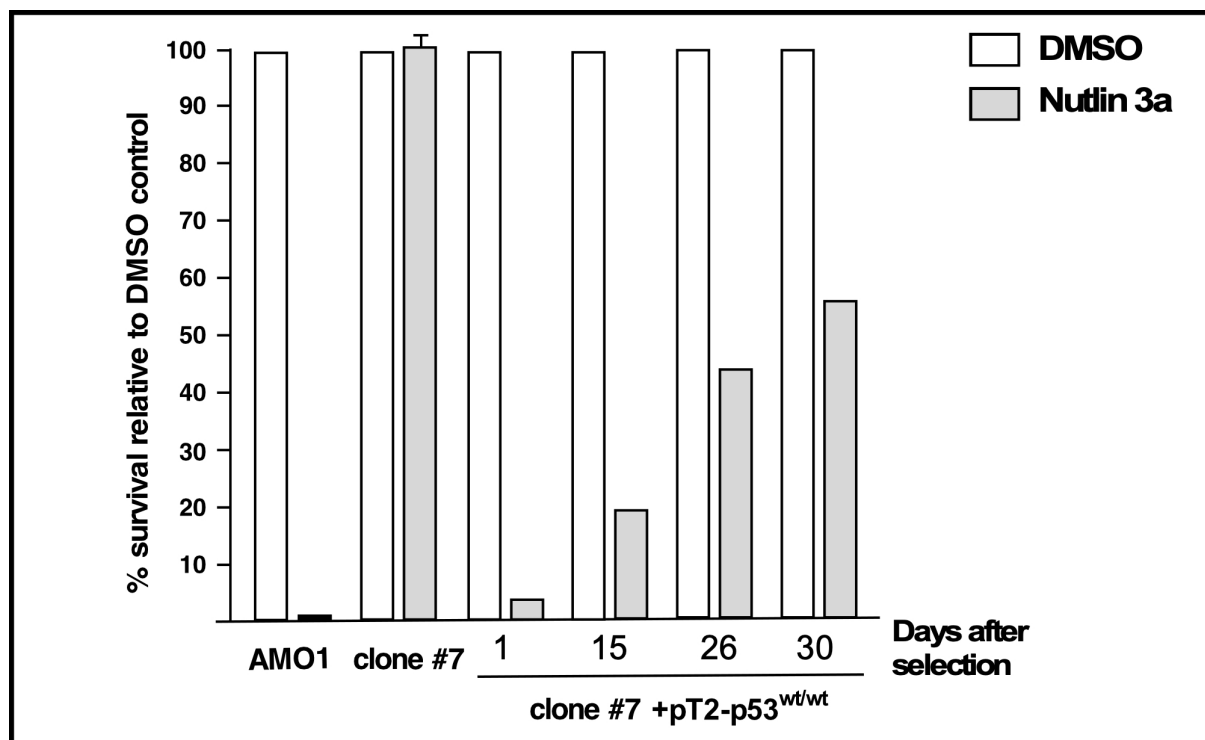
Figure 4.8: Analysis of limited stability of reestablished p53 system in *TP53-/-* clones. AMO1, clone #7 with and without reintroduced wt p53 were treated with 10 µM Nutlin 3a and cell survival analysis (Annexin V-PI staining) was performed after 3 days. Clone # 7 with reintroduced p53 was tested on different days after initial selection of a polyclonal culture.

4.4.2 Heterozygous *TP53* point mutations partially reinstate the p53 system

To modelize the heterozygous point mutations in *TP53* (mutation-first scenario), initially clone # 7 (*TP53-/-*) was stably transposed with the double cassette SB vector, expressing a combination of a wt *TP53* gene with either of the mutant *TP53* copy (R175H or R282W). Western analysis in Figure 4.9 (A) showed that clone # 7 + p53 wt/R282W had slightly higher steady-state levels of p53 protein (lane 7) as compared to the wildtype AMO1 culture (lane 1) and clone # 7 + p53wt/wt (lane 5). Overnight Nutlin treatment enhanced the p53 levels in the heterozygous situation, but not as much as seen in wildtype AMO1 cells or clone # 7 + p53 wt/wt (lanes 2, 6 and 8). There was not much increase in other components of the p53 system (MDM2 and p21) seen in clone # 7 + p53 wt/R282W and clone # 7 + p53 wt/R175H compared to wildtype AMO1 culture and clone # 7 + p53wt/wt cells. This indicated that the slight elevation seen in the p53 levels after Nutlin 3a treatment was not high enough to translate into the induction of other components of the p53 system.

Figure 4.9: Functional analysis of p53 system after stable transfection with pT2 expression vector in clone # 7. (A) (B) Clone # 7 stably transposed with double cassette SB vector performing CMV promotor driven gene expression of two wt *TP53* cDNA gene copies or a combination of a wt and a mutant p53 cDNA gene copy (p53wt/R282W or p53wt/R175H) to emulate mutation-first scenarios, or of a single mutant p53 cDNA gene to simulate a deletion plus mutation scenario. Western blot analysis of p53 system components; p53, MDM2 and p21 after overnight treatment with 10 µM Nutlin 3a. (C) Cell survival analysis (Annexin V-PI staining) of AMO1, clone # 7 and polyclonal clone # 7-derived subculture expressing different constellations of wildtype and mutant p53 after 3 days incubation with 10 µM Nutlin 3a or a DMSO equivalent solvent control. Data represents 2 independent experiments and s.e.m is depicted by error bars.

Likewise, this minor increase in p53 level did not prove to be enough to reinstate the normal function of p53 in cells, as it did not make cells sensitive towards the 3 days treatment with 10 μM Nutlin 3a. The cells with the heterozygous mutations showed almost no cell death when treated with MDM2 inhibitor Nutlin 3a in contrast to parental AMO1 cells or clone # 7 + p53 wt/wt cells (Figure 4.9 (C)).

Similar results were seen when clone # 7 was stably transposed with the vector expressing a p53wt/R175H combination. Even with this different mutant, cells showed higher elevated steady-state levels of p53 already on a par with induced p53 levels in wt AMO1 and clone #7 + p53 wt/wt cells. No significant increase in p53 level was seen after Nutlin 3a exposure over-night ((lane 7 and 8) Figure 4.9 (B)). Moreover, not much increase was seen in MDM2 and p21 levels in WB and this slight increase did not revoke the sensitivity against 3 days treatment with Nutlin 3a (Figure 4.9 (C)). Clone # 6 when transposed with a vector expressing heterozygous mutant p53 (wt/R282W) showed higher steady levels of p53 and a slight increase in p53 level after Nutlin overnight treatment, which caused a minor increase in MDM2 and p21 levels (lanes 5 and 6) as seen in Figure 4.10 (A). This limited increase in the levels of p53, MDM2 and p21 resulted in minor gains in sensitivity against prolonged Nutlin treatment (Figure 4.10 (B)) These results indicated that the molecular functionality of the p53 system gets significantly diminished in the mutant first scenario.

4.4.3 Expression of mutant p53 does not reinstate the p53 system

Mutation plus deletion scenario, characterized by overexpression of mutant p53 protein in the absence of wt p53, is a common situation seen in some MM cell lines and primary MM cells. The mutant overexpression may have dominant negative and potential gain of function effects as opposed to a single hit scenario: del 17p (simulated by CRISPR-mediated single *TP53* hit) causing haploinsufficiency, hence complements the work reproducing all possible *TP53*/p53 constellations.

To depict the biallelic inactivation (mutation plus deletion scenario), *TP53-/-* clone (clone # 7) was stably transposed with SB vector expressing cDNA of mutant p53 (R282W) Figure 4.9 (A). The culture depicting mutant (R282W) plus deletion combination showed a very high steady-state level of mutant p53 expression as compared to the wildtype AMO1 cells (lanes 9 and 1). Overnight Nutlin treatment did not further increase the level of mutant p53 or of MDM2 and p21. This indicated that at molecular level, the mutant plus deletion scenario led to complete abrogation of p53 function, worse than both types of single hit scenarios, which showed at least a minor increase in levels of p53 and its downstream targets MDM2 and p21.

Similar results were seen when another mutant of p53 (R175H) was expressed in a deletion background. No further increase in an already high level of p53 and no induction of MDM2 and p21 was seen in (lanes 9 and 10) Figure 4.9 (B) after Nutlin treatment. At a functional level none of these mutants provided any sensitivity of the transfected cells towards Nutlin treatment. Clone # 7 expressing these mutants remained completely insensitive to the prolonged Nutlin treatment as seen with Annexin V-PI staining performed 72 hours after the drug treatment (Figure 4.9 (C)).
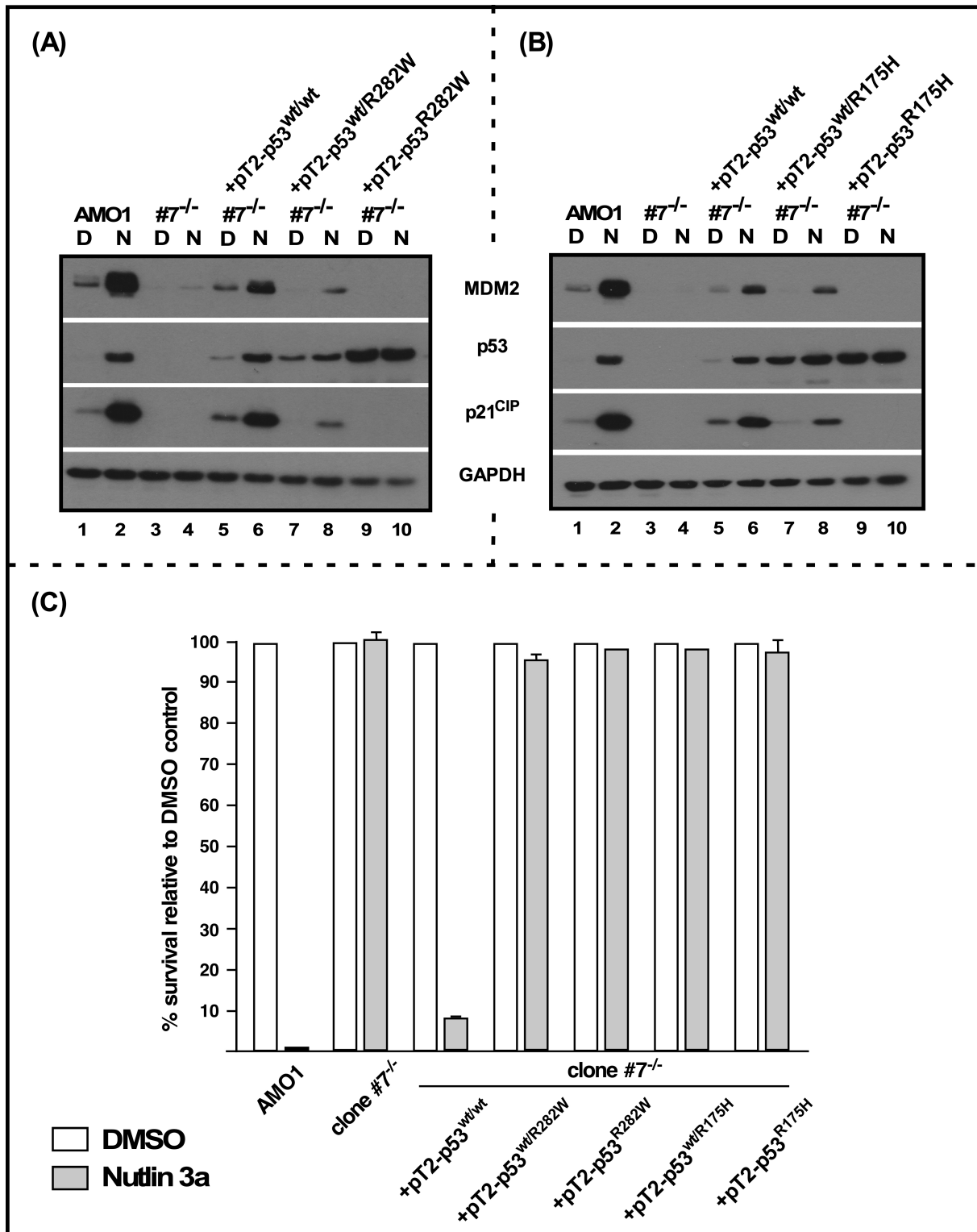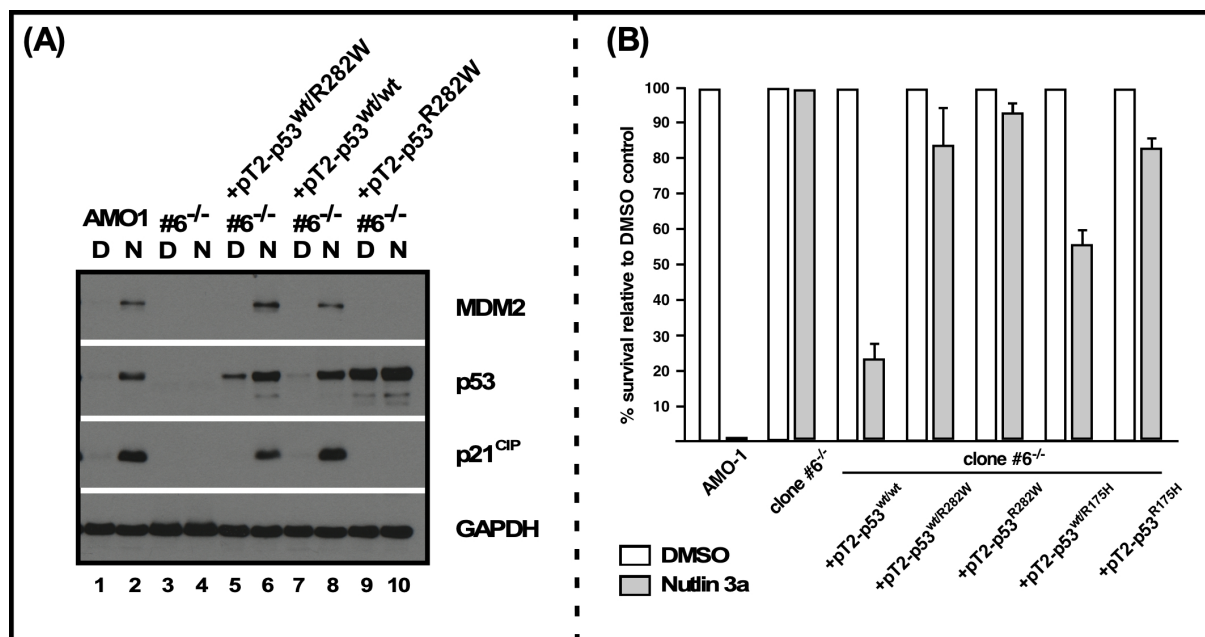
Figure 4.10: Functional analysis of p53 system after stable transfection with pT2 expression vector in clone # 6. (A) Clone # 6 stably transposed with double cassette SB vector performing CMV promotor driven gene expression of two wt p53 cDNA gene copies or a combination of a wt and a mutant p53 cDNA gene copy (p53wt/R282W) to emulate the mutation-first scenario, or of a single mutant *TP53* cDNA gene to simulate deletion plus mutation scenario. Western blot analysis of p53 system components; p53, MDM2 and p21 after overnight treatment with 10 µM Nutlin 3a. (B) Cell survival analysis (Annexin V-PI staining) of AMO1, clone # 6 and this clone expressing different constellations of wildtype and mutant p53 after 3 days incubation with 10µM Nutlin 3a or equivalent DMSO as solvent control. Data represents 2 independent experiments and s.e.m is depicted by error bars.

Furthermore, transposition of clone # 6 with only mutant p53 expressing vector resulted in a very high level of p53 in cells which after Nutlin treatment neither increased any more, nor induced expression of the downstream responsive proteins MDM2 and p21 (lane 9 and 10) (Figure 4.10 (A)). These cells almost completely survived 3 days Nutlin treatment with both mutant p53 types (282W and 175H) as seen in Figure 4.10 (B). This indicated that in the case of double hits, the p53 system is completely abolished at molecular and functional levels. In this way, AMO1 cell line models depicting all the MM related genomic lesions were obtained and characterized at molecular and functional levels.

4.5 *TP53* defective clones have abrogated melphalan sensitivity

After molecular and functional validation of models emulating different *TP53* lesions, they were examined for any alterations in response towards clinical drugs.

Initially, AMO1 parental cells, CRISPR/Cas9 generated hemizygous and double deleted *TP53* clones were tested for sensitivity against a clinically employed alkylating agent, melphalan. Both of the *TP53-/-* clones (clone 6 and 7) which were previously used for stable transpositions of p53 cDNA genes, and three *TP53+/-* clones (clone 2, 3 and 4) were treated with melphalan and an alamarBlue assay was performed after 3 days. Wildtype AMO1 cells (black) showed sensitivity to increasing concentrations of melphalan, whereas this melphalan effect was severely reduced in all 3 of the tested hemizygous clones (green,

magenta, orange) (Figure 4.11), indicating that melphalan sensitivity is directly or indirectly dependent on the p53 status of the cell. Melphalan sensitivity appeared virually abolished in both *TP53-/-* clones (brown, blue). Clone # 6 and # 7 did not show any significant difference in the growth even at the highest concentrations of melphalan, it further strengthened the observation that p53 status can potentially be important for the efficacy of this particular alkylating agent.
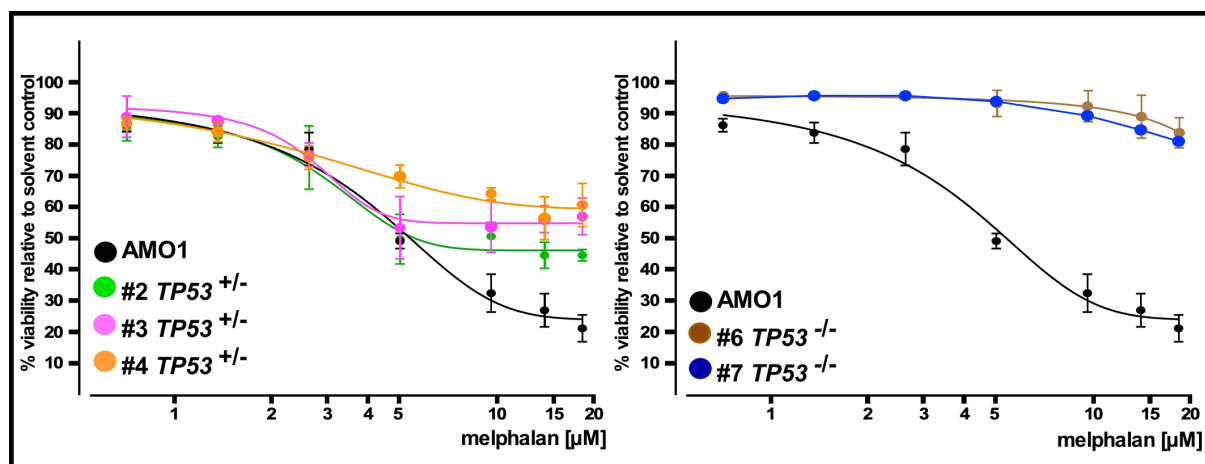
Figure 4.11: Analysis of melphalan sensitivity as function of *TP53*/p53 status. Wildtype AMO 1 (black) and clones with different p53 status (both or single alleles of *TP53* disrupted) were treated with Melphalan for 3 days and subjected to viability assay (alamarBlue). Two *TP53-/-* clones (brown and blue) used above for stable transpositions (clone 6 and 7) and 3 hemizygous clones (*TP53+/-*) (green, purple and orange) were used in this experiment. Data represents 3 independent experiments. SD is depicted by error bars.

Next, melphalan was tested on clone # 7, stably transposed with a sleeping beauty vector expressing two wildtype *TP53* cDNA copies, to see if reinstatement of the p53 system in *TP53-/-* clone reestablished the sensitivity towards melphalan. In Figure 4.12 (A) it can be seen that clone # 7 with exogenously expressed wt p53 acquired melphalan sensitivity and the response was very similar to the response seen in wt AMO1 cells (black and red). Expression of the wt + mutant (R282W) combination produced an attenuated melphalan response fairly identical to CRISPR/Cas9 generated hemizygous *TP53* clones (magenta and orange). It underpinned that heterozygous *TP53* mutation had a dominant negative effect and the adverse effects of 'mutation first' scenario and 'deletion first scenario' were analogous for the melphalan sensitivity. A similar effect was seen with another point mutation (R175H) when tested as heterozygous combination (wt/R175H) for its response towards melphalan treatment. Similar to the wt/R282W p53 heterozygous state, the culture representing mutant first scenario for R175H mutant p53 showed attenuated response towards melphalan treatment, and this response was on a par to the response of the *TP53* hemizygous clone (Figure 4.12 (A) left).

In addition, a *TP53 -/-* clone (clone # 7) when transposed with mutant p53 (R282W) expressing vector did not show any change in the melphalan sensitivity and remained equally insensitive. Equal impairment of the melphalan sensitivity in the heterozygous *TP53* mutation and hemizygous *TP53* situation, and complete abrogation in *TP53* double hit scenario implied the strong dependence of melphalan sensitivity on p53 status of this AMO1 MM model system.
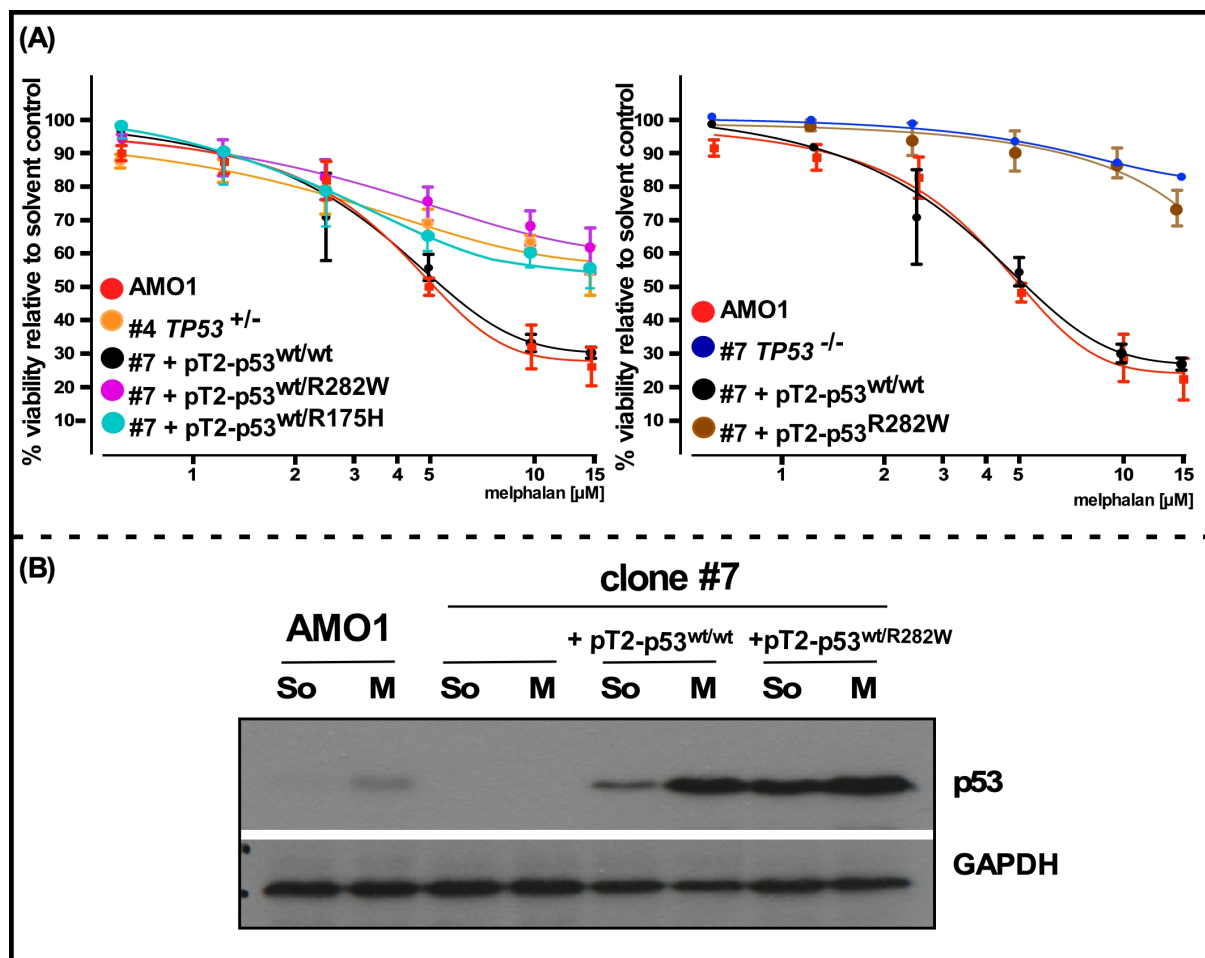
Figure 4.12: Analysis of melphalan sensitivity as a function of the *TP53*/p53 status. (A) Response to increasing concentrations of melphalan in AMO1 wildtype cells (red) *TP53-/-* cells clone # 7 (blue), clone # 7 stably transposed with sleeping beauty vector expressing two copies of wildtype p53 cDNA genes (black), combination of wt and mutant R282W p53 cDNA genes (purple) or mutant only R282W (brown). Clone # 4 (hemizygous for *TP53*) is added for comparison (orange). Cells were treated with melphalan or acidified ethanol equivalent to the highest concentration of melphalan as solvent control. After 3 days alamarBlue assay was performed. Data represents 3 independent experiments and error bars depict SD. (B) Western analysis of p53 levels after melphalan treatment. Cells were treated with 10µM melphalan (M) or equivalent amounts of acidified ethanol as solvent control (So) overnight and analyzed for p53 levels by Western blotting. GAPDH served as loading control.

Next, the impact of melphalan treatment on p53 levels in these cells was studied. Figure 4.12 (B) shows that melphalan treatment caused an increase in p53 levels in AMO1 cells, whereas this increase was not seen in clone # 7. A relative increase in the p53 level is higher in clone # 7 transposed with p53 wt/wt expressing vector as compared to wildtype AMO1 cells mainly due to the higher absolute steady-state p53 level in this particular clone. The cells expressing wt/R282W p53 showed no increase in p53 level after melphalan treatment because they already had a relatively high steady-state p53 level when compared to the wildtype AMO1 cells. This increase in p53 level after melphalan treatment further confirmed the dependence of melphalan activity on *TP53* status of the cells.
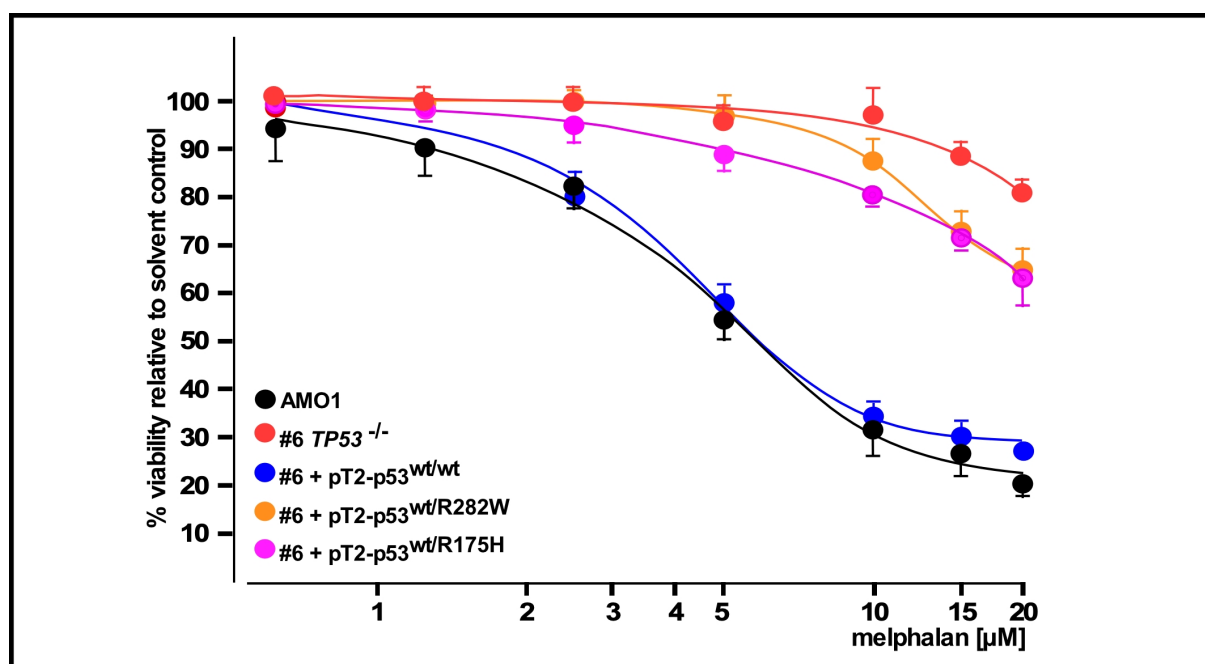
Figure 4.13: Response to increasing concentration of melphalan in AMO1 wildtype cells and clone # 6 transposed with sleeping beauty vectors expressing 2 copies of wt p53 cDNA genes or combination of wt p53 with either of two mutant p53 cDNA genes (R282W, R175H). Cells were treated with melphalan for 72 hours and subjected to alamarBlue assay. Data represents 3 independent experiments, SD is depicted by error bars.

Finally, the whole data was confirmed with another *TP53*-/- clone (clone # 6), transposed with vectors expressing different constellations of wildtype and mutant p53. Re-instatement of a functional p53 system re-sensitized the melphalan sensitivity which was decreased in a single hit to p53 system and completely diminished in the absence of any functional p53 (Figure 4.13).

4.6 Doxorubicin sensitivity is affected by the *TP53* status

Next, the impact of *TP53* status was investigated on response to another genotoxic drug, doxorubicin. Cells were treated with various concentrations of doxorubicin and alamarBlue assay was performed after 3 days. As seen in Figure 4.14, *TP53* -/- clone (clone # 7) showed an attenuated response against doxorubicin (blue curve) as compared to AMO1 wildtype cells (black). Clone # 7 when stably transposed with two wt *TP53* cDNA, reattained the lost sensitivity against doxorubicin (red curve), implying that efficacy of doxorubicin is potentially dependent on *TP53*/p53 status of the cell. When cells simulating a mutation-first scenario, using two different p53 mutations (R175H, R282W) in combination with a wt p53 copy were tested with this drug, a blunted response as compared to AMO1 cells was observed (brown and magenta). A marginal shift of kill curves to the right side was seen, which was not as stark as seen in the case of double *TP53* deleted cells. Subsequent disruption of the response in the cells representing different *TP53*/p53 constellations indicated the dependence of the antimyeloma activity of this drug on the p53 status in this AMO1 MM model system.
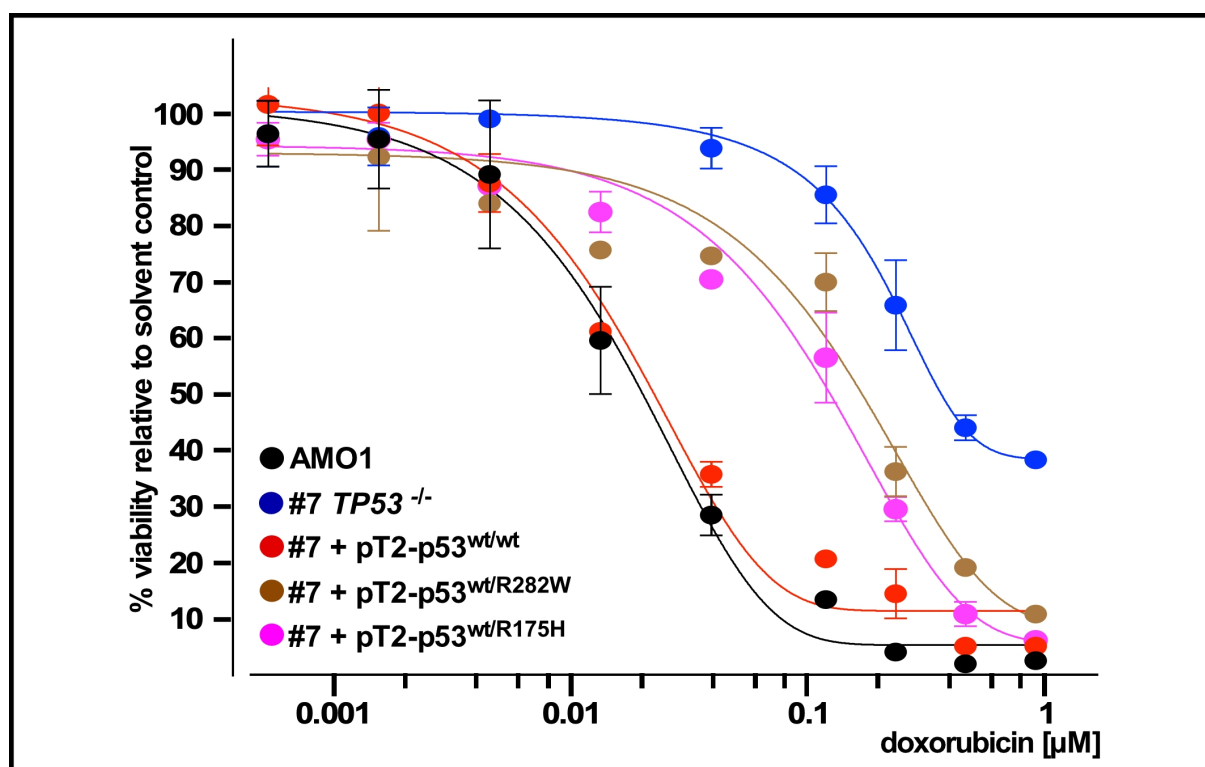
Figure 4.14: Response to doxorubicin in Parental AMO1 (black), *TP53−/−* cells (clone # 7) without (blue curve) or with stable expression of combinations of wildtype and mutant p53 cDNA genes via sleeping beauty (magenta and brown curves). Two different p53 mutant proteins (R175H, R282W) were tested in combination with wt p53. Clone # 7 transposed with two wildtype p53 cDNA gene copies (red) was also included for comparison. AlamarBlue was performed after 3-day drug treatment. Data was normalized with DMSO control and represents 3 independent experiments. Error bars depict S.D.

4.7 The *TP53* status does not influence proteasome inhibitors sensitivity

The last group of drugs tested comprised proteasome inhibitors (PIs), which show anti-myeloma activity by inhibiting different proteasome subunits in the cells. To test whether they depend on p53 for their activity, cells with different *TP53*/p53 status were treated with two different proteasome inhibitors, carfilzomib and bortezomib. After 3 days treatment with PIs, cells were subjected to Annexin V-PI staining to monitor apoptosis. Figure 4.15 (A) shows that wildtype AMO1 cells and the *TP53-/-* clone (clone # 7) did not show any variation in the sensitivity to carfilzomib. Clone # 7 stably transposed with two wt cDNA copies of p53 or with a mutant+wildtype combination also had similar responses. As none of the cells with different *TP53*/p53 constellation showed any variation, it confirmed that the p53 system appeared not to be significantly involved in carfilzomib-mediated apoptosis of MM cells.
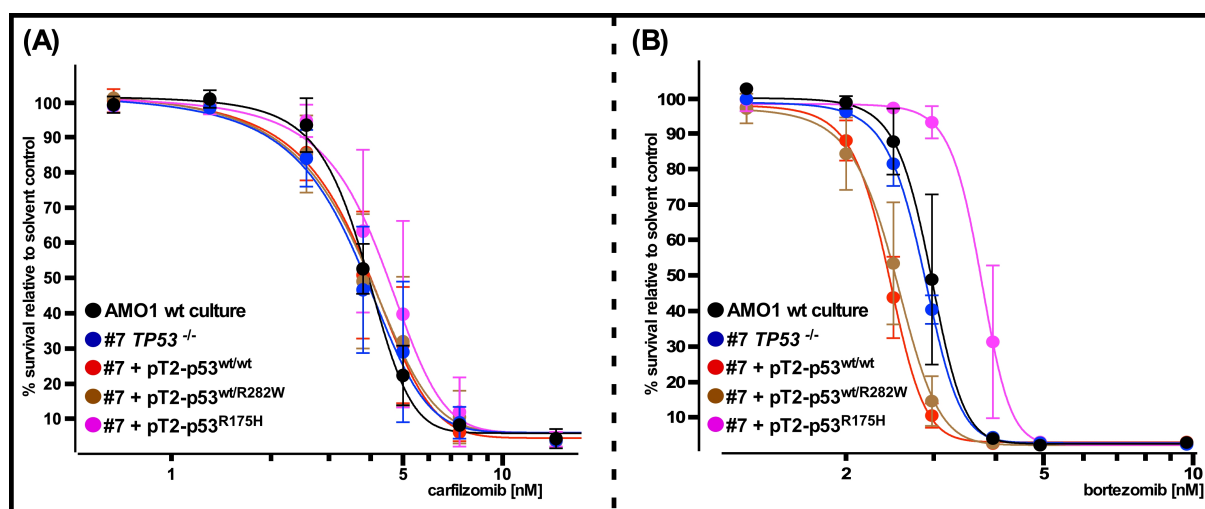
Figure 4.15: Response to proteasome inhibitors (A) carfilzomib. (B) bortezomib were tested on AMO1 parental cells and clone # 7 with and without SB-mediated expression of different arrangements of wt and mutant p53 cDNA genes. Cell survival assay (Annexin V-PI) was performed after 72 hours of drug treatment. Data represents 3 independent experiments. Error bars depict s.e.m

Figure 4.15 (B) shows that AMO1 wt and *TP53-/-* clone had no differences in the response when treated with bortezomib. Minor increase in the sensitivity was seen when CMV promotor driven expression of 2 wt p53 cDNA copies was performed in *TP53-/-* clone (clone # 7). Furthermore, a slight shift in the kill curve was seen when mutant p53 was expressed in the same clone. But these slim deviations do not indicate that bortezomib has dependancy on the p53 status for its anti-myeloma activity.

With the data set shown, the different constellations of mono- and biallelic *TP53* alterations, observed in MM patients, were approximated within the framework of a single cell line model, assessed for their potential to disrupt the functionality of the p53 system and to provide drug resistance. These results indicated that monoallelic alterations of *TP53* (as first hit), whether it is a mutation-first scenario (one allele gets mutation and other allele is wildtype) or deletion first scenario (complete loss of one allele of *TP53* due to del 17p), strongly impaired the functionality of the p53 system and at the same time provided resistance against genotoxic drugs (melphalan and doxorubicin). Biallelic alteration (second hit) which is normally represented by deletion 17p in a mutation-first scenario or by *TP53* mutation in a del 17p-first scenario, completely abolished the remaining functionality of the p53 system and further enhanced the resistance to genotoxic drugs, but the response to PIs remained unaltered. These results fit rather well with the clinically observable drive from normal MM cells to mono- and subsequently biallelic *TP53* alterations as seen in MM patients.

Parts of this data set have been published: Munawar et al. Assessment of *TP53* lesions for p53 system functionality and drug resistance in multiple myeloma using an isogenic cell line model; *Scientific Reports*, 2019.

4.8 Generation of fluorescently labeled multiple myeloma cell lines

After analyzing the impact of mono- and biallelic *TP53* alterations on the p53 system function and therapy response in myeloma, the next step was to analyze the long-term cell fitness of these *TP53* altered clones. A clonal competition assay (CCA) was developed to quantify the cellular fitness provided by any genomic alterations. In the CCA, the cells which need to be studied are selectively color coded through stable transposition with cDNA genes for fluorescent proteins, and subsequently co-cultured in the presence or absence of external pressure (drugs). Co-cultures in a CCA are maintained just like normal cell culture but monitored at regular intervals by simple flow cytometry to record the relative ratio of cells in co-culture over a period of time. To color code the cells with fluorescent proteins, SB vectors were prepared to express enhanced green fluorescent protein (EGFP) or red fluorescent protein (LSS-mKate2) by Nicole Müller (MD student). Wild-type and *TP53* defective AMO1 clones were stably transposed with these color coding vectors using an aminoglycosidase phosphotransferase gene (neo) as selection marker (G418 selection). Polyclonal cultures expressing EGFP, RFP or no fluorescent protein and respective mono- or biallelic *TP53* alterations were thus distinguishable by flow cytometry (Figure 4.16).
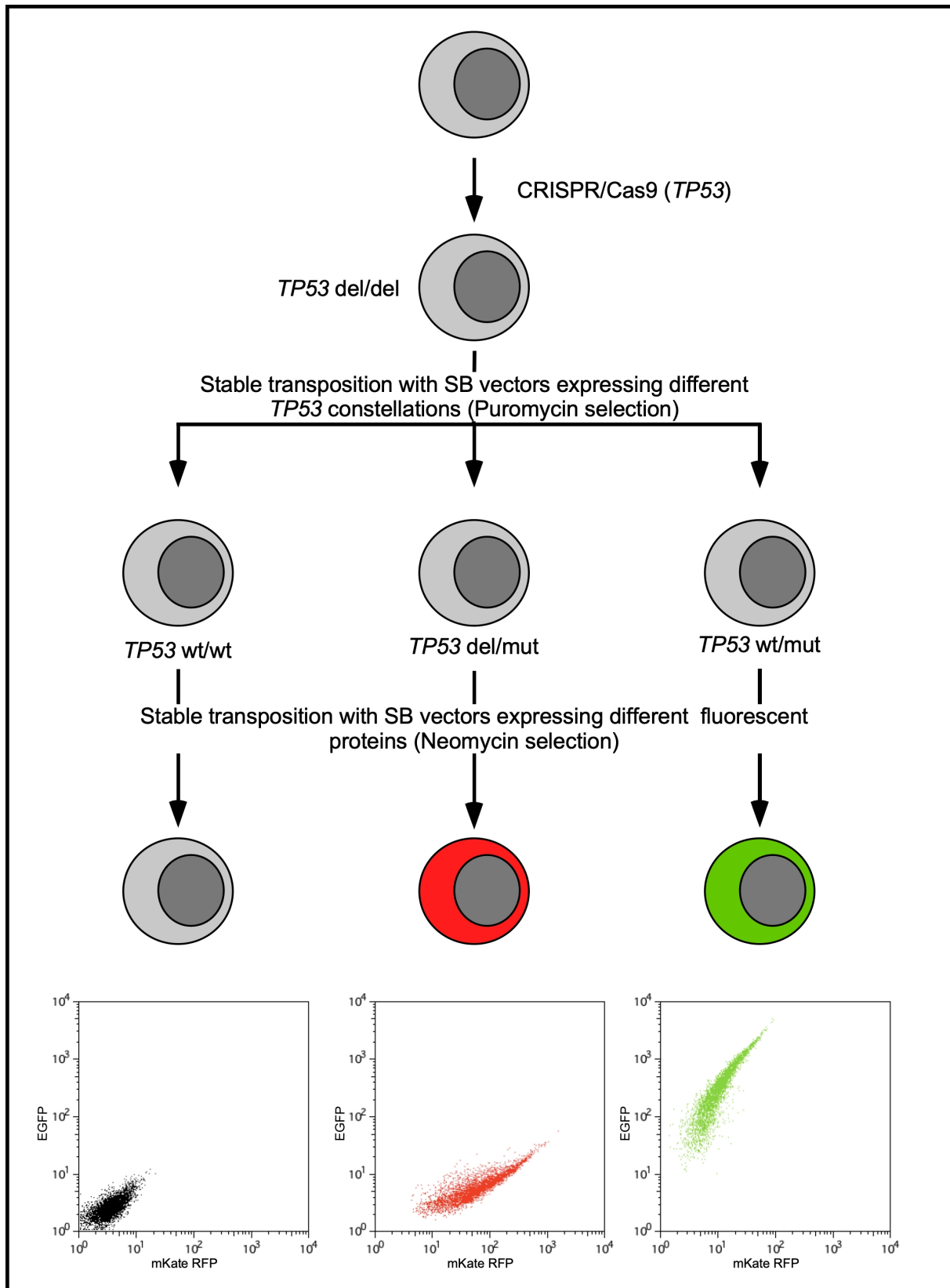
Figure 4.16: Diagrammatic representation of generation of fluorescently labeled cell lines for quantification of cell fitness. AMO1 cells which underwent a series of genetic changes with CRISPR/Cas9 and sleeping beauty transpositions to emulate genetic variations seen in MM were subjected to a second SB transposition to express EGFP or RFP.

4.9 Melphalan selects for the clone with no functional p53 system

To study if the alteration in *TP53* genomic status provides any fitness advantage to the cells in the presence of the drug melphalan, *TP53* -/- clone (clone # 7) expressing mutant p53 R282W (del/mut scenario) and wildtype AMO1 cells were color-coded with EGFP or RFP respectively. The CCA was set up by mixing wt AMO1 and *TP53* double hit clone, clone # 7 (del/R282W) in 9:1 in the presence or absence of sub-lethal concentration of melphalan. The relative ratio of the cells in the co-culture was monitored by FACS analysis at regular time intervals. Figure 4.17 shows that melphalan treatment selected the cells with a defective p53 system. The relative number of p53 double hit cells (del/R282W) increased from 10% (initial number) to 80% of the total culture in 30 days against wildtype AMO1 cells when exposed to the low dose of melphalan.

Meanwhile, even in the absence of melphalan, the p53 defective clone (del/R282W) was selected over wildtype cells. In 30 days, it increased in the number from 10% to 50% of the culture. The selection of p53 defective cells in the absence of selection pressure (melphalan), though not as fast as in the presence of melphalan, indicated that disruption of the p53 system provided a selection advantage to these cells over wildtype AMO1 cells. This suggested that the presence of the selection pressure, in the form of low dose melphalan, boosted an already existing fitness advantage of the p53 defective clone.
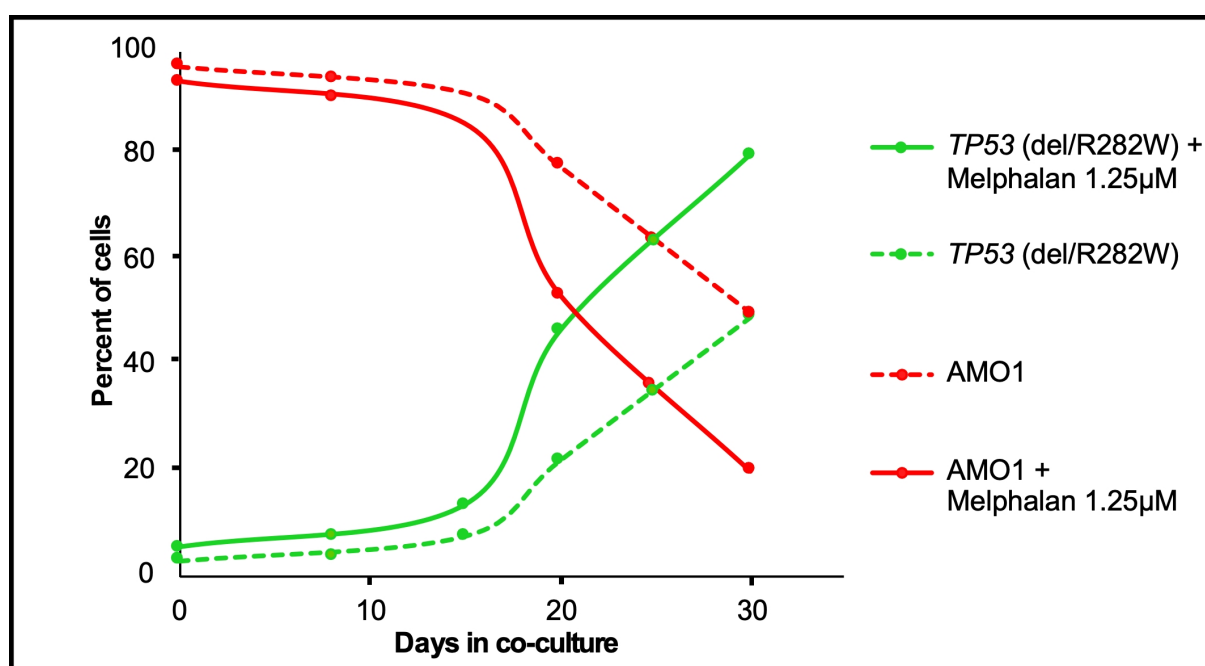
Figure 4.17: AMO1 wildtype cells and *TP53*-/- clone (clone # 7) expressing p53 mutant R282W were color coded with EGFP and RFP and mixed in a 9:1 ratio. The cells were treated with 1.25 µM melphalan. Solvent control was set up using equivalent volume of acidified ethanol. The co-culture was monitored every 5-7 days by flow cytometry. The cell culture was split regularly and the final concentration of melphalan was maintained throughout the experiment.

4.10 Double *TP53* hit cells have a fitness advantage over single *TP53* hit and wt cells

To quantify the fitness advantage of the clones with different *TP53*/p53 constellations in the absence of any external selective pressure further experiments were set up. In the first experiment, *TP53* biallelic hit cells (del/mut) were co-cultured with the parental *TP53* wildtype AMO1 cells at an initial ratio of 1:3. The *TP53* double-hit clone expanded significantly, reached almost 50% of the cell population by day 21 and took over more than 80% of the whole culture by day 40 (Figure 4.18 (A)). Similarly, the clone with one defective *TP53* copy (wt/mut), from a similar initial ratio, also outcompeted the AMO1 parental cells, but it took longer time (38 days) to get to 50% of the cell culture as seen in Figure 4.18 (B). By day 40 this clone represented almost 60% of the cell culture.
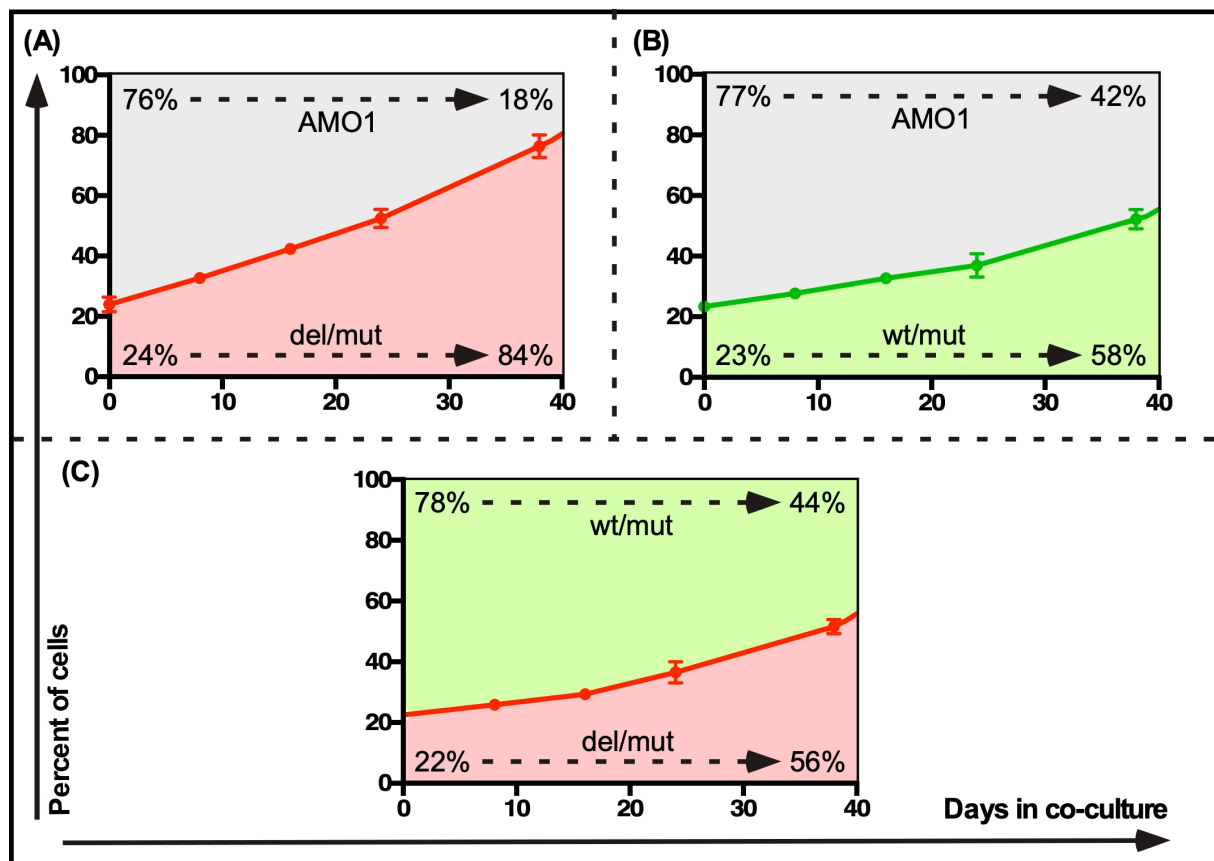
Figure 4.18: Clonal competition assays of double hit *TP53* (red), single hit *TP53* (green) and wildtype AMO1 cells (grey). The initial percentage of the subclone(s) at day 0 and at the end of the experiment is included in each figure. Regular cell culture was performed. The share of the different clones based on the fluorescence signals of EGFP and/or LSS-Kate2 RFP was determined regularly. Error bars represent the standard deviation based on 3 independent experiments.

Likewise, the double-hit *TP53* clone outcompeted the single-hit *TP53* clone under similar experimental settings as seen in Figure 4.18 (C). Over a period of 40 days, it took over more than half of the co-culture. Taken altogether, this data suggests that if one copy of *TP53* is defective in the cells, cells achieve fitness over the wildtype cells and this cell fitness is further enhanced when no functional p53 at

all is present in the cell (in double-hit *TP53* clones). In this model system, the proliferative/cell fitness thus increases according to the extent of loss of *TP53*.

4.11 Initial clonal burden determines the selection dynamics of the clone

Next, the impact of the initial clonal burden on the fitness dynamics was studied. Under similar settings, three experiments with varying initial concentrations of *TP53* biallelic hit clone versus AMO1 wildtype cells were set. When cells were mixed in a 1:3 ratio, the *TP53* defective clone took almost 21 days to take up 50% of the culture as seen in Figure 4.19 (A). The *TP53* defective clone took 45 days to take up 50% of the culture when co-culture stated at 1:9 initial ratio against wildtype AMO1 cells as seen in Figure 4.19 (B). In a co-culture set up with a 1:99 initial ratio between double hit *TP53* clone and AMO1 wildtype cells, the *TP53* del/mut clone took a longer time, 58 days, to attain 50% of the cell culture as shown in Figure 4.19 (C). In all 3 cases double-hit cells were able to take up most of the culture in the end.
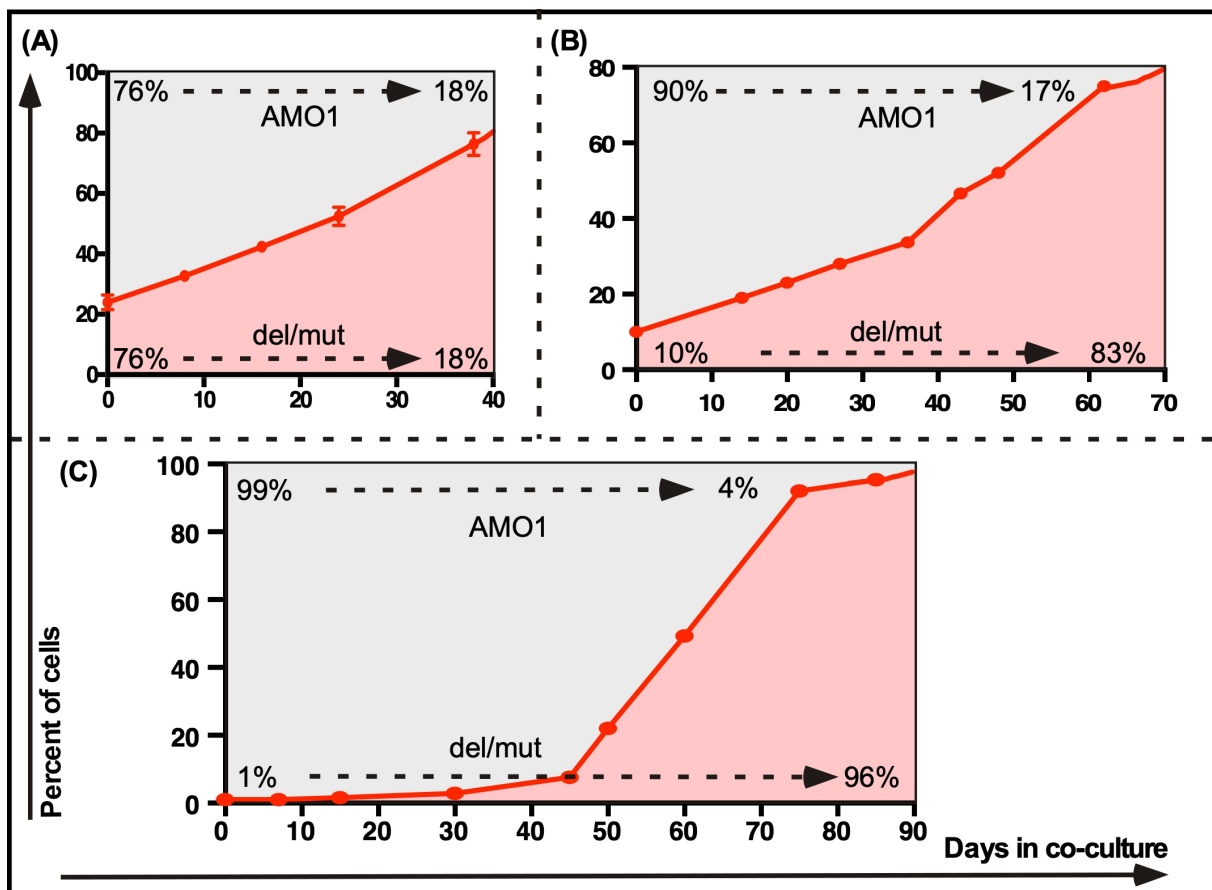
Figure 4.19: Clonal competition assay with varying initial clonal burden. *TP53* (del/mut) clone and wildtype AMO1 cells were mixed in different initial ratio 1:3 (A) 1:9 (B) and 1:99 (C) and were maintained in co-culture for the mentioned period of time. The culture was regularly monitored by flow cytometry to determine the relative number of both clones in the experiment.

These results demonstrated that the dynamics underlying the cell fitness competition were determined

by the initial amount of that particular clone present in the experiment. In the experiments with different initial clonal burdens, not only the time taken by the clone to dominate in the culture was different, but also the dynamics of the clonal growth. In the experiments with the higher initial clonal burden (25%), the growth pattern was linear, whereas with a very low initial clonal burden (1%), the clone showed a sigmoidal growth trajectory in the experiment. These results correspond to the mathematical models which describe the clonal progression in other cancers [102, 103].

4.12 Cells with no functional p53 have best fitness among p53 defective and wt cells

By now in different experiments, it was observed that cells with a double-hit to the p53 system had a fitness advantage over wildtype cells and cells with a single hit to the p53 system. To confirm this observation in a unified environment, a triple clonal competition assay was designed. The AMO1 cells (no color code) 90%, were mixed with *TP53* (wt/mut) cells (green) 5% and *TP53* (del/mut) cells (red) 5% in a single experiment. Normal cell culture was maintained and was regularly monitored by flow cytometry.

The results showed that initially both clones with a defective p53 system displayed superior fitness over the wildtype AMO1 cells, but with the passing of time, the double hit *TP53* clone showed superior fitness over both of the other clones and in the end dominated the culture (Figure 4.20). This further confirmed that proliferative fitness increases when one copy of *TP53* is affected but is further enhanced when both of the copies are defective.
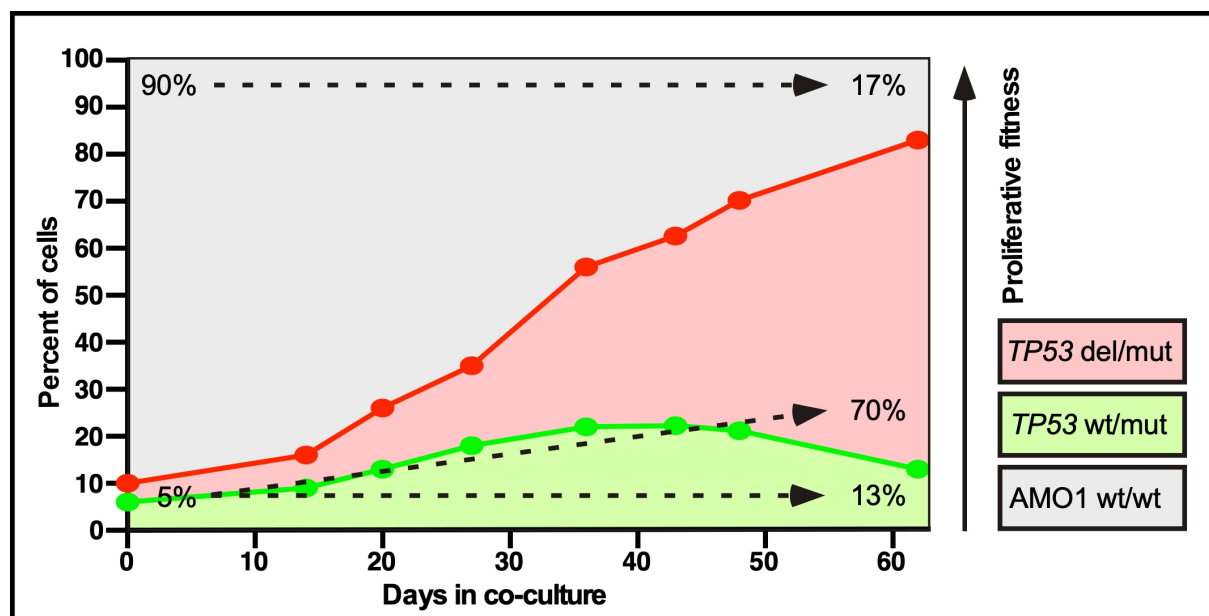
Figure 4.20: Triple clonal competition assay. Wildtype AMO1 cells 90% were mixed with *TP53* del/mut (red) and *TP53* wt/mut (green) cells 5% each. Cell culture was maintained and monitored regularly for the relative number of clones present in co-culture.

For the *TP53* del/del situation two different clones (Clones # 6 and 7) were tested, for del/mut and

wt/mut situations both mutations (R282W and R175H) were tested and results were reproduced with both clones and both mutants. This data set further illustrated the clinical drive towards the double hit *TP53* lesions seen in MM patients, by showing that increases in the proliferative fitness are influenced by the *TP53* status of the cells. Selection of the *TP53* double-hit clones over wildtype cells in the co-culture experiment was expedited in the presence of external selection pressure in the form of low dose melphalan.

This data set shown above became the part of the following publication. Munawar et al. Hierarchy of mono- and biallelic *TP53* alterations in multiple myeloma cell fitness, *Blood*, 2019.

4.13 *CUL4B* knock-out and determination of CRISPR-mediated genomic alterations

Genomic analysis from a colleague Dr. Santiago Barrio showed the increase in mutation frequency of the subunits of CRL4-CRBN complex [104]. This PhD work focused on one of the subunits of this protein complex, CUL4B. Two point mutations seen in *CUL4B* were selected to study their potential role in resistance against IMiDs. One of these *CUL4B* mutations R820S is a hotspot mutation, whereas, mutation D311H was found in an IMiD refractory patient in the mentioned analysis above. To functionally validate these mutations in a cell line, CRISPR/Cas9 and the sleeping beauty transposon vectors system were used.

The L363 cell line was selected as it is sensitive to IMiDs and has wildtype *CUL4B*. First of all, oligonucleotides were designed to target the exon 3 of *CUL4B* and cloned into the commercially available GeneArt CRISPR vector. L363 cells were electroporated with CRISPR vector and EGFP expression vector. The next day, positively electroporated cells were selected with CD4 microbeads and single green cells were plated in a 96 well plate (under fluorescent microscope) and were allowed to grow. After they had grown enough in number, they were screened for *CUL4B* knock out with Western blotting. Several clones were tested and 4 clones showed no expression of *CUL4B* as seen in Figure 4.21 (A).

Among these four clones, Clone # 3 and 4 were selected for further genomic analysis. To find the precise defect at the genomic level, PCR was performed using primers flanking target sequence of the guide RNA (used in CRISPR Vector). The PCR product was cloned into the pGEM-T easy vector and analyzed by Sanger sequencing. Sequencing results showed that in clone # 3, one allele of *CUL4B* had one bp insertion (A) which caused a frameshift and translation of a protein of only 121 amino acids in length (estimated size 12kDa). In the same clone, the second allele was also found to be affected by CRISPR/Cas9 and had a longer deletion of 124 bp causing the premature termination of translation potentially represented by a protein of 122 amino acids. This confirmed that clone #3 had both alleles of *CUL4B* affected by CRISPR/Cas9 (Figure 4.21 (B)).

The clone # 4 showed an insertion of one base pair (A) in all reads which caused the translation of a frame-shifted protein of only 121 amino acids in length. Since all the clones from T/A cloning showed a similar insertion, it was not possible to determine if both alleles had similar insertion or if one of the alleles has insertion and the other allele had deletion long enough that it did not get flanked by primers used in PCR. In either way there was no expression of CUL4B as analyzed by Western blotting (Figure

4.21 (B)). Clone # 3 was chosen for further functional analysis of mutations as the precise alteration of both alleles was known.
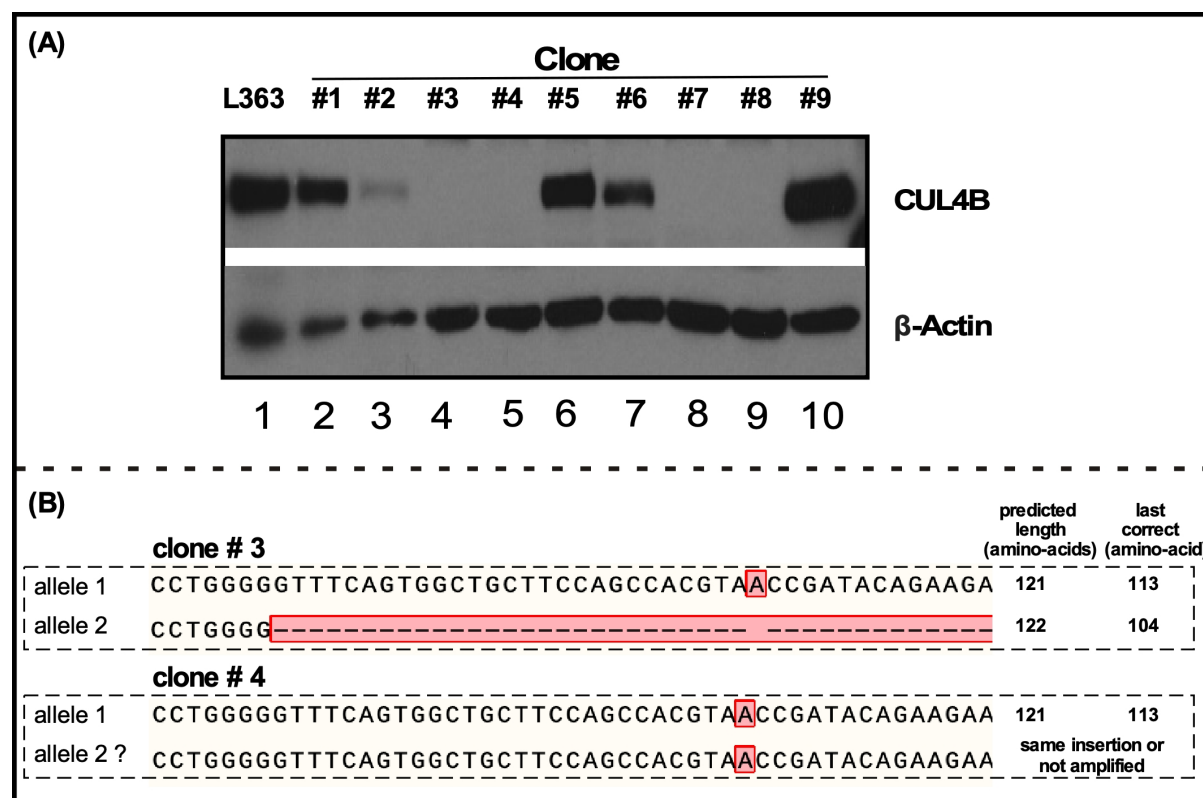
Figure 4.21: Analysis of L363 clones for *CUL4B* knockout. (A) Western analysis of L363 clones for expression of CUL4B. B-Actin acts as a loading control. (B) Analysis of CRISPR/Cas9-generated *CUL4B* alterations in AMO1 clones. Genomic DNA was used to amplify PCR products covering the CRISPR target region. PCR products were cloned in the pGEM®-T Easy vector. Several plasmid minipreparations were made and sequenced. Representative parts of each type of read are shown to indicate the CRISPR-induced defects in respective AMO1 clones. The predicted protein changes are indicated on the right side.

4.14 *CUL4B* plays a role in IMiD sensitivity

Next, the role of *CUL4B* was tested for IMiD sensitivity. Wildtype L363 cells were sensitive to lenalidomide treatment and showed viability of around 40% when treated for 5 days. The clone # 3 when treated with lenalidomide, showed resistance as compared to the wildtype cells and had nearly 75% viability after 5 days. The role of *CUL4B* in observed lenalidomide resistance/sensitivity was confirmed by a rescue experiment. Stable transposition of clone # 3 with sleeping beauty vector expressing wt CUL4B was performed. Exogenous expression of CUL4B in clone # 3 was marginally higher than the endogenous CUL4B expression in wildtype cells as seen in lanes 1, 5 and 6 in Figure 4.22 (A). Reintroduction of wildtype *CUL4B* reverted the lenalidomide sensitivity in otherwise IMiD resistant clone # 3 (Figure 4.22 (B)). This indicated the role of *CUL4B* in determining the lenalidomide response.
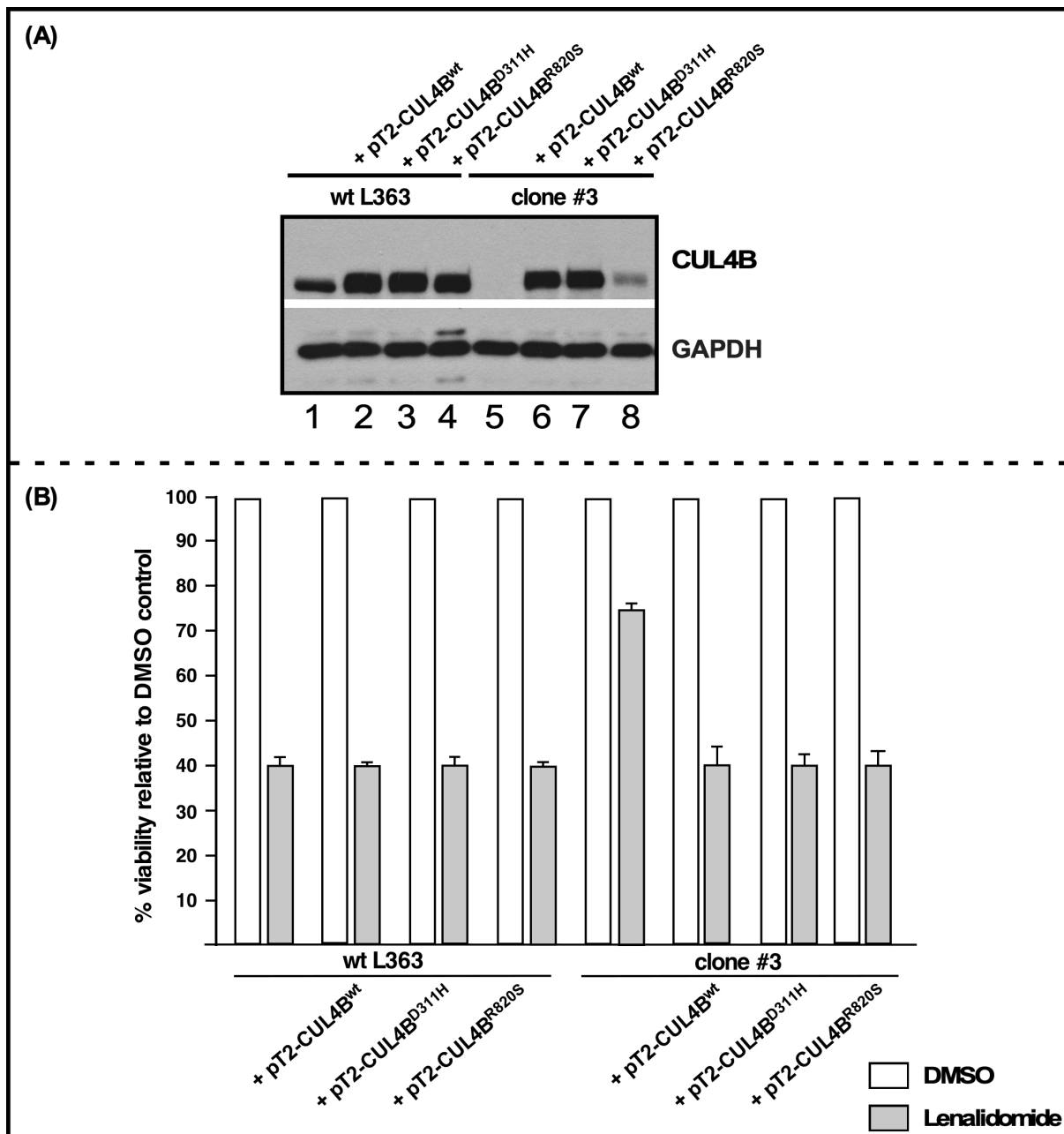
Figure 4.22: Analysis of sleeping beauty based *CUL4B* expression (wildtype and mutants) and its effects on lenalidomide resistance. (A) Western analysis of *CUL4B* wildtype and knocked out cells before and after the stable transposition of CUL4B wt and mutants expressing sleeping beauty vectors. (B) L363 and clone # 3 expressing different CUL4B variants were treated with 10 µM lenalidomide or equivalent DMSO concentration. Alamarblue assay was performed after 5 days of drug treatment. Data represents 2 independent experiments and error bars depict S.D

Both mutants of *CUL4B* were expressed in wildtype L363 cells and clone # 3. As seen in (lane 2, 3 and 4) Figure 4.22 (A) all three variants when expressed in wildtype L363 increased the overall CUL4B level in the cells. This exogenous expression did not cause any differences in response to lenalidomide in wildtype cells. Higher expression of wildtype CUL4B in L363 cells did not increase the lenalidomide sensitivity, expression of mutants did not act as dominant negativity and did not cause lenalidomide resistance as seen in Figure 4.22 (B).

Next, the role of mutant CUL4B was tested in maintaining the acquired resistance in clone # 3.

Mutant D311H showed good expression in Western analysis, whereas mutant R820S showed lower levels of protein, even though both mutants were being expressed from a similar promotor (CMV) (Lane 7 and 8) Figure 4.22 (A). In clone # 3, *CUL4B* deletion-acquired resistance was reverted to sensitivity with expression of both mutants of CUL4B as seen in Figure 4.22 (B).

It indicated that D311H and R820S were not providing any resistance/fitness against lenalidomide treatment and were most likely not functionally linked to relapse condition. This data set suggested that *CUL4B* as a whole protein was important for anti-myeloma activity of lenalidomide, but mutations seen in those patients did not seem to have importance towards lenalidomide resistance, reducing the potential importance of mutations seen in *CUL4B* in patients treated with lenalidomide for therapeutic guidance.

4.15 *CUL4B* K.O. provides negative fitness to cells in the absence of lenalidomide

A clonal competition assay was designed to study the long term fitness advantage of clone # 3 over wildtype L363 cells. The cells were transposed with EGFP or RFP expression vector and mixed in a 9:1 ratio for CCA in the presence or absence of a low dose of lenalidomide, 2.5 μM. In the presence of external selection pressure in the form of lenalidomide, clone # 3 was selected over the wildtype L363 cells, whereas, in the absence of lenalidomide such fitness was not seen (Figure 4.23 (A)). These results were confirmed in a CCA set with different initial ratios between cells. Wildtype L363 and clone # 3, were mixed in a 1:1 ratio in the absence of lenalidomide. L363 cells showed superior fitness to clone # 3 and dominated the culture initially but after the addition of lenalidomide in the same experiment on day 21, clone # 3 gained an advantage over L363 cells and was selected for. It eventually dominated the culture as seen in Figure 4.23. These results indicated that *CUL4B* was important for the cells to provide sensitivity against lenalidomide and cells without *CUL4B* had an advantage in the presence of lenalidomide. But in the absence of any selective pressure clones with defective *CUL4B* may disappear, as CUL4B must be required for other physiological functions in the cell.

These results suggest that treatment-driven alterations may provide fitness only in the presence of the treatment. If such alterations involve genes required for some other essential function in cells, this may act as negative contribution to fitness, as these cells will only be favored in the presence of selection pressure and may disappear once the drug is withdrawn.
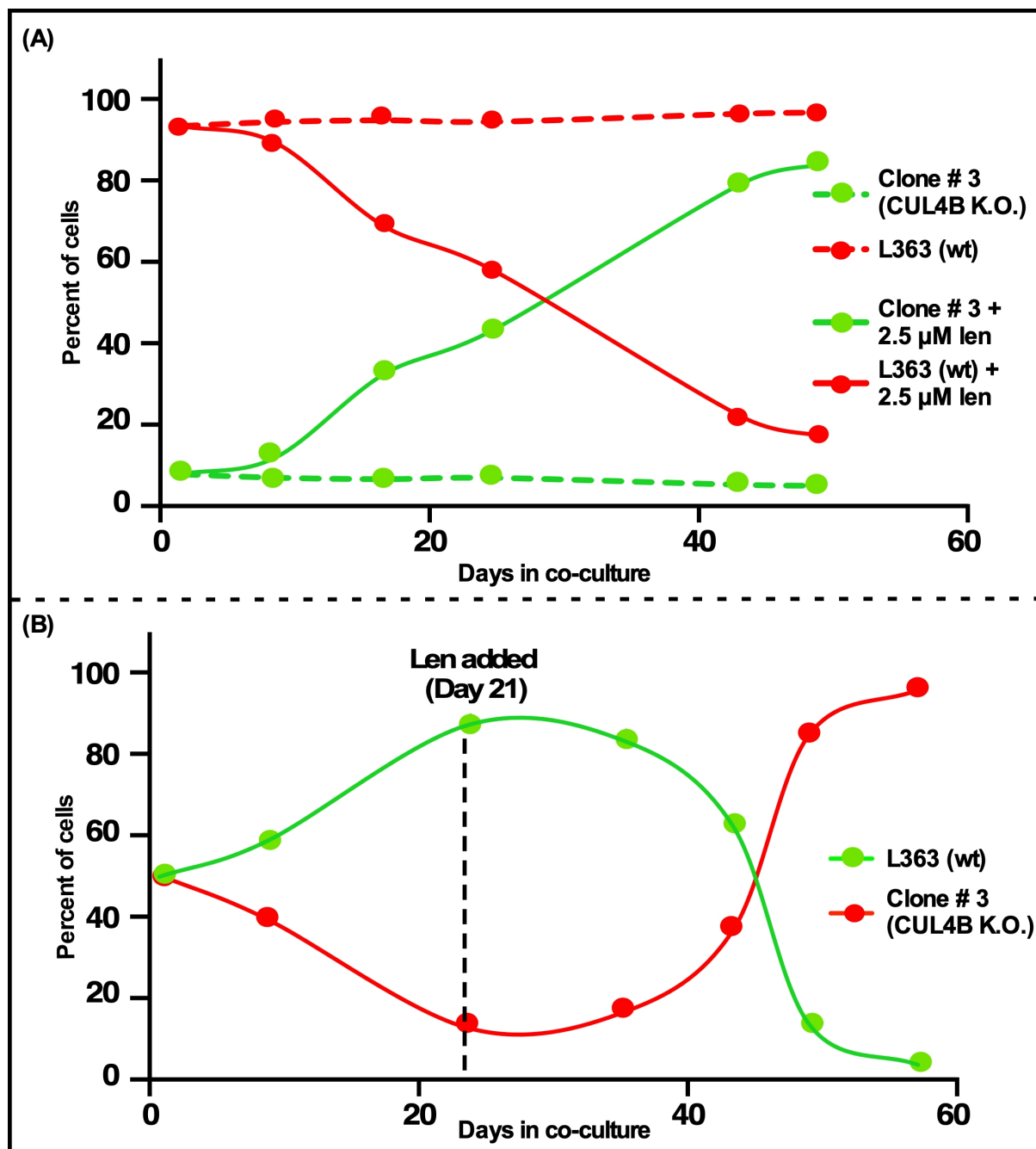
Figure 4.23: A clonal competition assay of wildtype L363 cells and clone # 3 (*CUL4B* K.O.). (A) Clonal competition was set between wildtype and knocked out cells in the presence or absence of a sublethal concentration of lenalidomide (2.5 µM). The cell culture was split regularly and drug concentration was maintained after every split. (B) Clonal competition assay was set with an initial 1:1 ratio between wildtype and clone # 3 cells. Cell culture was maintained and monitored regularly and 2.5 µM lenalidomide was added at day 21 and maintained till the end of experiments.

These data suggest that treatment driven alterations seen in the patient should be monitored regularly. Because if they provide fitness under treatment, a clone harboring these alterations may get selected during therapy. But at the same time if similar alterations provide negative fitness in the absence of treatment there is theoretical reason for these clones to disappear when treatment is discontinued. So regular monitoring of mutations/alterations in patients is recommended. This data set focusing on one protein of CRL4 complex along with other proteins of the same complex became the part of publication,

Barrio et al. IKZF1/3 and CRL4-CRBN E3 ubiquitin ligase mutations and IMiD resistance in multiple myeloma, *haematologica*, 2019. which focused on the importance of mutations found in IMiD refractory patients.

Chapter 5

Discussion

Despite the development of the novel therapies, MM remains generally incurable. MM is known to display complex genetic heterogeneity [59, 60] and various types of genetic alterations are known to be present already at diagnosis and with more acquired during disease progression [73, 74]. These genetic lesions are involved in determining high-risk features and have potential role in drug resistance mechanisms [57, 50, 51]. The current work focused on the functional characterization of various genetic lesions found in MM patients, particularly aberrations found in the *TP53* gene mono- and biallelic alterations. Furthermore, this study also analyzed the role of *CUL4B* and its mutations in IMiD refractory MM patients.

Patients with genetic lesions affecting tumor suppressor gene *TP53* form the poor prognosis/high-risk group. Both alleles of *TP53* are affected most commonly by the combination of deletion and point mutation [84, 80]. During the course of the disease, a switch into a high-risk class is often seen in patients, which acquire de novo first hit to p53 or/and progress from single hit to double hit arrangement [58, 87, 89]. As it has been shown (Figure 1.5) that these single and double hits to the *TP53* gene accrue during disease progression, it suggests that clones that harbor single hit to the *TP53* gene may have selection advantage and acquisition of a second hit further enhances the fitness and leads toward the intractable malignancy. Since these *TP53* single and double hit clones emerge and accumulate over the course of the disease, this current work evaluates the main types of *TP53* lesions detected in MM patients within the frame of a single isogenic MM cell line model, to analyze their impact on the functionality of p53 system and their potential role for resistance against anti-myeloma drugs.

Lack of p53 expression from one of the alleles is considered 'single hit' and mainly, two types of single hits can be found in MM. In the deletion-first scenario, one copy of the *TP53* allele is lost as a consequence of del 17p and it is found to be associated with haploinsufficiency [83]. The role of other genes present in the deleted region of chromosome 17 is not fully ruled out but the presence of *TP53* gene in minimally deleted region endorse the role of *TP53* but its functional aspect remains unexplained [81]. The second type of single hit is 'mutation-first scenario' in which one of the two *TP53* alleles has a point mutation and the other allele is wild type. This situation can be associated with dominant negativity [105] or in some cases gain of function attributes [106, 107]. The splice-site mutations can also be associated with no protein expression from one allele. There are two possible double hit scenarios; no expression of p53 in the case of both *TP53* alleles deleted (-/-) and overexpression of only mutant p53 protein in *TP53* deleted background (del/mut).

MM cell lines do not exactly represent these 'single hit' *TP53* genomic alterations. For instance, cell line JJN3 is hemizygous at the genomic level (one wild type and one deleted *TP53* allele) but phenotypically does not express p53, indicating that the wildtype *TP53* allele is kept silent somehow

[83]. MM cell lines representing wt/del and wt/mut scenario do not exist. Therefore, the AMO1 cell line was chosen to modelize the mentioned constellations of *TP53*. AMO1 cell line contains both wild type alleles of *TP53* and is shown to have a functional p53 system assessed by Nutlin 3a treatment, hence, by using the combination of techniques, CRISPR/Cas9 and sleeping beauty transposon-based expression system all genomic alterations could be represented within a framework of a single cell line. Using a single cell line, instead of different cell lines, excludes the influence of coexisting genetic and epigenetic alterations present in different cell lines. Understandably, since no single cell line can represent all aspects of MM patients, this work shows that AMO1 cell line is a dynamic model system to analyze and evaluate functional and pharmacological consequences of these alterations seen in the *TP53* status. This model system with clonal competition assay has demonstrated that these single and double hits have the potential to provide protection against genotoxic drugs and can contribute overall proliferative fitness to these *TP53* defective clones.

In the AMO1 cell line, after targeting *TP53* with CRISPR/Cas9, it was possible to screen for p53 defective clones with the help of WB and subsequent Sanger sequencing to confirm the status of *TP53* alleles in potentially defective clones. Non-homologous end joining repair (NHEJ) after CRISPR-induced double strand breaks caused frameshifts in the target sequence, which resulted in the disruption of *TP53* alleles and in some cases frameshift mutations even resulted in the expression of a stable p53 derivative but with corrupted C-terminal domain. In vivo inactivation of a *TP53* allele in the 'deletion-first scenario´ takes place by a different mechanism than frameshift induced by CRISPR. In a deletion-first scenario one allele of *TP53* is inactivated as a consequence of the deletion of a part of the p-arm of chromosome 17. *TP53* has been shown to be a part of the minimally deleted region and identified as a relevant gene and del 17p, therefore results in complete loss of the contribution of one allele to p53 protein expression [82]. In the current AMO1 cell line model, the CRISPR/Cas9 mediated *TP53* lesions, though limited to a comparatively minimal area of the genome, resulted in no contribution to p53 protein from one allele (thus approximating the consequences of del 17p) and opposed to strong overexpression of mutant p53 in the mutation-first scenario).

p53 system functionality of four different hemizygous clones (one *TP53* allele defective) was tested (clone # 2-5). These clones when treated with the MDM2 inhibitor Nutlin 3a and showed severely restricted p53 responses as compared to the wild type cells. Their response to genotoxic drugs was also strongly attenuated. Levels of p53 and its transcriptional targets MDM2 and p21 were not induced significantly. Variability in the intensity of the response among the four tested clones was observed and these differences were possibly based on the specific changes/frameshifts induced by NHEJ. Even though differences among different clones were seen, in general all clones had fairly attenuated p53 function and impaired response to genotoxic drug as compared to wild type cells. To rule out the possibility of clonal effects of individual clones, more than only one hemizygous clones were used in this study.

Several CRISPR-generated *TP53* double deleted/affected clones were tested for p53 functionality and they all showed complete abrogation of p53 expression/function. Their response to genotoxic drugs was even further impaired than in hemizygous clones. Sleeping beauty-based expression of wt p53 cDNA genes (pT2-p53^wt) was performed in several of the *TP53* double deleted clones in order to reinstate the

p53 system functionality. The function of p53 was not recovered in clones # 8 and 9 after exogenous expression of wt p53. Possibly p53 system components were damaged to the extent that it could not be reinstated. They showed the expression of exogenous p53 in Western analysis but did not integrate p53 in normal functioning system as they did not show significant changes in expression of p53 responsive proteins: MDM2 and p21. Conversely, pT2-p53^{wt} stable transposition reinstated the normal p53 function in clones # 6 and 7 as indicated by Western analysis and they attained back the Nutlin sensitivity. As different clones show different responses to exogenous wt p53 expression, it indicates that all AMO1 clones are not equal. Different types of CRISPR-induced alterations in both alleles could be potential underlying reason for such variability. In the end two workable clones (# 6 and 7) could be used as a good model to analyze the p53 system and to emulate other MM specific *TP53*/p53 constellations.

Reestablishment of the p53 system in *TP53-/-* clones was found to be a transient feature, as cells tend to lose the p53 expression and normal function gradually after stable transposition with pT2-p53^{wt}. Exogenous expression of wt p53 in cells that were endogenously devoid of p53 was not favored as the polyclonal culture was found to lose the acquired Nutlin sensitivity over time. Whether the expression of wt p53 is reduced in all cells of the culture or cells with relatively lower p53 expression are selected over time, is not clear. As the selected culture is polyclonal in nature, it may contain sufficient cells which initially received a relatively lower amount of plasmid and had in general lower expression of wt p53, and those cells over the time got selected over the cells which had received initially higher amount of plasmid and had higher p53 expression, high enough that they could not cope with it over time and slowly died, or the cells over time found a way to reduce the expression of wt p53 and ultimately shut it down, as these clones were normally growing without any check from p53 and exogenous p53 expression was not favorable for them in long run. Conversely, this transient feature was not observed with transposition of mutant *TP53*, cells maintained the overexpression of mutant p53 protein over long time. Therefore, a particular time-window of 10-14 days after stable transposition with wt p53 expressing vectors were used to set up experiments for testing different drugs on these clones.

In the mutation-first scenario, an equal expression from both alleles is expected. To emulate the mutation first scenario; a double cassette vector system was constructed to express two independent genes simultaneously at an equal level. pT2-p53^{wt/R175H} was transiently expressed in JJN3 cells and cDNA was prepared using a primer which could only amplify vector expressed genes. Sanger sequencing of amplified PCR product from cDNA showed equal peaks on the mut/wt base, implying the presence of equal mRNA level of both variants of p53 expressed from the vector.

Two different *TP53 -/-* clones (clone # 6 and 7) were subjected to sleeping beauty transposon-based expression of two individual copies of *TP53* cDNA, one wt copy and one mutant copy. Two different *TP53* hotspot mutations; R175H and R282W were tested and an attenuated response of the p53 system was observed after treatment with MDM2 inhibitor Nutlin 3a with the help of Western analysis and cell death assay. Impaired functionality of p53 seen in clones representing heterozygous *TP53* mutations was roughly on a par to the p53 function seen in hemizygous clones, implying that both types of single hit situations were functionally comparable and had abrogated p53 system compared to the wild type cells.

The current work focused on both possibilities of 'double hit' scenarios; no expression of p53 in the

case of both *TP53* alleles deleted (-/-) scenario and overexpression of only mutant p53 protein in *TP53* deleted background (del/mut) scenario. No functional p53 response was seen in all four -/- clones (clone # 6-9). In the case of clones # 6 and 7, a smaller size band of p53 was seen on WB, as predicted by Sanger sequencing/genomic analysis. The expressed variant of p53 in these clones must have corrupted C-terminal, and no downstream signaling was seen in Western analysis (MDM2 and p21). For clone #7, genomic analysis showed that all the clones sequenced after T/A cloning in pGEM®-T easy vector had similar insertion. That means that either both of the alleles have same nucleotide insertion at same position, which theoretically is possible but not very likely to happen or one of the alleles had deletion so long that primers used for PCR amplification from genomic DNA did not flank the whole deleted region and it did not get amplified at all and no clone for the second allele was seen. Either way, no function of the p53 system was seen in clone # 7 by western analysis. To avert the clonal effects of individual single cell derived clone two different -/- clones (clone # 6 and 7) were used for emulation of other *TP53* constellations. Current work indicated that p53 system in both double hit scenarios was completely abrogated and cells showed no response to the Nutlin treatment in the Western and cell survival analysis. Reinstatement of the p53 system after expression of two copies of wt *TP53* in -/- clones, entrenched the fidelity of the AMO1 models.

Next, the response to genotoxic drugs was tested on these different models and data showed that both types of single hit representing scenarios (deletion-first and mutation-first) had identically defective response towards melphalan. *TP53* -/- clones transposed with pT2-p53$^{\mathrm{wt/R175H}}$ or pT2-p53$^{\mathrm{wt/R282W}}$ had similar responses to genotoxic drugs like *TP53* hemizygous clones. Moreover, this resistance to genotoxic drugs was still further enhanced in the case of both double hit scenarios. However, these different models showed no variation in response against tested proteasome inhibitors.

These single *TP53* lesions were shown to provide proliferative advantage/survival fitness when tested with the clonal competition assay. Single *TP53* hit clones showed fitness over wildtype cells and this fitness was further enhanced in case of biallelic *TP53* alterations. Indicating that the defective p53 system provides fitness against genotoxic drugs and provide proliferative advantage even in the absence of the drugs. This provided the first evidence that the increase in the clones with altered *TP53* in relapsed MM is driven by increased proliferative advantage of these clones and can be independent of any selective pressure from therapy or microenvironment.

These results explain the rise of clones with monoallelic *TP53* alterations by accentuating the gains in proliferation fitness and drug resistance, that potentially arise from single *TP53* lesions. Furthermore, it underlines the importance of the second hit to the p53 system which further increases the survival potential of single hit AMO1 cells and coincides with the clinical drive from monoallelic to biallelic inactivation of *TP53* in MM (Figure 5.1). The quickest course to the expansion of relentless MM clones is probably by complete abrogation of the p53 system in the form of a biallelic hit to the *TP53*. Moreover, these results support the idea that in the deletion 17p scenario it is particular hit to the *TP53* gene that is liable to the poor clinical outcome and spread of intractable clones in MM.

As indicated by our experiments, if the functional consequence of both types of mono-allelic *TP53* alterations (deletion-first in the form of del 17p or mutation-first in the form of point mutation in one

allele) is similar and biallelic *TP53* hit is the most favored outcome then clinical drive towards double-hit situation and selection of biallelic *TP53* lesions (del 17p and mut) is plausible. If the cell gets the first hit in the form of del 17p then it is not suitable for the cell to have a second hit as a deletion because it will result in biallelic loss of other genes present in the minimally deleted region and this may not happen to be a very favourable case for the cell. Therefore, the second hit in the form of a point mutation in *TP53* is the most likely event in this case. This sequence of alterations could be observed in a patient sample analysed using M³P sequencing panel (NGS) by Dr. Santiago Barrio. In Figure 5.1 it can be seen that in germline, patient 2 has wt *TP53*. At time point 1, the patient lost one allele of *TP53* in tumor cells as a consequence of del 17p, detected by FISH. Later, at time point 2, myeloma cells from this patient showed a point mutation in *TP53* (T163C) in 88% of the sequencing reads, implying that a subclone has evolved and already dominates the tumor which has fully inactivated *TP53*. This NGS analysis on patient 2 confirmed the drive towards the double hit, in which the patient first lost one copy of *TP53* as a result of del 17p and inactivated the second *TP53* allele by point mutation.
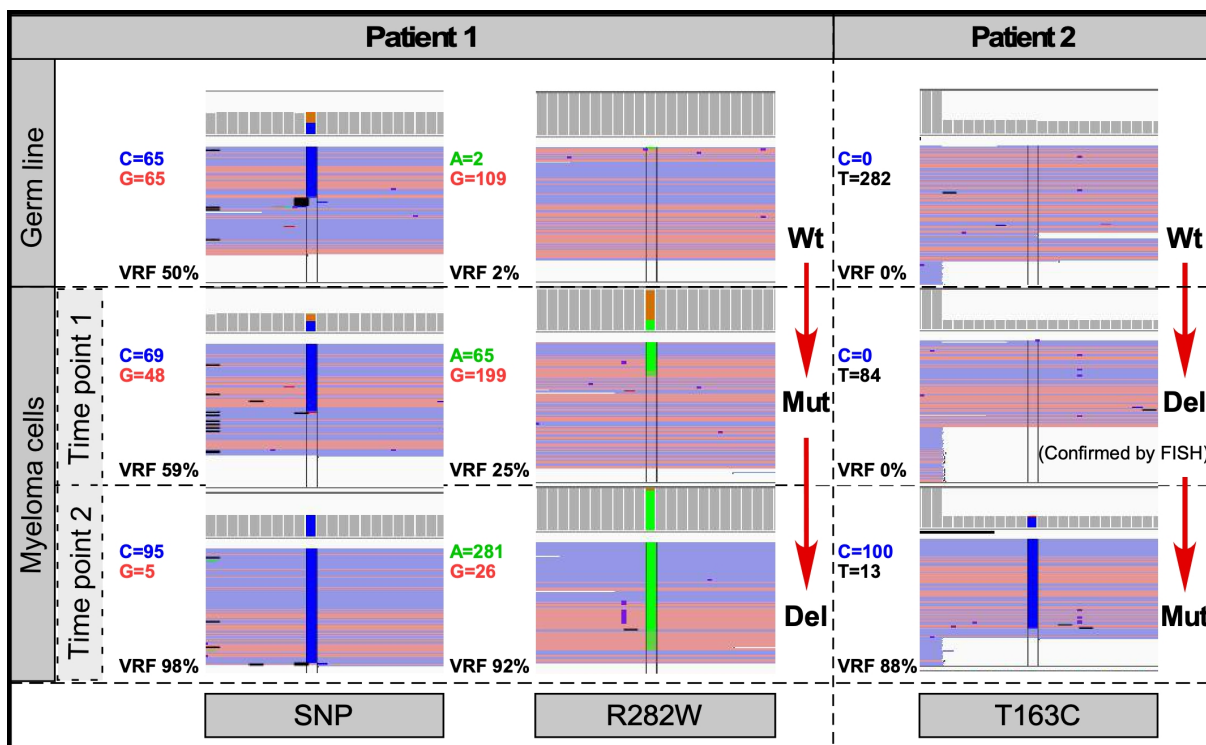
Figure 5.1: Next generation sequencing (NGS) of two MM patients at different time points during treatment using M³P sequencing panel [108]. Excerpts of the sequencing analysis focus on different regions of *TP53* gene in 2 different patients at different time points. Binary alignment map (BAM) files were visualized in integrated genomics viewer (IGV) and sequencing reads were aligned to hg19.

Furthermore, if the first hit to the *TP53* gene is a point mutation, it often is followed by the del 17p as a second hit, as cells with both alleles of *TP53* mutated or deleted are not seen frequently. A similar scenario was also observed in a patient analysed with NGS (using M³P sequencing panel [108]) as seen in Figure 5.1. In germ line, patient 1 does not show mutation R282W and has two alleles of *TP53* as seen from 50% variable read frequency (VRF) of a single nucleotide polymorphism (SNP). At time point 1, patient 1 developed a mutation, which seemed heterozygous in nature. Later, at time point 2, patient

1 completely lost the wildtype *TP53* allele, as seen in the SNP panel and had a VRF of more than 90% for the acquired mutation (R282W), which essentially indicates clonality. This is a good illustration of how a patient who acquired a first hit to *TP53* as a mutation, develops a second hit as a deletion, as attaining another specifically targeted change (in the form of point mutation) in *TP53* must be difficult as compared to losing a fairly unspecified part of chromosome 17. These observation made with NGS of patients samples follow the notion of attaining double hits to the p53 system by sequential acquisition of mutations and deletion (sequence may vary based on the type of first hit).

With the precise molecular diagnostics, it is possible now to monitor the presence or rise of the MM subclones with single or double hits and this information could be used for retrospective analysis to better understand the precise genetic feature responsible for poor clinal outcome in MM patients with defects in *TP53*. Therefore, for a longterm perspective there is a need to conduct studies with particular focus on monitoring the number of *TP53* defective clones because such studies can help us answer some eminent questions. Such as, if a person showing single hit clones should not be treated with genotoxic drugs anymore to reduce the risk of developing a second hit or when such single hit clones are seen in the patient, is it wise to use rather more powerful combination therapy to completely get rid of such clones and so to reduce the chance of attaining the second hit by eliminating single hit clones completely. If studies particularly focus on the genomic status of *TP53* of emerging clones, over time information would be gained to answer these crucial questions and this data provides a rationale to include monitoring of the *TP53* status in the MM cell population that emerges as remission fails, and, if a single or double-hit disease clone is detected, to consider extensive measures aimed at subduing or eradicating such subclones.

Conversely, MM cells are well adept at developing resistance against novel therapies irrespective of the *TP53* status. In recent studies we and others have shown the increase in the mutation incidence rate in CRL4 protein complex subunits; CRBN, IKZF1/3 and CUL4B [55, 104]. Mutations have been found to be present in binding domains of DDB1, near the binding domain in ROC1, IMiD and DDB1 binding region of CRBN. The focus of the current work was on one of the subunits of CRL4 complex, CUL4B, which is found to be mutated in 3% of the pretreated patients [104]. Since there was an increase in the incidence of mutations in IMiD treated patients it was hypothesized that these mutations could be responsible for causing IMiD resistance. L363 cell line was chosen to functionally analyze these mutations, as they are sensitive to IMiDs such as lenalidomide. These cells provided ease of use, good transfection and purification efficiency. The cells were subjected to CRISPR/Cas9 mediated destruction of *CUL4B* and several *CUL4B* knock out clones were generated and genomic analysis confirmed the aberrations *CUL4B* in clone # 3. In most of the other clones an insertion of adenosine (A) was seen, and this lesion was identical in all clones, so it was not clear if this represents some type of artefact. Clone #3 was used for the functional characterization of patient-specific mutations.

Cells with *CUL4B* knockout were found to be resilient to lenalidomide treatment as compared to the wildtype L363 cells and this resistance was overcome by the reintroduction of *CUL4B* wt using sleeping beauty transfections, implying the role played by *CUL4B* in lenalidomide sensitivity. This *CUL4B* knock out-acquired resistance effect was confirmed with CCA, in which lenalidomide exposure particularly selected for the *CUL4B* knocked out clones. Two different patient-specific point mutations

(D311H, R820S) were tested in this study and it was found that reintroduction of both point mutations reinstated the sensitivity against lenalidomide, indicating that these mutations had no role to play in lenalidomide resistance. *CUL4B* mutant R820S did not show high expression in the cells as its levels were not comparable to wildtype *CUL4B*, still it was able to revert lenalidomide resistance. This confirmed the role of *CUL4B* in the anti-myeloma activity of IMiDs.

The CCA showed that in the presence of lenalidomide the *CUL4B* K.O. clone was selected over wild type cells, this observation was in accordance with the result that cells acquire resistance against lenalidomide when devoid of *CUL4B* protein. Clonal dynamics of *CUL4B* K.O. clones became clear when wt and knock out cells were tested with equal starting numbers in CCA and clone # 3 showed negative selection in the absence of lenalidomide but the addition of lenalidomide after several days promoted the *CUL4B* knock out clone, which was initially selected against in the absence of any drug. These experiments imply that under therapy exposure, clones with certain aberrations can be selected, but in case of therapy withdrawal, these clones may disappear again. As *CUL4B* must be required for normal physiological activity of the cell, knocking it out is not a favorable outcome (as opposed to *TP53*, where knocking it out is a favored outcome for cancer cells) in the absence of external lenalidomide therapy and cells devoid of endogenous *CUL4B* expression (or lower expression level) may not be selected (if generated). Whereas in the presence of therapy (selection pressure) these clones are selected as they survive better in the presence of lenalidomide, but in the case that therapy is discontinued they may disappear again, as these acquired alterations provide negative fitness in the absence of selection pressure.

There is a clinical need for the close monitoring of such altered clones that arise during the course of treatment. With the precise molecular diagnostics, it is now possible to monitor generation, rise and dynamics of clones during the course of the disease. Assessment of the arising or established clones that may have positive fitness (*TP53* single/double hit clones) or negative fitness (*CUL4B* negative clones) provided by genomic alterations in patients can, in the long run, guide the therapy approach towards this unfavored group of patients. Functional validation of acquired mutations is desirable, as it can clarify the positive or negative role imparted by them and this information can be helpful in some clinical decisions, for example, considering alterations discussed in the current study, if clones with *TP53* alterations are detected, it is an indication that they will be resilient to genotoxic drugs (as shown by functional validation in the current study) so use of genotoxic drugs may be discontinued as it can potentially expedite the selection of these clones, or if *CUL4B* mutant clones are detected, they may not impact the therapy decisions as they were shown not to be involved in lenalidomide resistance. Therefore, a close monitoring of arising clones in MM patients, and functional validation of the acquired alterations is desirable for better clinical decisions for the MM patients.

Bibliography

[1] R. A. Kyle and S. V. Rajkumar, "Multiple myeloma," *New England journal of medicine*, vol. 351, no. 18, pp. 1860–1873, 2004. PMID: 15509819.

[2] A. J. Cowan, C. Allen, A. Barac, H. Basaleem, I. Bensenor, M. P. Curado, K. Foreman, R. Gupta, J. Harvey, H. D. Hosgood, *et al.*, "Global burden of multiple myeloma: a systematic analysis for the global burden of disease study 2016," *JAMA oncology*, vol. 4, no. 9, pp. 1221–1227, 2018.

[3] R. A. Kyle, M. A. Gertz, T. E. Witzig, J. A. Lust, M. Q. Lacy, A. Dispenzieri, R. Fonseca, S. V. Rajkumar, J. R. Offord, D. R. Larson, *et al.*, "Review of 1027 patients with newly diagnosed multiple myeloma," in *Mayo clinic proceedings*, vol. 78, pp. 21–33, Elsevier, 2003.

[4] R. Silbermann and G. D. Roodman, "Myeloma bone disease: pathophysiology and management," *Journal of bone oncology*, vol. 2, no. 2, pp. 59–69, 2013.

[5] A. Bouchnita, N. Eymard, T. K. Moyo, M. J. Koury, and V. Volpert, "Bone marrow infiltration by multiple myeloma causes anemia by reversible disruption of erythropoiesis," *American journal of hematology*, vol. 91, no. 4, pp. 371–378, 2016.

[6] Y. Beguin, "Erythropoiesis and erythropoietin in multiple myeloma," *Leukemia & lymphoma*, vol. 18, no. 5-6, pp. 413–421, 1995.

[7] T. O'Connell, T. J. Horita, and B. Kasravi, "Understanding and interpreting the serum protein electrophoresis," *American family physician*, vol. 71, no. 1, pp. 105–112, 2005.

[8] M. Mackenzie, K. Wuepper, G. Jordan, and H. Fudenberg, "Rapid renal failure in a case of multiple myeloma: the role of bence jones proteins," *Clinical and experimental immunology*, vol. 3, no. 6, p. 593, 1968.

[9] C. Blimark, E. Holmberg, U. Mellqvist, O. Landgren, M. Björkholm, M. Hultcrantz, C. Kjellander, I. Turesson, and S. Y. Kristinsson, "Multiple myeloma and infections: a population-based study on 9253 multiple myeloma patients," *Haematologica*, vol. 100, no. 1, pp. 107–113, 2015.

[10] M. A. Gertz and R. A. Kyle, "Hyperviscosity syndrome," *Journal of intensive care medicine*, vol. 10, no. 3, pp. 128–141, 1995.

[11] M. Hallek, P. L. Bergsagel, and K. C. Anderson, "Multiple myeloma: increasing evidence for a multistep transformation process," *Blood*, vol. 91, no. 1, pp. 3–21, 1998.

[12] G. Merlini and G. Palladini, "Differential diagnosis of monoclonal gammopathy of undetermined significance," *Hematology 2010, the American society of hematology education program book*, vol. 2012, no. 1, pp. 595–603, 2012.

[13] R. A. Kyle, T. M. Therneau, S. V. Rajkumar, J. R. Offord, D. R. Larson, M. F. Plevak, and L. J. Melton III, "A long-term study of prognosis in monoclonal gammopathy of undetermined significance," *New England journal of medicine*, vol. 346, no. 8, pp. 564–569, 2002.

[14] R. A. Kyle, T. M. Therneau, S. V. Rajkumar, E. D. Remstein, J. R. Offord, D. R. Larson, M. F. Plevak, and L. J. Melton III, "Long-term follow-up of igm monoclonal gammopathy of undetermined significance," *Blood*, vol. 102, no. 10, pp. 3759–3764, 2003.

[15] R. A. Kyle, D. R. Larson, T. M. Therneau, A. Dispenzieri, S. Kumar, J. R. Cerhan, and S. V. Rajkumar, "Long-term follow-up of monoclonal gammopathy of undetermined significance," *New England journal of medicine*, vol. 378, no. 3, pp. 241–249, 2018.

[16] R. G. Owen, S. P. Treon, A. Al-Katib, R. Fonseca, P. R. Greipp, M. L. McMaster, E. Morra, G. A. Pangalis, J. F. San Miguel, A. R. Branagan, *et al.*, "Clinicopathological definition of waldenstrom's macroglobulinemia: consensus panel recommendations from the second international workshop on waldenstrom's macroglobulinemia," in *Seminars in oncology*, vol. 30, pp. 110–115, Elsevier, 2003.

[17] S. V. Rajkumar, D. Larson, and R. A. Kyle, "Diagnosis of smoldering multiple myeloma," *New England journal of medicine*, vol. 365, no. 5, p. 474, 2011.

[18] W. M. Kuehl and P. L. Bergsagel, "Multiple myeloma: evolving genetic events and host interactions," *Nature reviews cancer*, vol. 2, no. 3, pp. 175–187, 2002.

[19] P. L. Bergsagel and W. M. Kuehl, "Chromosome translocations in multiple myeloma," *Oncogene*, vol. 20, no. 40, pp. 5611–5622, 2001.

[20] A. M. Roccaro, A. Sacco, B. Thompson, X. Leleu, A. K. Azab, F. Azab, J. Runnels, X. Jia, H. T. Ngo, M. R. Melhem, *et al.*, "Micrornas 15a and 16 regulate tumor proliferation in multiple myeloma," *Blood*, vol. 113, no. 26, pp. 6669–6680, 2009.

[21] P. L. Bergsagel and W. M. Kuehl, "Molecular pathogenesis and a consequent classification of multiple myeloma," *Journal of clinical oncology*, vol. 23, no. 26, pp. 6333–6338, 2005.

[22] R. Fonseca, B. Barlogie, R. Bataille, C. Bastard, P. L. Bergsagel, M. Chesi, F. E. Davies, J. Drach, P. R. Greipp, I. R. Kirsch, *et al.*, "Genetics and cytogenetics of multiple myeloma," *Cancer Research*, vol. 64, no. 4, pp. 1546–1558, 2004.

[23] W. J. Chng, S. A. Van Wier, G. J. Ahmann, J. M. Winkler, S. M. Jalal, P. L. Bergsagel, M. Chesi, M. C. Trendle, M. M. Oken, E. Blood, *et al.*, "A validated fish trisomy index demonstrates the hyperdiploid and nonhyperdiploid dichotomy in mgus," *Blood*, vol. 106, no. 6, pp. 2156–2161, 2005.

[24] K. K. Jovanović, G. Escure, J. Demonchy, A. Willaume, Z. Van de Wyngaert, M. Farhat, P. Chauvet, T. Facon, B. Quesnel, and S. Manier, "Deregulation and targeting of *TP53* pathway in multiple myeloma," *Frontiers in oncology*, vol. 8, p. 665, 2019.

[25] S. Solly, "Remarks on the pathology of mollities ossium; with cases," *Medico-chirurgical transactions*, vol. 27, p. 435, 1844.

[26] J. F. Holland, H. Hosley, C. Scharlau, P. P. Carbone, E. Frei Iii, C. O. Brindley, T. C. Hall, B. I. Shnider, G. L. Gold, L. Lasagna, *et al.*, "A controlled trial of urethane treatment in multiple myeloma," *Blood*, vol. 27, no. 3, pp. 328–342, 1966.

[27] N. Blokhin, L. Larionov, N. Perevodchikova, L. Chebotareva, and N. Merkulova, "Clinical experiences with sarcolysin in neoplastic diseases," *Annals of the New York academy of sciences*, vol. 68, no. 3, pp. 1128–1132, 1958.

[28] D. Bergsagel, C. Sprague, and S. Ross, "Evaluation of new chemotherapeutic agents in the treatment of multiple myeloma. plan of study," *Cancer chemotherapy reports*, vol. 21, 1962.

[29] B. Hoogstraten, P. R. Sheehe, J. Cuttner, T. Cooper, R. A. Kyle, R. A. Oberfield, S. R. Townsend, J. B. Harley, D. M. Hayes, G. Costa, *et al.*, "Melphalan in multiple myeloma," *Blood*, vol. 30, no. 1, pp. 74–83, 1967.

[30] R. Alexanian, A. Haut, A. U. Khan, M. Lane, E. M. McKelvey, P. J. Migliore, W. Stuckey, and H. E. Wilson, "Treatment for multiple myeloma: combination chemotherapy with different melphalan dose regimens," *JAMA*, vol. 208, no. 9, pp. 1680–1685, 1969.

[31] G. Gahrton, S. Tura, M. Flesch, A. Gratwohl, P. Gravett, G. Lucarelli, M. Michallet, J. Reiffers, O. Ringden, and M. Van Lint, "Bone marrow transplantation in multiple myeloma: report from the european cooperative group for bone marrow transplantation," *Blood*, vol. 69, pp. 1262–1264, 04 1987.

[32] B. Barlogie, R. Alexanian, K. A. Dicke, G. Zagars, G. Spitzer, S. Jagannath, and L. Horwitz, "High-dose chemoradiotherapy and autologous bone marrow transplantation for resistant multiple myeloma," *Blood*, vol. 70, no. 3, pp. 869–872, 1987.

[33] M. Attal, J. L. Harousseau, A. M. Stoppa, J. J. Sotto, J. G. Fuzibet, J. F. Rossi, P. Casassus, H. Maisonneuve, T. Facon, N. Ifrah, *et al.*, "A prospective, randomized trial of autologous bone marrow transplantation and chemotherapy in multiple myeloma," *New England journal of medicine*, vol. 335, no. 2, pp. 91–97, 1996.

[34] J. A. Child, G. J. Morgan, F. E. Davies, R. G. Owen, S. E. Bell, K. Hawkins, J. Brown, M. T. Drayson, and P. J. Selby, "High-dose chemotherapy with hematopoietic stem-cell rescue for multiple myeloma," *New England journal of medicine*, vol. 348, no. 19, pp. 1875–1883, 2003.

[35] W. McBride, "Thalidomide and congenital abnormalities," *The lancet*, vol. 2, no. 1358, pp. 90927–909278, 1961.

[36] S. Singhal, J. Mehta, R. Desikan, D. Ayers, P. Roberson, P. Eddlemon, N. Munshi, E. Anaissie, C. Wilson, M. Dhodapkar, *et al.*, "Antitumor activity of thalidomide in refractory multiple myeloma," *New England journal of medicine*, vol. 341, no. 21, pp. 1565–1571, 1999.

[37] P. G. Richardson, R. L. Schlossman, E. Weller, T. Hideshima, C. Mitsiades, F. Davies, R. LeBlanc, L. P. Catley, D. Doss, K. Kelly, *et al.*, "Immunomodulatory drug cc-5013 overcomes drug resistance

and is well tolerated in patients with relapsed multiple myeloma," *Blood*, vol. 100, no. 9, pp. 3063–3067, 2002.

[38] S. V. Rajkumar, S. R. Hayman, M. Q. Lacy, A. Dispenzieri, S. M. Geyer, B. Kabat, S. R. Zeldenrust, S. Kumar, P. R. Greipp, R. Fonseca, *et al.*, "Combination therapy with lenalidomide plus dexamethasone (rev/dex) for newly diagnosed myeloma," *Blood*, vol. 106, no. 13, pp. 4050–4053, 2005.

[39] P. G. Richardson, E. Blood, C. S. Mitsiades, S. Jagannath, S. R. Zeldenrust, M. Alsina, R. L. Schlossman, S. V. Rajkumar, K. R. Desikan, T. Hideshima, *et al.*, "A randomized phase 2 study of lenalidomide therapy for patients with relapsed or relapsed and refractory multiple myeloma," *Blood*, vol. 108, no. 10, pp. 3458–3464, 2006.

[40] M. Engelhardt, R. Wäsch, H. Reinhardt, and M. Kleber, "Pomalidomide," in *Small molecules in oncology*, pp. 359–372, Springer, 2014.

[41] J. Adams, V. J. Palombella, E. A. Sausville, J. Johnson, A. Destree, D. D. Lazarus, J. Maas, C. S. Pien, S. Prakash, and P. J. Elliott, "Proteasome inhibitors: a novel class of potent and effective antitumor agents," *Cancer research*, vol. 59, no. 11, pp. 2615–2622, 1999.

[42] R. Z. Orlowski, T. E. Stinchcombe, B. S. Mitchell, T. C. Shea, A. S. Baldwin, S. Stahl, J. Adams, D. L. Esseltine, P. J. Elliott, C. S. Pien, *et al.*, "Phase 1 trial of the proteasome inhibitor ps-341 in patients with refractory hematologic malignancies," *Journal of clinical oncology*, vol. 20, no. 22, pp. 4420–4427, 2002.

[43] P. G. Richardson, B. Barlogie, J. Berenson, S. Singhal, S. Jagannath, D. Irwin, S. V. Rajkumar, G. Srkalovic, M. Alsina, R. Alexanian, *et al.*, "A phase 2 study of bortezomib in relapsed, refractory myeloma," *New England journal of medicine*, vol. 348, no. 26, pp. 2609–2617, 2003.

[44] P. Moreau, A. Chanan-Khan, A. W. Roberts, A. B. Agarwal, T. Facon, S. Kumar, C. Touzeau, E. A. Punnoose, J. Cordero, W. Munasinghe, *et al.*, "Promising efficacy and acceptable safety of venetoclax plus bortezomib and dexamethasone in relapsed/refractory mm," *Blood*, vol. 130, no. 22, pp. 2392–2400, 2017.

[45] P. M. Voorhees, C. Rodriguez, B. Reeves, N. Nathwani, L. J. Costa, Y. Lutska, D. Hoehn, H. Pei, J. Ukropec, M. Qi, *et al.*, "Efficacy and updated safety analysis of a safety run-in cohort from griffin, a phase 2 randomized study of daratumumab (Dara), bortezomib (V), lenalidomide (R), and dexamethasone (D; Dara-Vrd) vs. vrd in patients (Pts) with newly diagnosed (ND) multiple myeloma (MM) eligible for high-dose therapy (HDT) and autologous stem cell transplantation (ASCT)," *Blood*, vol. 132, no. Suppl 1, p. 151, 2018.

[46] N. Raje, J. Berdeja, Y. Lin, D. Siegel, S. Jagannath, D. Madduri, M. Liedtke, J. Rosenblatt, M. V. Maus, A. Turka, *et al.*, "Anti-BCMA CAR T-cell therapy bb2121 in relapsed or refractory multiple myeloma," *New England journal of medicine*, vol. 380, no. 18, pp. 1726–1737, 2019.

[47] B. G. Durie, A. Hoering, M. H. Abidi, S. V. Rajkumar, J. Epstein, S. P. Kahanic, M. Thakuri, F. Reu, C. M. Reynolds, R. Sexton, *et al.*, "Bortezomib with lenalidomide and dexamethasone versus lenalidomide and dexamethasone alone in patients with newly diagnosed myeloma without intent for immediate autologous stem-cell transplant (swog s0777): a randomised, open-label, phase 3 trial," *The lancet*, vol. 389, no. 10068, pp. 519–527, 2017.

[48] A. Branagan, M. Lei, U. Lou, and N. Raje, "Current treatment strategies for multiple myeloma," *JCO oncology practice*, vol. 16, no. 1, pp. 5–14, 2020.

[49] D. Dingli, S. Ailawadhi, P. L. Bergsagel, F. K. Buadi, A. Dispenzieri, R. Fonseca, M. A. Gertz, W. I. Gonsalves, S. R. Hayman, P. Kapoor, *et al.*, "Therapy for relapsed multiple myeloma: guidelines from the mayo stratification for myeloma and risk-adapted therapy," in *Mayo clinic proceedings*, vol. 92, pp. 578–598, Elsevier, 2017.

[50] D. Brünnert, M. Kraus, T. Stühmer, S. Kirner, R. Heiden, P. Goyal, C. Driessen, R. C. Bargou, and M. Chatterjee, "Novel cell line models to study mechanisms and overcoming strategies of proteasome inhibitor resistance in multiple myeloma," *Biochimica et biophysica acta (BBA)-molecular basis of disease*, vol. 1865, no. 6, pp. 1666–1676, 2019.

[51] S. Barrio, T. Stühmer, M. Da-Viá, C. Barrio-Garcia, N. Lehners, A. Besse, I. Cuenca, A. Garitano-Trojaola, S. Fink, E. Leich, *et al.*, "Spectrum and functional validation of PSMB5 mutations in multiple myeloma," *Leukemia*, vol. 33, no. 2, pp. 447–456, 2019.

[52] L. Haertle, M. Bittrich, R. Potabattula, M. C. Da-Viá, U. Munawar, Y. Ruiz-Heredia, C. Vogt, T. Steinbrunn, A. Garitano-Trojaola, T. Stuehmer, *et al.*, "Focusing PI and IMiD resistance in multiple myeloma: Impact of DNA methylation," *Blood*, vol. 132, pp. 404–404, 11 2018.

[53] K. Kortüm, Y. Zhu, C. Shi, P. Jedlowski, and A. K. Stewart, "Cereblon binding molecules in multiple myeloma," *Blood reviews*, vol. 29, no. 5, pp. 329–334, 2015.

[54] E. S. Fischer, A. Scrima, K. Böhm, S. Matsumoto, G. M. Lingaraju, M. Faty, T. Yasuda, S. Cavadini, M. Wakasugi, F. Hanaoka, *et al.*, "The molecular basis of CRL4$^{\text{DDB2/CSA}}$ ubiquitin ligase architecture, targeting, and activation," *Cell*, vol. 147, no. 5, pp. 1024–1039, 2011.

[55] K. M. Kortüm, E. K. Mai, N. H. Hanafiah, C. X. Shi, Y. X. Zhu, L. Bruins, S. Barrio, P. Jedlowski, M. Merz, J. Xu, *et al.*, "Targeted sequencing of refractory myeloma reveals a high incidence of mutations in CRBN and Ras pathway genes," *Blood*, vol. 128, no. 9, pp. 1226–1233, 2016.

[56] K. Kortüm, E. Braggio, L. Bruins, S. Barrio, C. Shi, Y. Zhu, R. Tibes, D. Viswanatha, P. Votruba, G. Ahmann, *et al.*, "Panel sequencing for clinically oriented variant screening and copy number detection in 142 untreated multiple myeloma patients," *Blood cancer journal*, vol. 6, no. 2, pp. e397–e397, 2016.

[57] K. Kortüm, C. Langer, J. Monge, L. Bruins, Y. Zhu, C. Shi, P. Jedlowski, J. Egan, J. Ojha, L. Bullinger, *et al.*, "Longitudinal analysis of 25 sequential sample-pairs using a custom multiple

myeloma mutation sequencing panel (M^{3}P)," *Annals of hematology*, vol. 94, no. 7, pp. 1205–1211, 2015.

[58] K. M. Kortüm, C. Langer, J. Monge, L. Bruins, J. B. Egan, Y. X. Zhu, C. X. Shi, P. Jedlowski, J. Schmidt, J. Ojha, *et al.*, "Targeted sequencing using a 47 gene multiple myeloma mutation panel (M^{3}P) in-17p high risk disease," *British journal of haematology*, vol. 168, no. 4, pp. 507–510, 2015.

[59] N. Weinhold, C. Heuck, A. Rosenthal, S. Thanendrarajan, C. Stein, F. Van Rhee, M. Zangari, A. Hoering, E. Tian, F. Davies, *et al.*, "Clinical value of molecular subtyping multiple myeloma using gene expression profiling," *Leukemia*, vol. 30, no. 2, pp. 423–430, 2016.

[60] N. Bolli, H. Avet-Loiseau, D. C. Wedge, P. Van Loo, L. B. Alexandrov, I. Martincorena, K. J. Dawson, F. Iorio, S. Nik-Zainal, G. R. Bignell, *et al.*, "Heterogeneity of genomic evolution and mutational profiles in multiple myeloma," *Nature communications*, vol. 5, p. 2997, 2014.

[61] L. Rasche, S. Chavan, O. Stephens, P. Patel, R. Tytarenko, C. Ashby, M. Bauer, C. Stein, S. Deshpande, C. Wardell, *et al.*, "Spatial genomic heterogeneity in multiple myeloma revealed by multiregion sequencing," *Nature communications*, vol. 8, no. 1, pp. 1–11, 2017.

[62] L. R. Yates and P. J. Campbell, "Evolution of the cancer genome," *Nature reviews genetics*, vol. 13, no. 11, pp. 795–806, 2012.

[63] G. J. Morgan, B. A. Walker, and F. E. Davies, "The genetic architecture of multiple myeloma," *Nature reviews cancer*, vol. 12, no. 5, pp. 335–348, 2012.

[64] J. J. Keats, M. Chesi, J. B. Egan, V. M. Garbitt, S. E. Palmer, E. Braggio, S. Van Wier, P. R. Blackburn, A. S. Baker, A. Dispenzieri, *et al.*, "Clonal competition with alternating dominance in multiple myeloma," *Blood*, vol. 120, no. 5, pp. 1067–1076, 2012.

[65] C. A. Finlay, P. W. Hinds, and A. J. Levine, "The p53 proto-oncogene can act as a suppressor of transformation," *Cell*, vol. 57, no. 7, pp. 1083–1093, 1989.

[66] P. A. Muller and K. H. Vousden, "p53 mutations in cancer," *Nature cell biology*, vol. 15, no. 1, pp. 2–8, 2013.

[67] O. Laptenko and C. Prives, "Transcriptional regulation by p53: one protein, many possibilities," *Cell Death & Differentiation*, vol. 13, no. 6, pp. 951–961, 2006.

[68] P. D. Jeffrey, S. Gorina, and N. P. Pavletich, "Crystal structure of the tetramerization domain of the p53 tumor suppressor at 1.7 angstroms," *Science*, vol. 267, no. 5203, pp. 1498–1502, 1995.

[69] M. H. Kubbutat, S. N. Jones, and K. H. Vousden, "Regulation of p53 stability by MDM2," *Nature*, vol. 387, no. 6630, pp. 299–303, 1997.

[70] L. T. Vassilev, B. T. Vu, B. Graves, D. Carvajal, F. Podlaski, Z. Filipovic, N. Kong, U. Kammlott, C. Lukacs, C. Klein, *et al.*, "In vivo activation of the p53 pathway by small-molecule antagonists of MDM2," *Science*, vol. 303, no. 5659, pp. 844–848, 2004.

[71] J. N. Weinstein, E. A. Collisson, G. B. Mills, K. R. M. Shaw, B. A. Ozenberger, K. Ellrott, I. Shmulevich, C. Sander, and J. M. Stuart, "The cancer genome atlas pan-cancer analysis project," *Nature genetics*, vol. 45, no. 10, pp. 1113–1120, 2013.

[72] V. D. Li, K. H. Li, and J. T. Li, "*TP53* mutations as potential prognostic markers for specific cancers: analysis of data from the cancer genome atlas and the international agency for research on cancer *TP53* database," *Journal of cancer research and clinical oncology*, vol. 145, no. 3, pp. 625–636, 2019.

[73] J. Drach, J. Ackermann, E. Fritz, E. Kroemer, R. Schuster, H. Gisslinger, M. DeSantis, N. Zojer, M. Fiegl, S. Roka, *et al.*, "Presence of a p53 gene deletion in patients with multiple myeloma predicts for short survival after conventional-dose chemotherapy," *Blood*, vol. 92, no. 3, pp. 802–809, 1998.

[74] S. Manier, K. Z. Salem, J. Park, D. A. Landau, G. Getz, and I. M. Ghobrial, "Genomic complexity of multiple myeloma and its clinical implications," *Nature reviews clinical oncology*, vol. 14, no. 2, p. 100, 2017.

[75] H. Avet-Loiseau, M. Attal, P. Moreau, C. Charbonnel, F. Garban, C. Hulin, S. Leyvraz, M. Michallet, I. Yakoub-Agha, L. Garderet, *et al.*, "Genetic abnormalities and survival in multiple myeloma: the experience of the intergroupe francophone du myelome," *Blood*, vol. 109, no. 8, pp. 3489–3495, 2007.

[76] A. Palumbo, H. Avet-Loiseau, S. Oliva, H. M. Lokhorst, H. Goldschmidt, L. Rosinol, P. Richardson, S. Caltagirone, J. J. Lahuerta, T. Facon, *et al.*, "Revised international staging system for multiple myeloma: a report from international myeloma working group," *Journal of clinical oncology*, vol. 33, no. 26, p. 2863, 2015.

[77] G. An, Z. Li, Y. T. Tai, C. Acharya, Q. Li, X. Qin, S. Yi, Y. Xu, X. Feng, C. Li, *et al.*, "The impact of clone size on the prognostic value of chromosome aberrations by fluorescence in situ hybridization in multiple myeloma," *Clinical cancer research*, vol. 21, no. 9, pp. 2148–2156, 2015.

[78] A. Thakurta, M. Ortiz, P. Blecua, F. Towfic, J. Corre, N. V. Serbina, E. Flynt, Z. Yu, Z. Yang, A. Palumbo, *et al.*, "High subclonal fraction of 17p deletion is associated with poor prognosis in multiple myeloma," *Blood*, vol. 133, no. 11, pp. 1217–1221, 2019.

[79] H. Avet-Loiseau, N. J. Bahlis, W. J. Chng, T. Masszi, L. Viterbo, L. Pour, P. Ganly, A. Palumbo, M. Cavo, C. Langer, *et al.*, "Ixazomib significantly prolongs progression-free survival in high-risk relapsed/refractory myeloma patients," *Blood*, vol. 130, no. 24, pp. 2610–2618, 2017.

[80] S. Thanendrarajan, E. Tian, P. Qu, P. Mathur, C. Schinke, F. van Rhee, M. Zangari, L. Rasche, N. Weinhold, D. Alapat, *et al.*, "The level of deletion 17p and bi-allelic inactivation of *TP53* has a significant impact on clinical outcome in multiple myeloma," *Haematologica*, vol. 102, no. 9, p. e364, 2017.

[81] Y. Liu, C. Chen, Z. Xu, C. Scuoppo, C. D. Rillahan, J. Gao, B. Spitzer, B. Bosbach, E. R. Kastenhuber, T. Baslan, *et al.*, "Deletions linked to *TP53* loss drive cancer through p53-independent mechanisms," *Nature*, vol. 531, no. 7595, pp. 471–475, 2016.

[82] K. D. Boyd, F. M. Ross, W. J. Tapper, L. Chiecchio, G. Dagrada, Z. J. Konn, D. Gonzalez, B. A. Walker, S. L. Hockley, C. P. Wardell, *et al.*, "The clinical impact and molecular biology of del (17p) in multiple myeloma treated with conventional or thalidomide-based therapy," *Genes, chromosomes and cancer*, vol. 50, no. 10, pp. 765–774, 2011.

[83] P. Teoh, T. Chung, S. Sebastian, S. Choo, J. Yan, S. Ng, R. Fonseca, and W. Chng, "p53 haploin-sufficiency and functional abnormalities in multiple myeloma," *Leukemia*, vol. 28, no. 10, pp. 2066–2074, 2014.

[84] B. A. Walker, K. Mavrommatis, C. P. Wardell, T. C. Ashby, M. Bauer, F. Davies, A. Rosenthal, H. Wang, P. Qu, A. Hoering, *et al.*, "A high-risk, double-hit, group of newly diagnosed myeloma identified by genomic analysis," *Leukemia*, vol. 33, no. 1, pp. 159–170, 2019.

[85] R. Owen, S. Davis, J. Randerson, A. Rawstron, F. Davies, J. Child, A. Jack, and G. Morgan, "p53 gene mutations in multiple myeloma.," *Molecular pathology*, vol. 50, no. 1, p. 18, 1997.

[86] B. Leroy, J. L. Fournier, C. Ishioka, P. Monti, A. Inga, G. Fronza, and T. Soussi, "The *TP53* website: an integrative resource centre for the tp53 mutation database and tp53 mutant analysis," *Nucleic acids research*, vol. 41, no. D1, pp. D962–D969, 2013.

[87] M. Lionetti, M. Barbieri, M. Manzoni, S. Fabris, C. Bandini, K. Todoerti, F. Nozza, D. Rossi, P. Musto, L. Baldini, *et al.*, "Molecular spectrum of *TP53* mutations in plasma cell dyscrasias by next generation sequencing: an italian cohort study and overview of the literature," *Oncotarget*, vol. 7, no. 16, p. 21353, 2016.

[88] B. A. Walker, K. Mavrommatis, C. P. Wardell, T. C. Ashby, M. Bauer, F. E. Davies, A. Rosenthal, H. Wang, P. Qu, A. Hoering, *et al.*, "Identification of novel mutational drivers reveals oncogene dependencies in multiple myeloma," *Blood*, vol. 132, no. 6, pp. 587–597, 2018.

[89] M. Chin, J. Sive, C. Allen, C. Roddie, S. Chavda, D. Smith, P. Blombery, K. Jones, G. Ryland, R. Popat, *et al.*, "Prevalence and timing of *TP53* mutations in del (17p) myeloma and effect on survival," *Blood cancer journal*, vol. 7, no. 9, pp. e610–e610, 2017.

[90] W. Chng, T. Price-Troska, N. Gonzalez-Paz, S. Van Wier, S. Jacobus, E. Blood, K. Henderson, M. Oken, B. Van Ness, P. Greipp, *et al.*, "Clinical significance of *TP53* mutation in myeloma," *Leukemia*, vol. 21, no. 3, pp. 582–584, 2007.

[91] I. Adzhubei, D. M. Jordan, and S. R. Sunyaev, "Predicting functional effect of human missense mutations using polyphen-2," *Current protocols in human genetics*, vol. 76, no. 1, pp. 7–20, 2013.

[92] B. Reva, Y. Antipin, and C. Sander, "Predicting the functional impact of protein mutations: application to cancer genomics," *Nucleic acids research*, vol. 39, no. 17, pp. e118–e118, 2011.

[93] R. Vaser, S. Adusumalli, S. N. Leng, M. Sikic, and P. C. Ng, "Sift missense predictions for genomes," *Nature protocols*, vol. 11, no. 1, p. 1, 2016.

[94] L. Lodé, M. Eveillard, V. Trichet, T. Soussi, S. Wuillème, S. Richebourg, F. Magrangeas, N. Ifrah, L. Campion, C. Traullé, *et al.*, "Mutations in *TP53* are exclusively associated with del (17p) in multiple myeloma," *Haematologica*, vol. 95, no. 11, pp. 1973–1976, 2010.

[95] D. Reece, K. W. Song, T. Fu, B. Roland, H. Chang, D. E. Horsman, A. Mansoor, C. Chen, E. Masih-Khan, Y. Trieu, *et al.*, "Influence of cytogenetics in patients with relapsed or refractory multiple myeloma treated with lenalidomide plus dexamethasone: adverse effect of deletion 17p13," *Blood*, vol. 114, no. 3, pp. 522–525, 2009.

[96] S. Knop, C. Gerecke, P. Liebisch, M. S. Topp, U. Platzbecker, O. Sezer, C. Vollmuth, K. Falk, A. Glasmacher, U. Maeder, *et al.*, "Lenalidomide, adriamycin, and dexamethasone (RAD) in patients with relapsed and refractory multiple myeloma: a report from the german myeloma study group DSMM (Deutsche Studiengruppe Multiples Myelom)," *Blood*, vol. 113, no. 18, pp. 4137–4143, 2009.

[97] N. Issaeva, P. Bozko, M. Enge, M. Protopopova, L. G. Verhoef, M. Masucci, A. Pramanik, and G. Selivanova, "Small molecule RITA binds to p53, blocks p53-HDM-2 interaction and activates p53 function in tumors," *Nature medicine*, vol. 10, no. 12, pp. 1321–1328, 2004.

[98] A. P. Turnbull, S. Ioannidis, W. W. Krajewski, A. Pinto-Fernandez, C. Heride, A. C. Martin, L. M. Tonkin, E. C. Townsend, S. M. Buker, D. R. Lancia, *et al.*, "Molecular basis of USP7 inhibition by selective small-molecule inhibitors," *Nature*, vol. 550, no. 7677, pp. 481–486, 2017.

[99] J. M. Lambert, P. Gorzov, D. B. Veprintsev, M. Söderqvist, D. Segerbäck, J. Bergman, A. R. Fersht, P. Hainaut, K. G. Wiman, and V. J. Bykov, "PRIMA-1 reactivates mutant p53 by covalent binding to the core domain," *Cancer cell*, vol. 15, no. 5, pp. 376–388, 2009.

[100] C. C. Uphoff and H. G. Drexler, "Detecting mycoplasma contamination in cell cultures by polymerase chain reaction," in *Cancer Cell Culture*, pp. 319–326, Springer, 2004.

[101] T. Steinbrunn, M. Chatterjee, R. C. Bargou, and T. Stühmer, "Efficient transient transfection of human multiple myeloma cells by electroporation–an appraisal," *PLOS ONE*, vol. 9, no. 6, 2014.

[102] L. Norton, "A gompertzian model of human breast cancer growth," *Cancer research*, vol. 48, no. 24 Part 1, pp. 7067–7071, 1988.

[103] C. Baldow, L. Thielecke, and I. Glauche, "Model based analysis of clonal developments allows for early detection of monoclonal conversion and leukemia," *PLOS ONE*, vol. 11, no. 10, 2016.

[104] S. Barrio, U. Munawar, Y. X. Zhu, N. Giesen, C.-X. Shi, M. Da Viá, R. Sanchez, L. Bruins, T. Demler, N. Müller, *et al.*, "IKZF1/3 and CRL4-CRBN E3 ubiquitin ligase mutations and IMiD resistance in multiple myeloma," *Haematologica*, pp. haematol–2019, 2019.

[105] S. Boettcher, P. G. Miller, R. Sharma, M. McConkey, M. Leventhal, A. V. Krivtsov, A. O. Giacomelli, W. Wong, J. Kim, S. Chao, K. J. Kurppa, X. Yang, K. Milenkowic, F. Piccioni, D. E. Root, F. G. Rücker, Y. Flamand, D. Neuberg, R. C. Lindsley, P. A. Jänne, W. C. Hahn, T. Jacks, H. Döhner, S. A. Armstrong, and B. L. Ebert, "A dominant-negative effect drives selection of tp53 missense mutations in myeloid malignancies," *Science*, vol. 365, no. 6453, pp. 599–604, 2019.

[106] R. Brosh and V. Rotter, "When mutants gain new powers: news from the mutant p53 field," *Nature reviews cancer*, vol. 9, no. 10, pp. 701–713, 2009.

[107] M. G. van Oijen and P. J. Slootweg, "Gain-of-function mutations in the tumor suppressor gene p53," *Clinical cancer research*, vol. 6, no. 6, pp. 2138–2145, 2000.

[108] S. Barrio, M. DáVia, L. Bruins, T. Stühmer, T. Steinbrunn, M. Bittrich, H. Einsele, A. K. Stewart, E. Braggio, and K. M. Kortüm, "Protocol for m 3 p: A comprehensive and clinical oriented targeted sequencing panel for routine molecular analysis in multiple myeloma," in *Multiple Myeloma*, pp. 117–128, Springer, 2018.

Appendices

List of publications

- U. Munawar, L. Rasche, N. Müller, C. Vogt, M. Da-Via, L. Haertle, P. Arampatzi, S. Dietrich, M. Roth, A. Garitano-Trojaola, *et al.*, "Hierarchy of mono-and biallelic *TP53* alterations in multiple myeloma cell", *Blood*, 134(10), pp.836-840, 2019.

- U. Munawar, M. Roth, S. Barrio, H. Wajant, D. Siegmund, R.C. Bargou, K.M. Kortüm, and T. Stühmer, "Assessment of *TP53* lesions for p53 system functionality and drug resistance in multiple myeloma using an isogenic cell line model", *Scientific Reports*, 9(1), pp.1-9, 2019.

- S. Barrio, U. Munawar, Y.X. Zhu, N. Giesen, C.X. Shi, M. Da-Viá, R. Sanchez, L. Bruins, T. Demler, N. Müller, *et al.*, IKZF1/3 and CRL4-CRBN E3 ubiquitin ligase mutations and resistance to immunomodulatory drugs in multiple myeloma, *Haematologica*, 105(5), p.e237, 2019

- M.C. Da Via, A.G. Solimando, A. Garitano Trojaola, S. Barrio, U. Munawar, S. Strifler, L. Haertle, N. Rhodes, E. Teufel, C. Vogt, *et al.*, CIC Mutation as a Molecular Mechanism of Acquired Resistance to Combined BRAF MEK Inhibition in Extramedullary Multiple Myeloma with Central Nervous System Involvement, *The Oncologist*, 25(2), p.112, 2020.

Conference contributions

- U. Munawar, S. Barrio, M. Roth, H. Einsele, R.C. Bargou, T. Stuehmer, M. Kortum, "Implications of *TP53* alterations for therapy response in multiple myeloma," *Blood*, 132(Supplement 1), pp.3189-3189, 2018 (Poster presentation, 60th annual American society of hematology meeting, San Diego, USA)

- U. Munawar, S. Barrio, M. Roth, H. Einsele, R.C. Bargou, M. Kortum, T. Stuehmer, "Implications of *TP53* alterations for therapy response in multiple myeloma," *Oncology research treatment*, 41(Supplement 4), p.134, 2018 (Oral presentation, Deutsche Gesellschaft für Hämatologie und Medizinische Oncology, Vienna, Austria)

- U. Munawar, L. Haertle, L. Martin, I. Cuenca, C. Vogt, M. Da-Via, A. Garitano-Trojaola, L. Rasche, M. Gallardo, T. Stuehmer, J. M. Lopez, M. Kortum, S. Barrio, "Clonal competition assays to understand progression and resistance in multiple myeloma," (Poster presentation, Spanish national cancer research center, Madrid, Spain)

Curriculum Vitae

Curriculum Vitae

• • •

Curriculum Vitae

Curriculum Vitae

• • •

Affidavit

I hereby confirm that my thesis entitled **Functional analysis of oncogenic lesions in multiple myeloma with potential significance for refractory disease** is the result of my own work. I did not receive any help or support from commercial consultants. All sources and / or materials applied are listed and specified in the thesis.

Furthermore, I confirm that this thesis has not yet been submitted as part of another examination process neither in identical nor in similar form.

Würzburg, 06.07.2020

Place, Date   Signature

Eidesstattliche Erklärung

Hiermit erkläre ich an Eides statt, die Dissertation **Funktionelle Analyse onkogener Läsionen beim Multiplen Myelom mit potenzieller Bedeutung für einen refraktären Krankheitsverlauf** eigenständig, d.h. insbesondere selbständig und ohne Hilfe eines kommerziellen Promotionsberaters, angefertigt und keine anderen als die von mir angegebenen Quellen und Hilfsmittel verwendet zu haben.

Ich erkläre außerdem, dass die Dissertation weder in gleicher noch in ähnlicher Form bereits in einem anderen Prüfungsverfahren vorgelegen hat.

Würzburg, 06.07.2020

Ort, Datum   Unterschrift

Acknowledgement

Many people have contributed to the success of this work. At this point, I would like to say special thanks to some of them. First of all, I convey my gratitude and thanks to Prof. Bargou for providing me an opportunity to work in his lab and to my thesis committee members Prof. Wajant and Prof. Meierjohann for their valuable comments during our meetings. Besides my thesis committee, I wish to express my heartiest gratitude to my mentor Dr. Thorsten Stühmer for his continuous guidance, support, valuable scientific ideas and discussions during the whole duration of my stay in the lab. I would like to especially thank Dr. Santiago Barrio for his invaluable assistance, ideas, comments, insight into different projects and a very nice company in the lab.

I am grateful to all lab members, Pooja Shah, Markus Roth, Evelyn Brandt, Leonard Glück, Nicole Müller, Carlotta Höschle, Stefanie Kirner, Heike Schraud for creating a very pleasant working environment and for a nice company, particularly Dr. Daniela Brünnert for her invaluable help in the lab and thesis corrections. I would like to pay my special regards to Dr. Larissa Haertle for her assistance and time during writing and correcting this thesis, for being a nice colleague, friend and a food buddy along with Seungbin Han and Johanna Lehmann. I would like to say thanks to my friends back home and here in Germany, especially to Dr. Muhammad Khalid for his help support encouragement and guidance during my stay in Würzburg and Hifza Idress for her help in corrections of the thesis.

Special thanks to the whole team of Graduate School of Life Sciences for their continuous support from my very first day in Würzburg till now, without them, it would not have been possible.

Most importantly, I would like to extend my heartiest gratitude to my parents and my family for their unparalleled love, prayers and support.
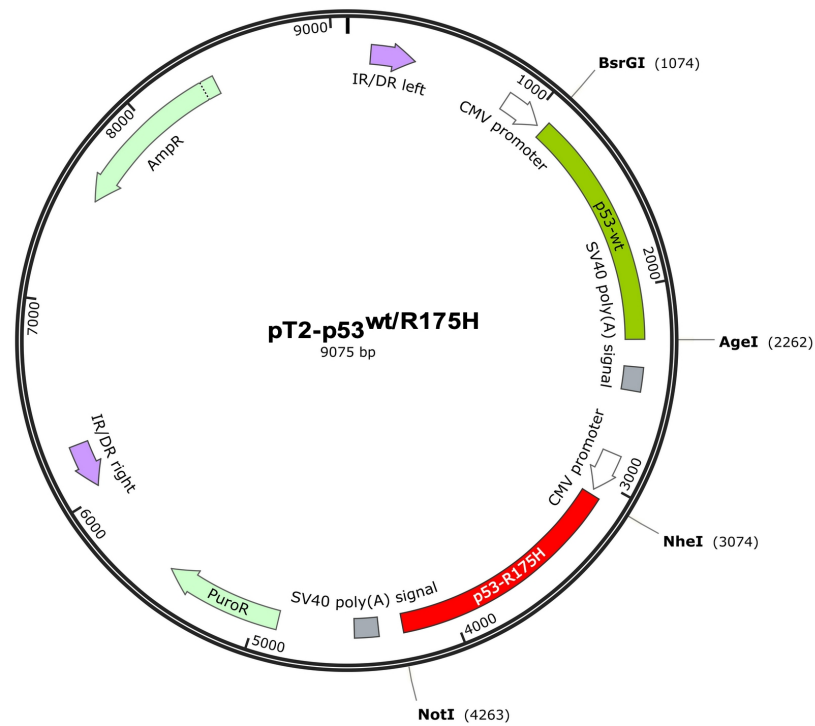
Vector maps
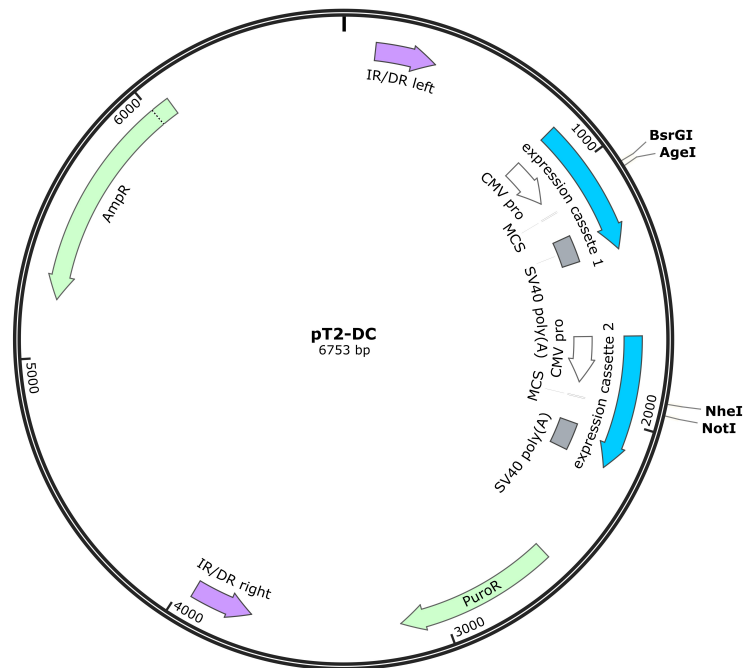
Vector 1: pT2-DC. Sleeping beauty expression vector with two identical but individually addressable expression cassettes
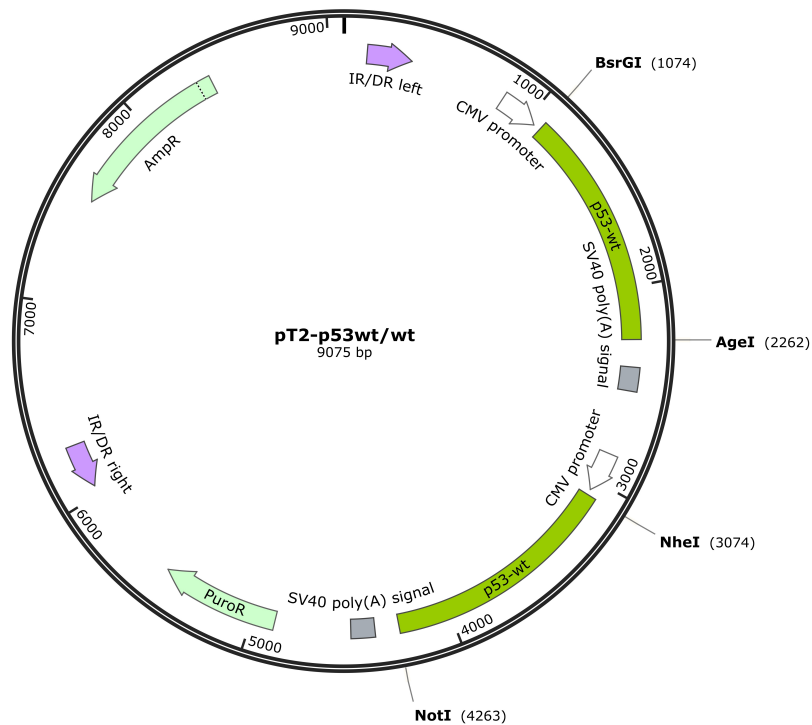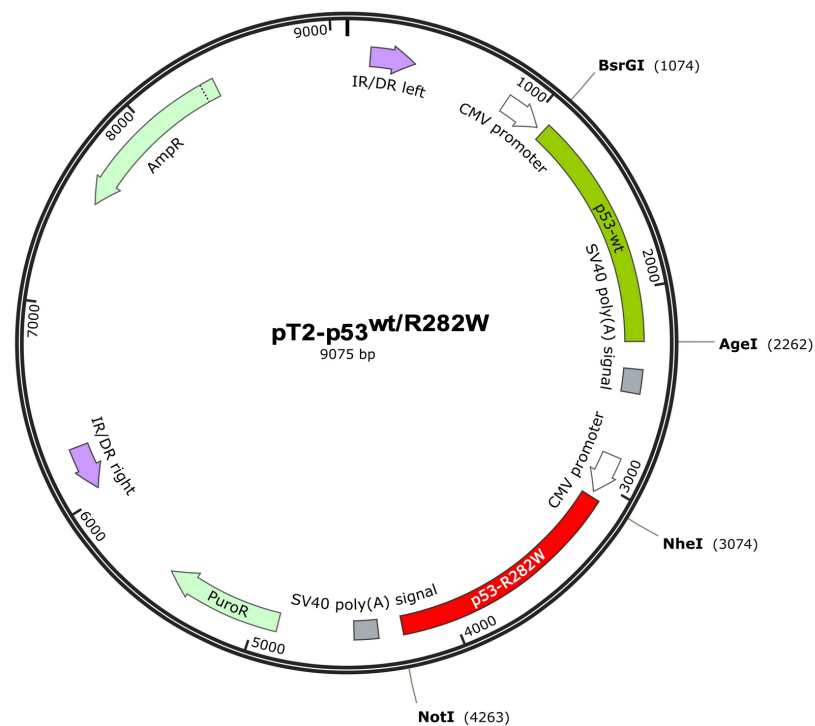

Vector 2: pT2-p53$^{\mathrm{wt/wt}}$. Sleeping beauty expression vector with two wildtype *TP53* cDNA copies
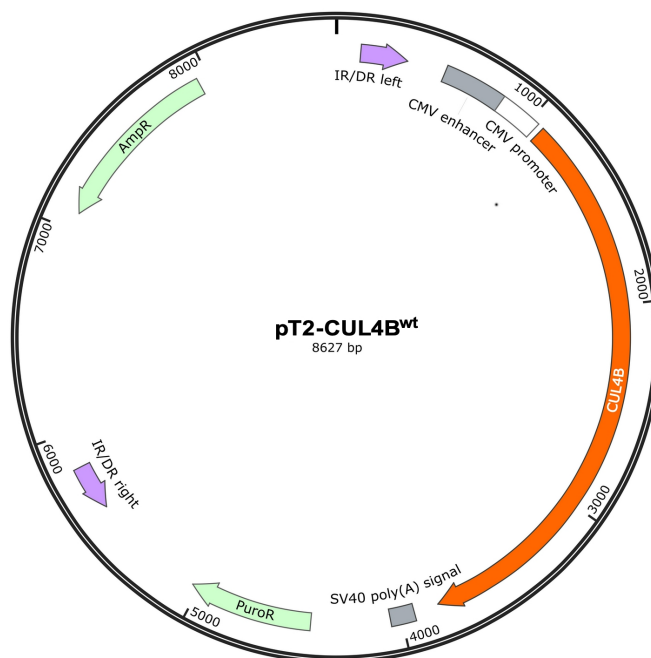
Vector 3: pT2-p53^{wt/R175H}. Sleeping beauty expression vector expressing a combinations of a wildtype and a mutant (R175H) *TP53* cDNA copies

Vector 4: pT2-p53^{wt/R282W}. Sleeping beauty expression vector expressing a combination of a wildtype and a mutant (R282W) *TP53* cDNA copies

Vector 5: pT2-CUL4B^{wt}. Sleeping beauty expression vector with a wildtype *CUL4B* cDNA copy